UNIVERSIDAD DE ANTIOQUIA

NOPYL ACETATE PRODUCTION BY ESTERIFICATION OF ACETIC ACID AND NOPOL OVER HETEROGENEOUS CATALYSTS

LUIS FERNANDO CORREA MONTES

Universidad de Antioquia

Engineering Faculty, Chemical Engineering Department

Medellín, Colombia

2019

CC BY NC ND

NOPYL ACETATE PRODUCTION BY ESTERIFICATION OF ACETIC ACID AND NOPOL OVER HETEROGENEOUS CATALYSTS

LUIS FERNANDO CORREA MONTES

Thesis to fulfill requirements for Ph.D. in Chemical Engineering

Director

Ph.D Aída Luz Villa Holguín

Universidad de Antioquia
Engineering Faculty, Chemical Engineering Department,
Environmental Catalysis Research Group
Medellín, Colombia
2019

NOPYL ACETATE PRODUCTION BY ESTERIFICATION OF ACETIC ACID AND NOPOL OVER HETEROGENEOUS CATALYSTS

LUIS FERNANDO CORREA MONTES

"Reproduction forbidden without author´s express authorization"

UNIVERSIDAD DE ANTIOQUIA
Medellín
2019

To God.

To the memory of my parents.

To my family.

ACKNOWLEDGMENTS

I want to thank my deceased parents, Professor Consuelo Montes de Correa and Luis Fernando Correa A., for their infinite support and dedication throughout my personal and professional career. To my family for their unconditional support throughout my life. I would like to thank Dr. Aída Luz Villa, professor at Universidad de Antioquia, for her valuable guidance in the execution of the project. I also thank Dr. Edwin Alarcón and Dr. Lina María González for their collaboration, the staff of the Environmental Catalysis Research Group, Comité para el Desarrollo de la Investigación (CODI) through project MDC11-1-12 and the Chemical Engineering graduate program.

ABSTRACT

Nopyl acetate is an artificial fragrance compound with a fruity odor of fresh wood which is not present in nature and it is used in the preparation of soaps, detergents, creams, lotions and perfumes. It is conventionally prepared by the carbonyl-ene reaction of β-pinene and paraformaldehyde with subsequent acetylation of the intermediary nopol with acetic anhydride. As the esterification reaction in the absence of a catalyst is slow and reversible and water is one of the by-products, a hydrothermal stable material is required as catalyst.

There are few reports about the synthesis of nopyl acetate. It was reported that the reaction at 200 °C of β-pinene with paraformaldehyde in the presence of acetic anhydride produces nopyl acetate with a 60 % yield after 5 h. For nopol esterification with carboxylic chloride acids in triethanol amine and dichloromethane solution, nopyl acetate yields of 79 % (5 to 25 °C) were achieved. Nopyl acetate may be synthesized from acetic anhydride and sodium acetate, with 84 % yield (3 h, 90 ° C) after its separation and purification. It is possible to obtain yields of 98 % (150 °C, 1 h) by reacting nopol with acetic anhydride in the presence of toluene or chlorobenzene, removing the carboxylic acid by-product by azeotropic distillation. The synthesis of nopyl acetate with acetic anhydride in the presence of triethylamine and dimethylaminopyridine (DMAP) in dichloromethane as solvent at room temperature, with quantitative yields, has been reported. Using ammonium and cerium nitrate catalyst, $(NH_4)Ce(NO_3)_6$ in CH_2Cl_2 as solvent at 40-50 °C, nopyl acetate is obtained with a 92 % yield. Costa *et al.* reported in 2016 the use of tungstophosphoric heteropoly acid $H_3PW_{12}O_{40}$ (HPW) and its acidic Cs salt $Cs_{2.5}H_{0.5}PW_{12}O_{40}$ (CsPW) for the liquid phase acetylation of nopol. The reaction occurs at room temperature with low catalyst loadings and can be performed solvent-free with stoichiometric amounts of acetic anhydride providing excellent yields (100%).

Recently, environmental and economic considerations have promoted innovation processes towards the use of cleaner technologies. Therefore, there is a great challenge of using heterogeneous catalysts that can perform under mild reaction conditions, for

example at low temperatures and pressures, while avoiding the use of harmful substances such as amines and chlorinated compounds.

Systems reported for the esterification of other alcohols could be considered as possible alternatives for the esterification of nopol. Tin modified mesoporous materials (MCM-41 and SBA-15) could be attractive alternatives with voluminous organic molecules like nopol. Ionic exchange resins like Amberlyst – 15, with functional group $–SO_3H$, have been used in the esterification of primary alcohols with acetic acid.

Sn-SBA-15 is an acid catalyst, with a mesoporous support that would avoid mobility restriction of reactants and products. Additionally, Sn-MCM-41 has been found to be a suitable mesoporous material for nopol production. The use of Sn supported on SiO_2 is an economical option, as well as Amberlyst-15. *p*-toluenesulfonic acid (PTSA) has the potential to be used as a substitute for conventional acidic catalytic materials. It is characterized by the mildness of the reaction conditions, inexpensive chemical and the excellent functional group tolerance, allowing the formation of the corresponding esters in good to excellent yields.

The objective of this research is to determine the most adequate catalyst and reaction conditions for nopyl acetate synthesis in order to achieve highest reaction rate.

Sn-MCM-41, Sn-SBA-15 and Sn-SiO_2 heterogeneous catalysts were synthesized by incipient wetness impregnation using $SnCl_2 \cdot 2H_2O$ as precursor at room temperature. Physicochemical properties of the materials were determined by surface area BET (Brunauer, Emmett and Teller), SEM (Scanning Electron Microscopy), AAS (Atomic Absorption Spectroscopy) of Sn, NH_3-TPD (Ammonia Temperature Programmed Desorption), FTIR (Fourier-transform Infrared Spectroscopy), UV-vis (Ultraviolet–visible spectroscopy), Raman spectroscopy, XRD (X-ray Diffraction), and TGA (Thermal Gravimetric Analysis).

Characterization of MCM-41 and SBA-15 materials verified that synthesized catalysts have ordered hexagonal mesostructures. The XRD patterns of Sn-SBA-15 and Sn-MCM-

41 were very similar to those of the supports. SEM micrographs indicated that SBA-15 and Sn-SBA-15 showed the characteristic morphology of SBA-15, represented in domains in the form of loops that are added to a microstructure similar to wheat. The N_2 adsorption and desorption isotherms of the materials were type IV, which is typical of mesoporous materials. The BET areas of SBA-15 and Sn-SBA-15 were 531 and 471 m^2/g respectively. Surface area of MCM-41 decreased from 596 to 576 m^2/g by incorporating tin. SiO_2 and Sn-SiO_2 surface areas were 434 and 364 m^2/g, respectively. TPD analysis established the presence of strong (1.42 mmol NH_3/g cat), medium (0.08 mmol NH_3/g cat) and weak acid sites (0.24 mmol NH_3/g cat) in the materials. For kinetic tests with Amberlyst-15 and Sn-SBA-15, an average particle size of 58-76.5 μm and stirring speeds between 500 and 1000 rpm were used for guarantying the absence of diffusion effects for kinetic tests.

Acetic acid and acetic anhydride were used as esterifying agents. In presence of n-hexane, nopyl acetate selectivity over Sn-SBA-15 was 15.2 % and Sn-MCM-41 displayed best ester selectivity (17.8 %) in toluene at a 2:1 acetic acid: alcohol molar ratio. Amberlyst-15 reaches 100 % nopol conversion in presence of toluene at acetic acid: alcohol ratios of 1:2, 1:1 and 2:1. Synthesis of nopyl acetate was satisfactory using homogeneous catalyst *p*-toluenesulfonic acid (*p*-TSA), achieving a selectivity of 45.6 % and a nopol conversion of 99.7 % compared to Amberlyst-15 with 9 % ester selectivity and 57.6 % alcohol conversion. Using acetic anhydride, Sn-SiO_2 reaches 75 % nopol conversion at 60 min making it an active and selective material for nopyl acetate synthesis.

Amberlyst-15 exhibited best and more stable catalytic activity and with Sn-SiO_2 catalyst, best nopyl acetate selectivity was attained. Catalyst reusability was performed separating the material by decantation; washing it three times with acetone under continuous stirring and drying it in an oven at 80 °C overnight. This procedure was carried out before every reuse. The reusability tests were carried out with Amberlyst-15 that was the material that showed the highest nopol conversion, and it was found that the material loses catalytic activity in the fourth cycle, although leaching of the active species does not occur. The

structural properties of Sn-SBA-15, the high catalytic performance and the economic viability of Sn-SiO_2 make these materials potential to replace homogeneous acid catalysts in the nopol esterification reaction. Best nopyl acetate selectivity (100 %) is obtained over Sn-SiO_2, achieving a 75 % nopol conversion at 60 min, with a 3:1 acetic anhydride: alcohol molar ratio in presence of toluene, 80 °C and 750 rpm. Using Amberlyst-15, nopyl acetate selectivity reaches 8.2 % and 65.8 % nopol conversion at reaction times 90-120 min, 6.1 mg/mL catalyst loading, 80 °C, 750 rpm, nopol/ toluene solution 0.25 M and a 2:1 acetic acid: alcohol molar ratio.

CONTENT

LIST OF TABLES

LIST OF FIGURES

APPENDIXES

CHAPTER 1

CHAPTER 1. INTRODUCTION

1.1 Generalities

1.1.1 Essential Oils

Essential oils, volatile oils or etheric oil essences are secondary metabolites isolated from plants that are widely used in various branches of industry, medicine and many products used in everyday life. The essence is a complex mixture of volatile compounds of very diverse chemical nature; they are characterized by their smell, generally pleasant, intense, that evokes the fragrance of the plant, or of the fruit or the wood, from which it comes. The essence may remember the smell, for example, of one, a freshly cut grass, or vanilla, sweet and cloying, among other characteristics that possess an essential oil, formed by a complex range of volatile substances with different fragrant notes and different thresholds for their perception [1].

The essential oils obtained from aromatic plants are composed mostly of terpenes (monoterpenes, $C_{10}H_{16}$ and sesquiterpenes, $C_{15}H_{24}$) and their oxygenated derivatives (alcohols, aldehydes, ketones and, less frequently, acids), which together are called terpenoids. Numerous studies confirmed the varied biological activity of terpenoids as chemopreventive agents, active principles and adjuvants in the treatment of atherosclerosis, thrombosis and as a vehicle to facilitate the transdermal penetration of many topically applied drugs. Essential oils or their components are anti-bacterial, antifungal agents, exhibit anti-diabetic and antiviral properties. The key to success in using some essential oils to remove bacteria, *e.g.*, *Staphylococcus aureus*, *E. coli*, resistant to traditional antibiotics and various pathogenic fungi, is related to the very complex composition of oils, which are multi-component mixtures formed by substances with diverse biological activity, often enhanced precisely thanks to this unique combination of several components, which exert a notorious synergism [1].

Plants containing essential oils have been used since furthest antiquities as spices and remedies for the treatment of diseases and in religious ceremonies because of their healing properties and their pleasant odors. In spite of the obscured beginning of the use

of aromatic plants in prehistoric times to prevent, palliate, or heal sicknesses, pollen analyses of Stone Age settlements indicate the use of aromatic plants that may be dated to 10,000 BC [2].

The history of production of essential oils dates back to ca. 3500 BC when the oldest known water distillation equipment for essential oils was employed. Ancient India, China, and Egypt were the locations where essential oils were produced and widely used as medicaments, flavors, and fragrances [3].

Whatever may be regarded as the date of their industrial production, essential oils, together with a range of related products - pomades, tinctures, resins, absolutes, extracts, distillates, concretes, and so on - were the only ingredients of flavor and fragrance products until the late nineteenth century. At this stage, the growth in consumption of essential oils as odoriferous and flavoring materials stimulated the emergence of a great number of manufacturers in France, the United Kingdom, Germany, Switzerland, and the United States (Table 1.1).

Table 1.1 First industrial manufacturers of essential oils, flavors, and fragrances [3]

Company	Location	Establishment year
Antoine Chiris	France (Grasse)	1768
Cavallier Freres	France (Grasse)	1784
Dodge & Olcott Inc.	United States (New York)	1798
Roure Bertrand Fils and Justin Dupont	France (Grasse)	1820
Schimmel & Co.	Germany (Leipzig)	1829
J. Mero-Boyveau	France (Grasse)	1832
Stafford Allen and Sons	United Kingdom (London)	1833
Robertet et Cie	**France (Grasse)**	**1850**
W.J. Bush	United Kingdom (London)	1851
Payan–Bertrand et Cie	**France (Grasse)**	1854
A. Boake Roberts	United Kingdom (London)	1865
Fritzsche–Schimmel Co.	United States (New York)	1871
V. Mane et Fils	**France (Grasse)**	**1871**

Haarmann & Reimer	Germany (Holzminden)	1974
R.C. Treatt Co.	**United Kingdom (Bury)**	**1886**
N.V. Polak und Schwartz	Holland (Zaandam)	1889
Ogawa and Co.	**Japan (Osaka)**	**1893**
Firmenich and Cie	**Switzerland (Geneva)**	**1895**
Givaudan S.A.	**Switzerland (Geneva)**	**1895**
Maschmeijer Aromatics	Holland (Amsterdam)	1900

Note: Companies continuing to operate under their original name are printed in bold.

1.1.2 Turpentine

Turpentine, which occurs in many natural forms, is a component of conifer balsam and plays an important role in the ecosystem of the pine forest. It is part of the plant metabolism, and its individual components are important for the protective system of the conifers: for rapid closure of wounds to the bark by resin formation, for repelling insects (e.g., myrcene repels the pine beetle), and for protection against attack by bacteria (effect of, e.g., 3-carene) [4].

Turpentine (oil of turpentine, turpentine oil, spirit of turpentine) is the collective name for the volatile components of the crude resins (balsam or oleoresin, Latin: resina tere-binthi) from conifers, particularly the pine family. The turpentines represent a subgroup of plant and tree saps (essential oils) [4].

The main components of turpentines are mono- and bicyclic monoterpenes ($C_{10}H_{16}$; M_r (relative molecular mass) = 136.2). They also contain smaller quantities of terpene – oxygen compounds (e.g., terpene alcohols), sesquiterpenes ($C_{15}H_{24}$), and other compounds (see Fig. 1.1) [4]. α-Pinene is the main component of most turpentine oils. Many turpentines also contain large quantities of β-pinene, *d*- or *l*-limonene (or its racemate dipentene), 3-carene, or α-terpinene (sometimes up to 15 %).

The composition of different turpentines depends on the species of pine from which they are extracted. About 105 species and varieties have now been described which can be distinguished to only a limited extent on the basis of turpentine composition (their “terpene pattern”). Table 1.2 gives a simplified overview of the species of pine that are important

for turpentine extraction, the average composition and physical properties of various turpentines and producer country [4].

Besides the components listed in Table 1.2, turpentines can also contain α- and γ-terpinene, α- and β-phellandrene, terpinolene, myrcene, p-cymene, bornyl acetate, anethole, sesquiterpenes (such as longifolene; up to 20 % in *Pinus longifolia* Roxb.), heptane, nonane, and many other compounds [4].

Table 1.2 Simplified overview of the composition of turpentines of different origins [4]

Material	Proportion in wt % of					Density at
	α-Pinene	β-pinene	Camphene	3-Carene	Limonene (dipentene)	20 °C, g/mL
Gum turpentine						
Greece	92-97	1-3	ca. 1	0 - 1	0 - 2	0.860 – 0.865
Mexico	70-95	2-15	2 -15	1 - 2	0 - 4	0.862 – 0.868
China	70-95	4-15	1 - 2	0 - 5	1 - 3	0.860 - 0.865
Portugal	70-85	10-20	ca. 1		1 - 4	0.860 - 0.870
South America	45-85	5-45	1 - 3	0 - 2	2 - 4	0.860 - 0.870
Indonesia	65-85	1-3	ca. 1	10 - 18	1 - 3	0.865 - 0.870
France	65-75	20-26	ca. 1		1 - 5	0.860 - 0.871
Russia	40-75	4-15	1 - 5	0 - 20	0 - 5	0.855 - 0.865
Poland	40-70	2-15	ca.1	0 - 25	1 - 5	0.855 - 0.865
USA - Canada	40-65	20-35	ca.1	0 - 4	2 - 20	0.860 - 0.870
New Zealand	30-50	40-60				
India	20-40	5-20	1 - 5	45 - 70		0.850 - 0.865
Sulfate turpentine						
Finland	55-70	2-6	ca.1	7 - 30	ca. 4	0.860 – 0.870
Sweden	50-70	4-10	ca.1	15 - 40	1 – 3	0.860 – 0.870
USA	40-70	15-35	1 - 2	2 - 10	5 – 10	0.864 – 0.870
Russia	55-70	1-5	1 - 8	10 - 25	3 – 8	0.858 – 0.868
Wood turpentine						
USA	75-85	0-3	4 - 15		5 – 15	0.860 – 0.875

1.1.2.1 Composition

The main components of turpentines are mono- and bicyclic monoterpenes ($C_{10}H_{16}$; Mr = 136.2). They also contain smaller quantities of terpene – oxygen compounds (e.g., terpene alcohols), sesquiterpenes ($C_{15}H_{24}$), and other compounds (see Fig. 1.1) [4].

1.1.2.2 Transformations of the main components of turpentine

Typical reactions include isomerization, disproportionation, and polymerization catalyzed by acids, acid salts, surfactants, or Friedel – Crafts catalysts. Hydrates can be formed in the presence of water. Addition reactions take place with halogens, hydrogen halides, and nitrosyl chloride. Turpentine reacts with phosphorus pentasulfide and hydrogen sulfide to form complex sulfur compounds and thiols. Esterification of carboxylic acids gives esters, and acid condensation of alcohols gives ethers. Pyrolysis yields mixtures of acyclic and monocyclic terpenes, pyronenes, hydroterpenes, and *p*-cymene. Moist air leads to autoxidation of α-pinene to sobrerol (*trans*-p-menth-6-ene-2,8-diol) and resins [4].

One of the first syntheses of a new fragrance chemical from turpentine sources used formaldehyde with β-pinene in a Prins reaction to produce the alcohol, nopol (Chemical Abstract Service (CAS) Registry Number: [*128-50-7*]) (see Fig. 1.1). The corresponding acetate (nopyl acetate) can be made by direct esterification of nopol [*128-50-7*].

Hydrogenation of either α-pinene [*80-56-8*] or β-pinene [*127-91-3*] gives pinane [*473-55-2*] and pyrolysis of this produces citronellene. Treatment of α-pinene [*80-56-8*] with aqueous acid gives α-terpineol [*98-55-5*], whereas anhydrous acid gives camphene [*79-92-5*]. Pyrolysis of α-pinene [*80-56-8*] gives a mixture containing dipentene [*138-86-3*] and ocimenes [*673-84-7*]. Linalool [*78-70-6*] and geraniol [*106-24-1*] are produced from α-pinene [*80-56-8*]. Their process starts with hydrogenation of α-pinene [*80-56-8*] using a special catalyst that gives a high selectivity for cis-pinane. Autoxidation followed by catalytic hydrogenation of the intermediate hydroperoxide gives pinanol [*473-54-1*]. The pinanols are distilled, and then pyrolyzed to give linalool [*78-70-6*]. This pyrolysis is run at relatively low conversion in order to minimize the formation of plinols (alcohols formed by ene cyclization of linalool [*78-70-6*]). Before conversion to geraniol [*106-24-1*], the linalool [*78-70-6*] must be freed of impurities boiling close to the former. The isomerization is carried out over a vanadate catalyst, which process is improved by first converting the linalool to its borate ester. This gives a mixture of geraniol [*106-24-1*] and nerol in a purity of 99 % and with a geraniol/nerol ratio of 68/32 [5].

One of the first syntheses of a new fragrance chemical from turpentine sources used formaldehyde with β-pinene in a Prins reaction to produce the alcohol, nopol (Chemical Abstract Service (CAS) Registry Number: [*128-50-7*]). The corresponding acetate (nopyl acetate) can be made by direct esterification of nopol [*128-50-7*]. 3-Carene [*498-15-7*] is less widespread in nature than the pinenes. However, it is found in many turpentines and can be extracted from them by fractional distillation.

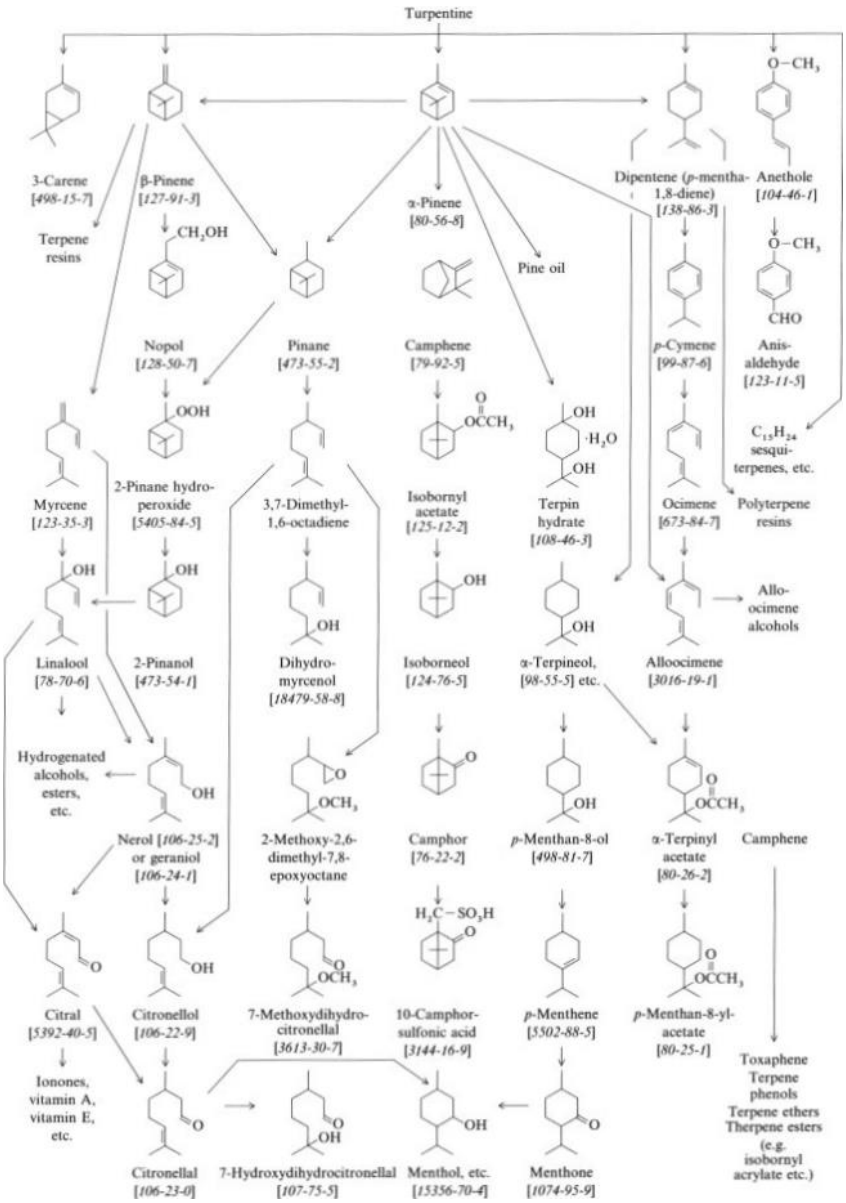

Figure 1.1 Turpentine constituents and downstream products with Chemical Abstract Service (CAS) Registry Number [4].

1.1.2.3 Turpentine properties

Turpentines are colorless to pale-yellow liquids with low viscosity and a characteristic odor. In gum turpentine this odor is pleasantly aromatic. The physical properties can vary within certain limits, depending on composition (see Table 1.3) [4]:

Table 1.3 Physical properties of turpentine [4]

Boiling range (101.3 kPa)	150 -177 °C
Solidification point	< -40 °C
ρ (20 °C)	0.855 -0.872 g/mL
$[\alpha]_D^{20}$	-40 to +48°
n_D^{20}	1.465 – 1.478
Relative evaporation rate (diethyl ether: 1)	ca. 170
Calorific value (CV)	ca. 40 000 kJ/kg

$[\alpha]_D^{20}$: specific rotation, n_D^{20}: index of refraction

Turpentines are miscible with most organic solvents, but immiscible with water. They are also good solvents for hydrocarbon resins, waxes, paints and coatings, fats, and oils. Approximately 0.06 wt % of water is absorbed at 20 °C [4]. The chemical properties of turpentine are determined by its main components, particularly the reactive pinenes.

1.1.2.4 Turpentine uses

The direct use of turpentine is now limited mainly to that as a solvent or dilution agent, e.g., for natural or modified binders (mainly alkyd resins), for oils, coatings, resins, paints (also artists' paints), and floor and shoe polishes. It accelerates, for example, the drying of coatings and paints by peroxide formation, in particular of those based on drying oils or other film-forming agents [4].

Higher-boiling turpentine fractions (containing large quantities of 3-carene) are suitable as pesticides for use in forestry. Although the importance of unfractionated turpentine as a solvent has decreased owing to the use of cheaper petrochemical products, turpentine has attracted increasing interest as a raw material for the chemical industry [4].

The following possible uses of turpentine and its downstream products are known [4]:
1) Flavors and fragances

2) Pharmaceuticals (e.g., camphor, menthol)

3) Disinfectants (e.g., terpineol, *p*-cymene)

4) Pesticides (e.g., toxaphene, 3-carene, terpene halides and thiocyanates)

5) Cleaning agents (e.g., dipentene, d- or l-limonene)

6) Solvents (e.g., turpentine and its individual components *p*-cymene, *p*-menthane, and pine oil)

7) Resins (e.g., β-pinene polymers)

8) Varnish resins (e.g., terpene phenols, isobornyl acrylate, and terpene – maleate resins)

9) Melt adhesives (e.g., terpene polymers, terpene phenols)

10) Polymerization accelerators for rubber (e.g., pinane or *p*-menthane hydroperoxide)

11) Antioxidants (e.g., isobornyl phenols)

12) Plasticizers (e.g., camphor, esters of pinic acid)

13) Lubricating oil additives (e.g., sulfur-containing terpenes)

14) Traction fluids (e.g., terpene ethers)

15) Textile auxiliaries (e.g., terpineol, pine oil)

16) Flotation aids (e.g., pine oil)

In case of overproduction sulfate turpentine may occasionally be used as a fuel (e.g., in Canada).

1.2 Esterification reactions

Esterification converts carboxylic acids into esters by nucleophilic substitution in presence of an acid as catalyst. The hydroxyl group (-OH) of the carboxylic acid is replaced by an alcoxy group (–OR_2) to form esters via a condensation reaction catalyzed by strong acids (Figure 1.2).

Figure 1.2 Esterification reaction.

Because the esterification is an equilibrium reaction (often with an unfavorable equilibrium constant), clever techniques are often required to achieve good yields of esters; for example, the use of a large excess of the alcohol or the acid. Adding a dehydrating agent removes water (one of the products), driving the reaction to the right. There is a more powerful way to form an ester, however, without having to deal with an unfavorable equilibrium. An alcohol reacts with an acid chloride in an exothermic reaction to give an ester (Figure 1.3) [6].

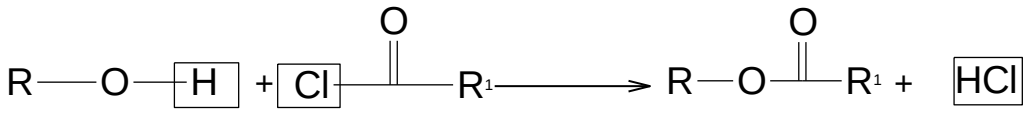

Figure 1.3 Esterification with an acid chloride [6].

The direct reaction between alcohol and carboxylic acid is conventionally conducted under acid or base catalysis conditions; without catalyst, the reaction must be carried out at high temperatures [6].

Esterification is conventionally carried by using a non-stoichiometric ratio of alcohol and carboxylic acid with homogeneous acid catalysts such as sulfuric acid, hydrochloric acid, *p*-toluenesulfonic acid, which leave traces of inorganic impurities, impart odor and color to the final product. In view of the stringent environmental and health concerns, the use of heterogeneous acid catalysts is now actively pursued since they offer better yields, selectivity, reusability and economy [7].

Esters are usually synthesized by the Fischer esterification of an acid with an alcohol (Figure 1.4a) or by the reaction of an acid choride (or anhydride) with an alcohol (Figure 1.4b, c). Methyl esters can be made by treating the acid with diazomethane (Figure 1.4b). The alcohol group in an ester can be changed by transesterification (Figure 1.4d), which can be catalyzed by either acid or base [6].

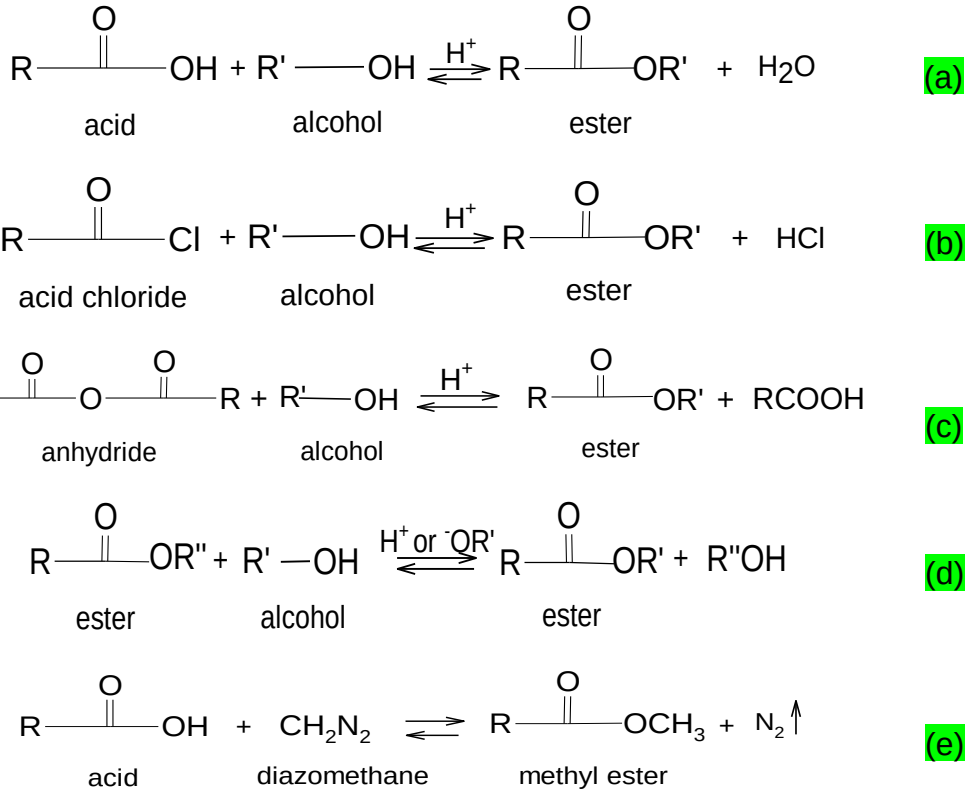

With R, R´, R´´: any group of atoms.

Figure 1.4 Synthesis of esters [6].

1.3 Applications of esters

Esters, which include a wide category of organic compounds ranging from aliphatic to aromatic, are generally used in the chemical industry such as drugs, plasticizers, food preservations, pharmaceuticals, solvents, perfumes, cosmetics, and chiral auxiliaries. In Table 1.4 common esters with their application and fragrance are presented.

Table 1.4 Application and fragrance of common esters [8]

Ester	Application	Fragrance
Benzyl acetate	In perfume formulation and as a solvent	Peach
Isomayl acetate	Flavor esters in the food industry	Banana
tert-Amyl acetate	In perfume formulation and as a solvent	Banana
Dodecyl acetate	Dodecyl acetate is the first repellent allomone	Characteristic odor
Octyl acetate	Flavorings	Orange, jasmine
Methyl acetate	Solvent in lacquers and paint removers and to make pharmaceuticals	Sweet

Ethyl acetate	Solvent in lacquers and paint removers and in pharmaceuticals	Fruity
Isobutyl acetate	Lacquers	Polish remover
Ethyl propionate	Solvent, flavoring agent and fragrance	Pear
Isobutyl propionate	Solvent or lacquer thinner, in perfumes and flavors	Rum
Isoamyl propionate	Flavorings	Pineapple, apricot
Benzyl propionate	An additive in tobacco products, alcoholic lotion, antiperspirant, deo-stick, detergent perborate, detergent TAED, fabric softener, shampoo and soap	Sweet, apple, banana, jam
Methyl acrylate	Ingredients in paints, coatings, textiles, adhesives and in polymer industry	Sharp fruity
Ethyl acrylate	Ingredients in paints, coatings, textiles, adhesives, and used in making acrylic resins	Sharp, ethereal rum
Isoamyl acrylate	Manufacturing polymers and as a feedstock for synthesis	Sharp fruity

1.4 Acetic acid

The most important commercial aliphatic acid is acetic acid. Vinegar is a 5 % aqueous solution of acetic acid used in cooking and in prepared foods such as pickles, ketchup, and salad dressings. Vinegar for food is produced by fermentation of sugars and starches. An intermediate in this fermentation is ethyl alcohol. When alcoholic beverages such as wine and cider are exposed to air, the alcohol oxidizes to acetic acid. This is the source of "wine vinegar" and "cider vinegar", Figure 1.5 [6].

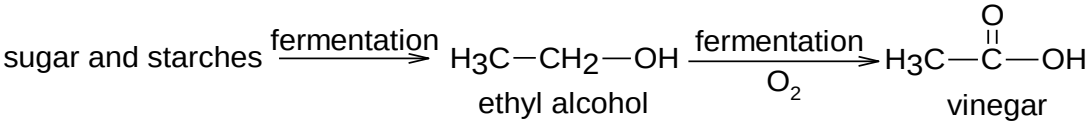

Figure 1.5 Synthesis of vinegar [6].

Acetic acid is also an industrial chemical. It serves as a solvent, a starting material for synthesis, and a catalyst for a wide variety of reactions. Some industrial acetic acid is produced from ethylene, using a catalytic oxidation to form acetaldehyde, followed by another catalytic oxidation to acetic acid, Figure 1.6 [6].

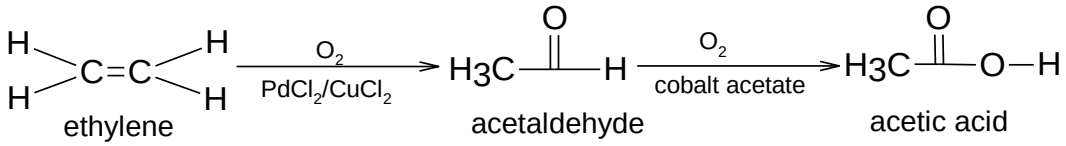

Figure 1.6 Synthesis of acetic acid from ethylene [6].

Methanol can also serve as the feedstock for an industrial synthesis of acetic acid. The rhodium-catalyzed reaction of methanol with carbon monoxide requires high pressures, so it is not suitable for a laboratory synthesis, Figure 1.7 [6].

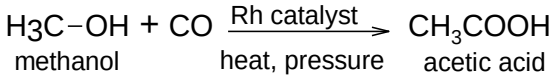

Figure 1.7 Synthesis of acetic acid from methanol [6].

1.5 Acetic anhydride

Acetic anhydride is the most important carboxylic acid anhydride. It is produced at the rate of about 4 billion pounds per year, primarily for synthesis of plastics, fibers, and drugs. Acetic anhydride consists of two molecules of acetic acid, minus a molecule of water. The most common industrial synthesis begins by dehydrating acetic acid to give ketene, Figure 1.8. At a sufficiently high temperature (750 °C), the equilibrium favors the products. Triethyl phosphate is added as a catalyst to improve the rate of the reaction [6].

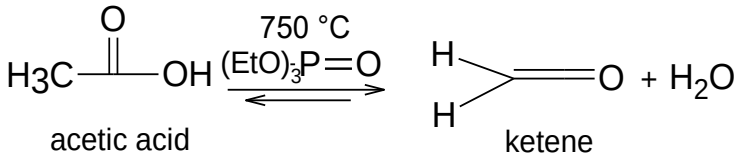

Figure 1.8 Synthesis of ketene from acetic acid [12].

Ketene (a gas at room temperature) is fed directly into acetic acid, where it reacts quickly and quantitatively to give acetic anhydride, Figure 1.9. This inexpensive large-scale manufacture makes acetic anhydride a convenient and inexpensive acylating reagent [6].

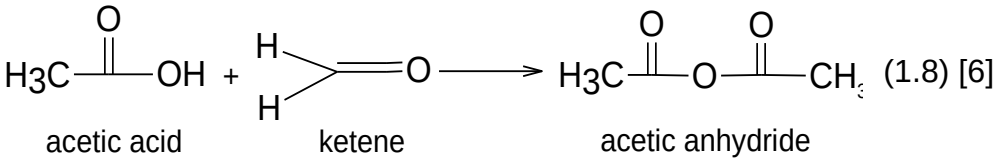

Figure 1.9 Synthesis of acetic anhydride from ketene [12].

1.6 Acid catalysts for esterification reactions

Esterification reactions can be carried out without a catalyst, although the reaction is extremely slow. Consequently, esterification is enhanced by an acid catalyst, which acts as a proton donor to the acid. Both homogeneous and heterogeneous catalysts are used in esterification reactions. Typical homogeneous catalysts are mineral acids, such as H_2SO_4, HCl, HF, $ClSO_2OH$ [8].

Acid sites are commonly regarded as the active centers on certain oxides to catalyze many reactions involving hydrocarbons (e.g. catalytic cracking, isomerization, alkylation, cationic polymerization and reforming). The acid sites on oxide surfaces are of two types as described by Lewis and Brønsted. A proton transfer occurs at the Brønsted site from the solid to the adsorbed molecule as an ion is emerged and an ion dipole interaction with the solid takes place, while Lewis acid sites accept electrons from the adsorbed molecule and a coordinate bond with the surface is formed [9].

When the substrate in the reaction is acid - resistant, it is usually carried out in the presence of a Brønsted acid such as HCl, HBr, H_2SO_4, $NaHSO_4$, $ClSO_3H$, NH_2SO_3H, H_3PO_4, HBF_4, AcOH camphorsulfonic acid [10]. Despite rather harsh conditions, the Brønsted acid - catalyzed reaction sometimes exhibits good selectivities.

Lewis acids in general, are milder than Brønsted acids and, more importantly, template effects are to be expected as they are sterically bulkier than a proton. Table 1.5 shows Lewis acids are classification according to elements [10].

Table 1.5 Classification of Lewis acids [10]

Element	Compounds
B	$BF_3{\cdot}OEt_2$; BCl_3; 3,4,5-$F_3C_6H_2B(OH)_2$
Al	$AlCl_3$ (immobilized); Al/NaI/CH_3CN; $AlCl_3$ /$ZnCl_2$
Zn	ZnO; $ZnCl_2$; Zn(OTf); $Zn(ClO_4)_2{\cdot}6H_2O$
In	$InCl_3$

Sn	$SnCl_2$; Bu_2SnO $(XR_2SnOSnR_2Y)_2$; $(XRf_2SnOSnRf_2X)_2$; Ph_2SnCl_2
Ti	$TiO(acac)_2$
Mn	$Mn(OAc)_3 \cdot 2H_2O$
Fe	$Fe(ClO_4)3$; $Fe_2(SO_4)_3 \cdot H_2O$; $Fe_2(SO_4)_3 \cdot nH_2O/H_2SO_4$;$FeCl_3$
Ni	$NiCl_2 \cdot 6H_2O$
Mo	$MoO(acac)_2$
Sc	$Sc(OTf)_3$
Zr; Hf	$ZrCl_4 \cdot 2THF$ and $HfCl_4 \cdot 2THF$; $ZrOCl_2 \cdot 8H_2O$ and $HfOCl_2 \cdot 8H_2O$; $Zr(O^iPr)_4$ or $Hf(O^iPr)_4$/ / $Fe(O^iPr)_3$
I	I_2

$BF_3 \cdot OEt_2$ is the oldest Lewis acid employed as an esterification catalyst, since the BF_3/CH_3OH complex had been known to be used for conversion of simple carboxylic acids to their methyl esters prior to GLC (gas-liquid chromatography) analysis. $AlCl_3$ is one of the most popular Lewis acids, but it is not employed in esterification because of its too strong acidity [10].

Khire *et al.* tested different grades of acid catalysts for esterification of ethanol with acetic acid at 80-85 °C and 2.5 h. *p*-TSA gives maximum conversion of ethanol to ethyl acetate (67 %). Among the solid acid catalysts, Amberlyst-15, SZ/silica-H and SZ-H catalysts showed respectively ethyl acetate selectivity of 66 %, 65 % and 64 % which was higher than selectivities obtained with HZSM-5 (15 %) and *γ*-alumina (5 %) catalysts [11].

Generally, esterification of alcohol with acetic acid is known to be catalyzed by the protons associated with $–SO_3H$ group of *p*-TSA and Amberlyst-15 and SO_4^{2-} groups of sulfated catalysts (SZ/silica-H, and SZ-H). The better perfomance of *p*-TSA for esterification is due to its liquid form in the reactant mixture, and hence the dispersion and accessibility of protons of $–SO_3H$ groups to the reactant molecules are expected to be higher as compared to that of solid catalysts. Among the three solid acid catalysts (Amberlyst-15, SZ/silica-H and SZ-H), the SZ/silica –H shows superior performance which is attributed not only to better dispersion of sulfated zirconia on porous silica support but also to the higher surface area and larger size pores that could enable easy accessibility of reactant

molecules to the active sites. In case of unsupported sulfated zirconia SZ-H catalyst and Amberlyst-15, the higher concentration of active sites (SO_4^{2-} and $–SO_3H$) and comparatively lower surface area result into inferior dispersion of active sites [11].

Liu *et al.* studied the acetic acid esterification with methanol using a commercial Nafion/silica nanocomposite catalyst (SAC-13) and H_2SO_4. The resin/silica composite is strongly acidic, with highly accessible sites and sufficient robustness to withstand reasonably high temperatures (~200 °C) and attrition stress. When only protons are available as active acid sites similar to H_2SO_4, one might expect SAC-13 to exhibit catalytic behavior resembling that of the homogeneous catalyst. Thus, the similarity between these two catalysts provides a good way to examine the effect of the heterogeneous catalyst surface on catalyst activity [12].

Comparing the reactivity of acetic acid esterification at 60 °C catalyzed by sulfuric acid and Nafion/silica nanocomposite catalyst SAC-13, the homogeneous acid catalyst was more active than the heterogeneous catalyst. Using a very small amount of H_2SO_4 (0.011 g/45 mL), acetic acid conversion reached 82 % after 11 h at 60 °C with 2 times stoichiometric methanol. On the other hand, a hundredfold greater amount of SAC-13 (1.09 g/45 mL) was required to yield a similar reaction profile with 75 % transformation of acetic acid after 11 h. The better catalytic activity of H_2SO_4 can be attributed to its greater density of acid sites per gram (1 mol H^+ /1 mol H_2SO_4) [12].

1.6.1 Solid acids

Various solid acids are utilized for esterification, although the substrates that can be employed suffer from considerable limitations due to the strong acidity. Nevertheless, solid acids have a great advantage because they can be removed from the reaction mixture by filtration and thus applied to large-scale production [10].

1.6.1.1 Nafion

Nafion is one of the most versatile acid catalysts that contain terminal sulfonic acid groups attached to a perfluoroalkyl polymeric backbone. The presence of electron-withdrawing

fluorine atoms in the structure significantly increases the acid strength of the terminal sulfonic acid groups, which is quite comparable to that of pure sulfuric acid [13].

Nafion - H is the oldest solid acid utilized as an esterification catalyst. When a mixture of carboxylic acid and alcohol is allowed to flow over this catalyst at 95 – 125 ° C, high yields of the corresponding esters are obtained with a contact time of ~ 5 s [10].

1.6.1.2 Amberlyst-15

Ion-exchange-resin catalysts have been used for years in esterification processes and are the most commonly used solid catalysts. They have been proved to be effective in liquid phase esterification. Typical resin catalysts are sulfonic acids fixed to polymer carriers, such as polystyrene cross-linked with divinylbenzene (DVB). Solid ion-exchange resins as catalysts have several advantages: the catalyst can be removed from the reaction product; continuous operation in column reactors is enabled; the product purity is high, since side reactions can be suppressed or completely eliminated; reaction intermediates can be isolated; and, furthermore, ion-exchange resins can discriminate between small and large molecules [14].

α-Hydroxy esters and α-amino acids are successfully converted into the corresponding esters over Amberlyst-15, while catechol undergoes esterification with acrylic acid to afford 7-hydroxy coumarin. A detailed kinetic study on esterification of acetic acid with 1-butanol with Amberlyst-15 has appeared more recently [10].

1.6.1.3 Zeolites

It is possible to say that zeolites are the most widely used catalysts in industry. They are crystalline microporous materials which have become extremely successful as catalysts for oil refining, petrochemistry, and organic synthesis in the production of fine and speciality chemicals, particularly when dealing with molecules having kinetic diameters below 10 Å. The reason for their success in catalysis is related to the following specific features of these materials: (1) they have very high surface area and adsorption capacity; (2) the adsorption properties of the zeolites can be controlled, and they can be varied

from hydrophobic to hydrophilic type materials; (3) active sites, such as acid sites for instance, can be generated in the framework and their strength and concentration can be tailored for a particular application; (4) the sizes of their channels and cavities are in the range typical for many molecules of interest (5-12 Å), and the strong electric fields existing in those micropores together with an electronic confinement of the guest molecules are responsible for a preactivation of the reactants; (5) their intricate channel structure allows the zeolites to present different types of shape selectivity, i.e., product, reactant, and transition state, which can be used to direct a given catalytic reaction toward the desired product avoiding undesired side reactions; (6) all of these properties of zeolites, which are of paramount importance in catalysis and make them attractive choices for the types of processes listed above, are ultimately dependent on the thermal and hydrothermal stability of these materials. In the case of zeolites, they can be activated to produce very stable materials not just resistant to heat and steam but also to chemical attacks [15].

The rare earth-exchanged (RE) H-Y zeolite is the best of the various zeolite catalysts. Heating of alcohol solutions of carboxylic acids in the presence of the freshly activated zeolite at 150 °C provides good to excellent yields of esters. Reactions between acetic acid and C_2–C_4 alcohols with Hβ, HY and ZSM-5 zeolites are the subject of extensive studies [10].

Several zeolites such as modified H-Y, H-Beta and H-ZSM-5, have been employed as esterification catalysts. In order to expel the water formed, hydrophobicity of the zeolite lattice is expected to be an important parameter. Which zeolite is eventually most suitable for a specific reaction depends on the polarity and miscibility of the acid and alcohol reactants [16].

1.6.1.4 Mesoporous silica

Porous solids are everywhere due to their many advantages such as a large surface area, an enhanced accessibility and the ability to anchor different chemical functionalities on their surface. The use of molecular and supramolecular templates, especially surfactants, has been one of the most successful strategies for the production of materials with a

controlled porosity. Since the discovery of MCM-41, a myriad of surfactant-templated solids has populated the research efforts of many groups, dealing with their synthesis, characterization and application. Some of the main advantages of this methodology are: their versatility, robustness, simplicity and ability to produce very complex and interconnected porous structures. Sol–gel chemistry techniques are typically used in combination with different surfactants to produce a wide variety of porous metal oxides. Both soft templates, such as surfactant and polymers and hard templates such as carbon and metaloxides and carbonates which can be burned-off or easily dissolved at a certain pH, have been extensively used to introduce controlled mesoporosity in a wide variety of solids. The combination of these strategies has yielded new hierarchical materials, whose unique porous structures provide significant advantages [17] such as a hexagonal arrangement of uniformly sized unidimensional mesopores. Another exciting property is the possibility of controlling the internal diameter of the mesopores between 2 and 10 nm by varying the chain length of the micellar surfactant template. Moreover, their high thermal and hydrothermal stability, uniform size and shape of the pores, and large surface areas make them of interest as catalysts [18].

Al-MCM-41 molecular sieves effect reactions between various acids and alcohols in the vapor phase: acetic acid/amyl alcohol; acetic acid/butyl alcohols; terephthalic acid/methanol; butyric acid/1 - pentanol. Microporous titanosilicate ETS - 10 molecular sieves are also effective for esterification of long – chain carboxylic acids with alcohols. Sulfonic acid - functionalized mesoporous silicas are utilized for esterification of fatty acids with methanol and glycerol. Hydrophobic sulfonic acid -functionalized mesoporous benzene/silica is more active than Nafion-H for esterification of acetic acid with ethanol. A similar hydrophobic SO_3H - modified catalyst is accessible from mesoporous ethylene/silica. Mesoporous MCM-41 and SBA-15 functionalized with perfluoro-alkane sulfonic acid are more active for esterification of long - chain fatty acids with alcohols than Nafion/silica composite [10].

It is noteworthy that MCM-41 and SBA-15 mesoporous materials with metallic species have been widely used as catalysts. Particularly, Selvaraj & Choe reported that Cr, Mn,

Sn, Ga, Al and Nb, have been successfully incorporated into SBA-15 by direct hydrothermal method with adjustable pH. Characterization results of those materials have shown that they have greater hydrothermal stability than the corresponding supported MCM-41 catalysts with these species [19].

1.6.1.5 Heteropolyacids

Catalysis by heteropoly acids (HPAs) and related compounds is a field of increasing importance, several features making them economically and environmentally attractive. They are very strong acids, approaching the superacid region, and they are efficient oxidants exhibiting fast reversible multielectron redox transformations under rather mild conditions. Their acid-base and redox properties can be varied over a wide range by changing the chemical composition. Solid HPA possess an ionic structure comprising fairly mobile basic structural units – heteropolyanions and countercations (H^+, H_3O+, $H_5O_2^+$, etc.) – unlike the network structure of e.g. zeolites and metal oxides. This unique structure manifests itself by extremely high proton mobility and a 'pseudoliquid phase' manifested by the ability of heteroployanions to stabilize cationic organic intermediates. Above all, HPAs are very soluble in polar solvents and fairly thermally stable in the solid state. These properties render them potentially promising acid, redox, and bifunctional catalysts in homogeneous as well as in heterogeneous systems. In the 80s and 90s, the broad utility of HPAs was demonstrated by a wide variety of synthetically useful selective transformations of organic substrates. Several new industrial processes based on HPA catalysis, such as oxidation of methacrolein, hydration of olefins and polymerization of tetrahydrofuran have been developed and commercialized [16].

Various bromoacetates are obtained by treatment of bromoacetic acids (1.0 mol) with alcohols (1.1 mol) in the presence of 12 - tungstophosphoric acid, $H_3PO_{40}W_{12}\cdot H_2O$. Its partially substituted Cs and K salts are also useful catalysts for esterification. The corresponding ammonium salt catalyzes selective reactions between aliphatic carboxylic acids and alcohols in the presence of aromatic carboxylic acids. $H_{14}[NaP_5W_{30}O_{110}]$ can be employed for esterification of salicylic acid with aliphatic and benzylic alcohols. Cobalt-

containing polyoxometalate, $K_5CoW_{12}O_{40}\cdot 3H_2O$, is suitable for esterification of mandelic acid [10].

1.7 Nopyl acetate and its uses

Nopyl acetate, also known as lignyl acetate; 6,6-dimethylbicyclo- (3,1,1) -2-heptene-2-ethyl acetate (Figure 1.10), is an artificial fragrance compound with a fruity odor of fresh wood that is not present in nature [20]. Its formula and molecular weight are $C_{13}H_{20}O_2$ and 208.30 g/mol, respectively. It has a boiling point of 253 °C at 1.5 kPa and a density of 0.9811 g/mL at 20 °C [21]. Nopyl acetate is prepared by the carbonyl-ene reaction of β-pinene (1) and paraformaldehyde (2) with subsequent acetylation of the intermediary nopol (3) with acetic anhydride (Figure 1.10) [20].

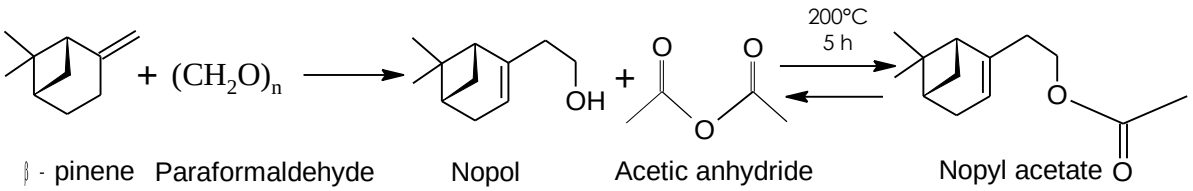

Figure 1.10 Nopyl acetate synthesis from β – pinene.

Nopyl acetate has been use since the 1950s. It is used in the preparation of soaps, detergents, creams, lotions, perfumes, cosmetics, shampoos, household and food products such as bakery, soft and alcoholic beverages, ice creams and candies. In 1979 its use in fragrances in the United States amounted to 200 000 lb/year. Table 1.6 shows the final concentration of nopyl acetate present in some products [22].

Table 1.6 Nopyl acetate final concentration in various products [22]

	Soap	Detergent	Creams, lotions	Perfume
Usual (%)	0.03	0.003	0.015	0.3
Maximum (%)	0.25	0.025	0.1	1

1.8 Nopyl acetate synthesis

Due to its high commercial demmand, nopyl acetate constitutes the main application of nopol [23]. Although it can be obtained directly from the Prins reaction of β-pinene and paraformaldehyde in acetic acid solution [24], with yields between 50 and 85 %, the by-products (1,3,5 – cycloheptatriene, bicyclo[3.1.1]heptan-2-one, 6,6-dimethyl-, (1R), spiro (4,4) none – 1,3 – diene, 1,2 –dimethyl) decreases yields towards the acetate, and consequently, it is more convenient to effect the esterification of nopol with acetic anhydride or acetic acid with continuous removal of water [16].

The synthesis of nopyl acetate has been reported using several systems. The thermal reaction at 200 °C of β-pinene with paraformaldehyde was carried out in the presence of acetic anhydride in which nopyl acetate is produced with 60 % yield after 5 h [25]. In the case of the esterification of nopol and carboxylic acid chlorides in solution of triethanol amine and dichloromethane, a nopyl acetate yield of 79 % (5 - 25 °C) was reached [26].

Nopyl acetate can be synthesized from acetic anhydride and sodium acetate, with yields of 84 % (3 h, 90 °C) after separation and purification [27][28][29]. It is possible to obtain yields up to 98 % (150 °C, 1 h) by the reaction of nopol with acetic anhydride in the presence of toluene or chlorobenzene, eliminating the by-product carboxylic acid by azeotropic distillation [30].

Nopyl acetate has been synthesized with acetic anhydride in the presence of triethylamine and dimethylaminopyridine (DMAP) with dichloromethane as solvent at room temperature, with quantitative yields [31]. Using a cerium and ammonium nitrate catalyst, $(NH_4)Ce(NO_3)_6$ in CH_2Cl_2 as solvent at 40–50 ºC, nopyl acetate is obtained from nopol and acetic anhydride with a 92 % yield [32].

Performing the esterification at room temperature over $Cs_{2.5}H_{0.5}PW_{12}O_{40}$ catalyst in acetic acid solution, in the presence of acetic anhydride with over-stoichiometric amounts respect to nopol, ensures 100 % selectivity to nopyl acetate and complete nopol conversion at 1.5 h [33].

Nopyl acetate has been synthesized from nopol and acetic acid under microwave irradiation (105 °C, 85 min) over solid superacid (SO_4^{2-}/ZrO_2-TiO_2) dosage 2.5 % achieving 81.3 % yield [34]. Nopyl acetate can also be synthesized by the reaction of nopol with acetic anhydride under heating with a 98 % yield [35].

1.9 β- Pinene

β-Pinene is a colorless liquid with a woody-green pine-like smell; it is soluble in alcohol, but not water and occurs naturally in rosemary, parsley, dill, basil and rose. There are two structural isomers found in nature: α-pinene and β-pinene. As the name suggests, both forms are important constituents of pine resin; they are also found in the resins of many other conifers, and more widely in other plants. Both are also used by many insects in their chemical communication system. Selective oxidation of pinene with some catalysts gives many components for pharmacy, artificial odorants and so on. The primary oxidation product is verbenone [36].

Figure 1.11 shows some of the major routes to terpenoids starting from β-pinene (**4**).

Nopol (**12**) is synthesized by the Prins condensation reaction of β-pinene with formaldehyde. Its acetate (nopyl acetate) (**13**) is used as a fragrance ingredient [37].

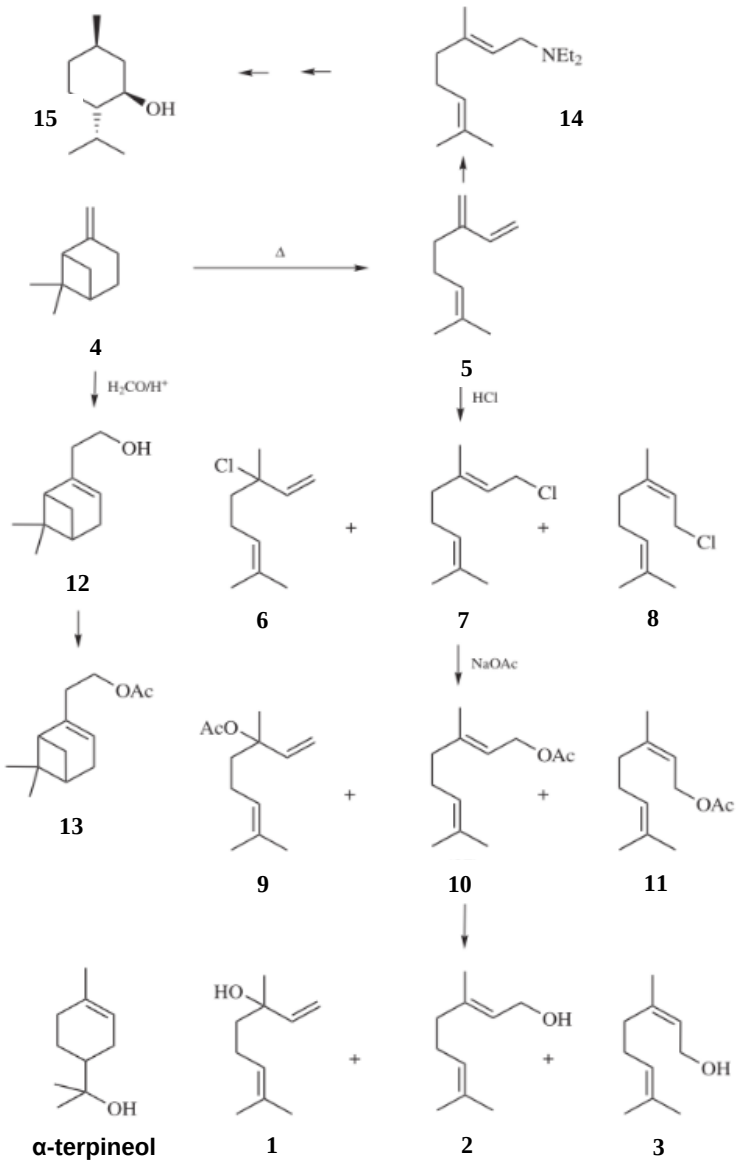

Figure 1.11 Major products from β-pinene involving reactions of pyrolysis, hydrochlorination, isomerization, hydrolysis, condensation, addition [37].

1.10 Nopol and its uses

Nopol, 6,6-dimethylbicyclo[3.1.1]hept-2-ene-2-ethanol, is an unsaturated primary bicyclic alcohol that acts as a perfume or flavoring agent (Figure 1.12). Nopol is found up to 15 % in the japanese cedar species *Anthemis werneri* grown in Greece, 32 % in the species *Curcuma solensis* of the family *Zingiberaceae* and up to 22 % in turmeric (curcuma)

volatile oil. It exhibits contents of less than 2 % in the japanese cedar species *Cryptomeria japonica*, (2005) the species of Norwegian cedar *Chamaecyparis lawsoniana*, turpentine of Turkey, carrots and blackberries [38].

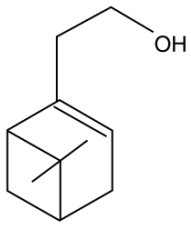

Figure 1.12 Nopol molecule

There are patents that describe nopol formulations in fragrances, besides being reported of having potential antibacterial activity. Nopol and other oxygenated monoterpenoids found in *Criptomeria japonica* cedar oil are active ingredients in preservative formulations of ophthalmic components, given their lower toxicity than other compounds used in such formulations such as benzalkonium chloride or n-alkyl methyl benzyl ammonium chloride. This alcohol has been useful in the inhibition of sulfur autoxidation, significantly altering the kinetics of acid rain formation in the clouds [38].

Nopol and other terpene alcohols such as terpineol (a mixture of α- and γ-terpineol) act as biodegradable solvents in the formulation of printing inks. Its application in biodegradable formulations of reactive paints is emphasized, avoiding the use of compounds harmful to the environment such as methylene chloride, phenol, methanol, toluene, acetone and caustic or corrosive compounds [38].

It has been found that nopol immobilized in the pores of a polyethylene membrane is effective for the enantioselective transport of amino acid hydrochlorides. Nopol casting with sodium hydroxide and its sulfonated or phosphorous derivatives has been successfully applied in lubricating grease formulations. Nopol and other terpene alcohols are valuable in formulations of pesticides and leaf fertilizers as they increase the adhesion of the active ingredients in the leaves. Finally, nopol, dinopyl ether, and other terpene derivatives are by-products of the essential tobacco oil, used in formulations of bioinsecticides [38].

Table 1.7 Nopol physical and chemical properties [39]

Formula	$C_{11}H_{18}O$
Molecular weight	166.26 g/mol
Purity	98 %
Optical activity	[α]24/D −37°, neat
Refractive index	n20/D1.493(lit.)
Boiling point	230-240 °C (lit.)
Flash point	98°(208°F)
Density	0.973g/mL at 25 °C (lit.)

Although nopol is present in nature, it is mainly obtained through synthetic processes, Figure 1.13. In the 1940s, Bain made the first report on the synthesis of nopol by homogeneous catalysis or thermal synthesis. In 2002, the Environmental Catalysis Research Group of Universidad de Antioquia reported the use of heterogeneous catalytic processes to obtain nopol. Synthetic methods for the synthesis of nopol are the saponification of nopyl acetate and the Prins condensation between β-pinene and formaldehyde from an anhydrous source (paraformaldehyde) with Lewis acids in homogeneous phase, by autoclaving at high temperature (150- 230 °C) or by heterogeneous catalytic processes (Figure 1.13) [24].

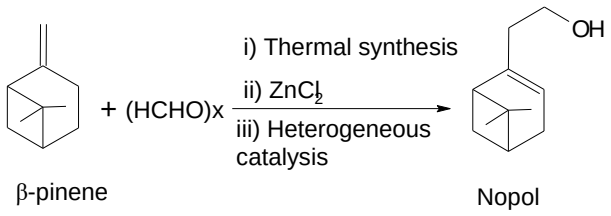

Figure 1.13 Nopol synthesis reaction.

Nopol synthesis was studied also by the author of this doctoral thesis in his Master in Chemical Sciences “Síntesis de nopol empleado los catalizadores Sn-SBA-15 y Sn-MCM-41” [38].

For the synthesis of nopol, several active heterogeneous catalytic systems have been proposed, such as the mesoporous Sn-MCM-41 material. As MCM-41 presents low hydrothermal and thermal stability, because its thin pore walls and large number of silanol

groups, the mesoporous molecular sieve SBA-15 that has uniform hexagonal channels, presents microporosity and has a greater hydrothermal and thermal stability was also tested for nopol production. In the Master research, the solvent effect on the activity of Sn-MCM-41 and Sn-SBA-15 catalysts synthesized by impregnation was studied; the solvents evaluated were toluene, hexane, acetonitrile, ethyl acetate, ethanol, methanol and tert-butanol [38].

Materials obtained by incipient wetness impregnation with $SnCl_2.2H_2O$ as a source of tin, have the advantage of being synthesized at moderate conditions, once the adequate mesoporous support is available. The materials were characterized by X-ray diffraction, BET surface area, programmed temperature desorption (TPD), ultraviolet, infrared and Raman spectroscopy, scanning electron microscopy, and thermogravimetry. The particle size and the speed of agitation were established to guarantee the absence of diffusional effects during the reaction. The solvent effect on the production of nopol was evaluated according to the results of catalytic activity (expressed in TOF) obtained with Sn-SBA-15 and Sn-MCM-41 in the presence of each solvent. Calorimetric analyzes were performed on the catalysts synthesized in contact with the solvents and each solvent individually. Leaching tests were performed on Sn-MCM-41 and Sn-SBA-15 catalysts.

The characterization of the materials allowed to verify that the synthesized catalysts have ordered hexagonal mesostructures. The BET area of SBA-15 and Sn-SBA-15 was around 744 m^2/g; while the surface area of the MCM-41 decreased from 1417 to 725 m^2 /g with tin incorporation. The XRD patterns of Sn-SBA-15 and Sn-MCM-41 were very similar to that of the supports. The TPD analyzes allowed to establish the presence of moderate and weak acid sites in both materials. Thermogravimetric analysis revealed that Sn-SBA-15 has a lower affinity for water than Sn-MCM-41. The SEM micrographs indicated that SBA-15 and Sn-SBA-15 showed the characteristic morphology of SBA-15, represented in domains in the form of loops that are added to a microstructure similar to wheat. The N_2 adsorption-desorption isotherms of the materials were type IV, which is typical of mesoporous materials.

An average particle size of 42 *μ*m and a minimum agitation speed of 1400 rpm ensured the absence of diffusional effects. There was no production of nopol in the presence of polar solvents such as methanol and tert-butanol. Sn-SBA-15 was more active for the transformation of β-pinene and production of nopol than Sn-MCM-41 in non-polar solvents such as hexane and toluene; no significant differences were found in the activity of these materials in the presence of other tested solvents. According to Table 1.8, the order of activity observed for the production of nopol over Sn-MCM-41 and Sn-SBA-15 was: toluene> hexane> acetonitrile> ethyl acetate> ethanol = tert-butanol and for consumption of β -pinene was: hexane = toluene> acetonitrile = ethyl acetate> ethanol = tert-butanol.

Table 1.8 TOF values for nopol production and β-pinene consumption

Material	Solvent	TOF (h^{-1})	
		β-pinene*	nopol**
Sn-MCM-41	Acetonitrile	2467	1084
	Ethyl acetate	2447	135
	Ethanol	1346	0
	Hexane	3261	1318
	Tert-butanol	1720	0
	Toluene	3130	2402
Sn-SBA-15	Acetonitrile	2134	894
	Ethyl acetate	2498	89
	Ethanol	1343	0
	Hexane	4375	1252
	Tert-butanol	1850	0
	Toluene	4256	3286

*mole of β-pinene transformed per mole of Sn per hour. **mole of nopol produced per mole of Sn per hour.

Sn-SBA-15 presented better performance for the production of nopol than Sn-MCM-41, in apolar solvents such as toluene. The presence of weak and moderate acid sites, with higher tin content and surface area, accompanied by a low affinity for water, confer superior characteristics to Sn-SBA-15.

Calorimetric analysis revealed that toluene with Sn-MCM-41 and Sn-SBA-15 forms a solvent-catalyst system with the highest temperature values for the endothermic peaks obtained in the calorimetric profile, making these systems more stable to the thermal

effects that occur in a chemical reaction. The leaching tests and three reuses of the materials Sn-MCM-41 and Sn-SBA-15, indicated that the production of nopol is due to the supported catalyst and not to metal species in solution.

Then, the results of the research carried out in the Master of the author of this thesis, suggest that Sn-MCM-41 and Sn-SBA-15 could be good catalysts for the next transformation of nopol to nopyl acetate and a possible one step transformation of β-pinene into nopyl acetate.

1.11 Domestic trade of essential oils

In our domestic context, turpentine exports do not exceed the ton per year. Between 2010 and 2012 turpentine exports increased considerably from 698.59 to 919.78 kg, nevertheless from 2013 to 2016 turpentine exports decreased (860.89 - 242.81 kg) Figure 1.14.

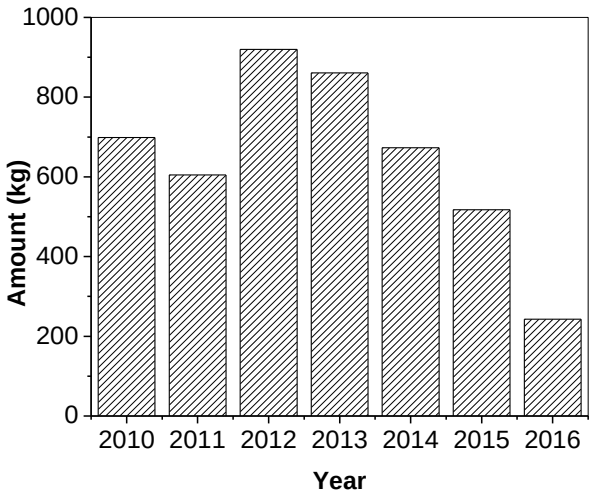

Figure 1.14 Colombian annual turpentine exports [40].

In Figure 1.15 statistics of alcoholic terpene exports between 2010 and 2016 are shown. The foreign requirement of acyclic alcoholic terpenes increased significantly in 2012 with respect to other years. After this year exports reached only between 3 and 2215.5 kg of alcoholic acyclic terpenes. Annual pine oil demand increased from 2010 (4834 kg) to 2011

(8930 kg), decreasing considerably in 2012 (2070 kg) and 2013 (3568.25 kg). In 2014 there was a dramatic decrease in both alcoholic acyclic terpenes (1605 kg) and pine oil (100 kg). This trend continued in 2015 and 2016.

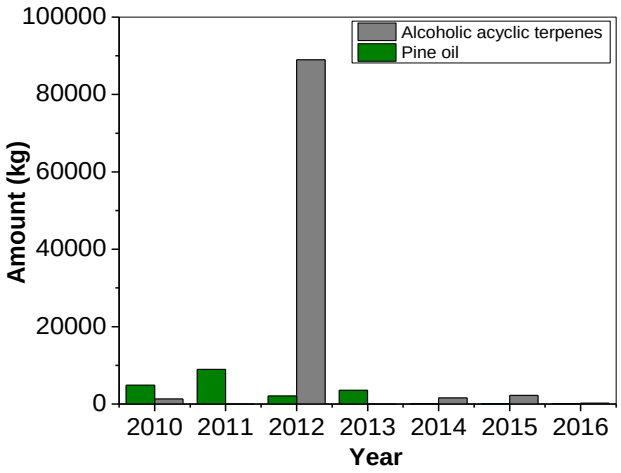

Figure 1.15 Colombian annual exports of alcoholic acyclic terpenes and pine oil (α-terpineol as main component) [40].

1.12 Global trade of essential oils

The rapid development of the fragrance and flavor industry in the nineteenth century was generally based on essential oils and related natural products. In 1876, however, Haarmann and Reimer started the first production of synthetic aroma chemicals (vanillin and then coumarin, anisaldehyde, heliotropin, and terpineol). Although aroma chemicals made a revolution in fragrances with top discoveries in the twentieth century, for many decades both flavors and fragrances were manufactured with constituents of natural origin, the majority of which were essential oils [3].

The range of applications for essential oils in different sectors and branches of industry is wide. Essential oils are used in large quantities in the production of foods, pharmaceuticals, flavors, cleaning agents, personal care products and cosmetics [1]. More oils are used in flavors than in fragrances, which today are mainly based on aroma chemicals, especially in large-volume compounds used in detergents and household products [3].

The largest world consumer of essential oils is the flavor industry, especially for soft drinks. However, this is limited to a few essential oils, mainly citrus (orange, lemon, grapefruit, mandarin, lime), ginger, cinnamon, clove, and peppermint. Similar oils are used in confectionery, bakery, desserts, and dairy products, although the range of oils may be wider and include some fruity products and spices. The spicy oils are widely used in numerous salted chips, which are commonly consumed along with beverages and long drinks. Also, the alcoholic beverage industry is a substantial user of essential oils, for example, anis in numerous specialties of the Mediterranean region, herbal oils in liqueurs, ginger in ginger beer, and peppermint in mint liquor and in many other flavored alcohols (Table 1.9) [3].

Next in importance to beverages in the food sector is the sweet, dairy, confectionery, dessert (fresh and powdered), sweet bakery, and cream manufacturing sector (Table 1.10), for which the main oils used are citrus, cinnamon, clove, ginger, and anis [3].

The fast-food and processed food industries are also substantial users of essential oils, although the main demand is for spicy and herbal flavors. The main oils used are coriander (especially popular in the United States), pepper, pimento, laurel, cardamom, ginger, basil, oregano, dill, and fennel, which are added to the spices with the aim of strengthening and standardizing the flavor [3].

Table 1.9 Main applications of essential oils [3]

Oil name	Main applications
Orange	Soft drinks, sweets, fragrances
Cornmint (*Menta arvensis*)	Oral care, chewing gum, confectionery, fragrances, menthol crystals
Peppermint	Oral care, chewing gum, confectionery, liquors, tobacco, fragrances
Eucalyptus (*Eucalyptus globulus*)	Oral care, chewing gum, confectionary, pharmaceuticals, fragrances
Lemon	Soft drinks, sweets, diary fragrances household chemicals
Citronella	Perfumery, toiletries, household chemicals
Eucalyptus (*Eucalyptus citriodora*)	Confectionery, oral care, chewing gum, pharmaceuticals, fragrances

Clove leaf	Condiments, sweets, pharmaceuticals, tobacco, chewing gum, confectionery
Spearmint (*Mentha spicata*)	Oral care, toileries, household chemicals
Cedarwood (*Virginia*)	Perfumery, toiletries, household chemicals
Lime	Soft drinks, sweets, diary, fragrances
Lavandin	Perfumery, cosmetics, toiletries
Litsea cubeba	Citral for soft drinks, fragrances
Cedarwood (from China)	Perfumery, toiletries, household chemicals
Camphor	Pharmaceuticals
Coriander	Condiments, pickles, processed food, fragrances
Grapefruit	Soft drinks, fragrances
Star anise	Liquors, sweets, bakery, household chemicals
Patchouli	Perfumery, cosmetics, toiletries
Basil	Condiments, processed food, perfumery, toiletries
Mandarin	Soft drinks , sweets, liquors, perfumery, toiletries

Table 1.10 Average content of flavors in food products and of essential oils in flavors [3]

Position	Product	Average dosage of fragrance compound in product (%)	Average content of essential oils in fragrance (%)
1	Alcoholic beverages	0.05 – 0.15	3 – 100
2	Soft drinks	0.10 – 0.15	2 – 5
3	Sweets	0.15 – 0.25	1 - 100
4	Bakery (cakes, biscuits, etc)	0.10 – 0.25	1 - 50
5	Ice creams	0.10 – 0.30	2 - 100
6	Dairy products, desserts	0.05 – 0.25	1 - 50
7	Meat and fish products (also canned)	0.10 – 0.25	10 - 20
8	Sauces, ketchup, condiments	0.10 – 0.50	2 - 10
9	Food concentrates	0.10 – 0.50	1 - 25
	Snacks	0.10 – 0.15	2 - 20

The consumption of essential oils in perfumed products varies according to the product (Table 1.11): from a very high level in perfumes (due to the high concentration of fragrance compounds in perfumes and the high content of natural ingredients in perfume fragrances) and in a wide range of natural cosmetics and toiletries to relatively low levels in detergents and household chemicals, in which fragrances are based on readily available low-priced aroma chemicals. However, it must be emphasized that although the concentration of essential oils in detergents and related products is low, the large-volume

sales of these consumer products result in substantial consumption of the oils. It should be noted that in many cases, the actual figures for individual products can be significantly different [3].

Table 1.11 Average dosage of fragrances in consumer products and content of essential oils in fragrance compounds [3]

Position	Product	Average dosage of fragrance compound in product (%)	Average content of essential oils in fragrance (%)
1	Perfumes	10.0 – 25.0	5 – 30[a]
2	Toilet waters	3.0 – 8.0	5 – 50[a]
3	Skin care cosmetics	0.1 – 0.6	0 - 10
4	Deodorants (inclusive deoparfum)	0.5 – 5.0	0 - 10
5	Shampoos	0.3 – 2.0	0 - 5
6	Body cleansing products (liquid soaps)	0.5 - 3.0	0 - 5
7	Bath preparations	0.5 – 6.0	0 - 10
8	Soaps	0.5 – 3.0	0 - 5
9	Toothpastes	0.5 – 2.5	10 - 50[b]
10	Air fresheners	0.5 – 30.0	0 - 20
11	Washing powders and liquids	0.1 – 0.5	0 - 5
12	Fabric softeners	0.1 – 0.5	0 - 10
13	Home care chemicals	0.5 – 5.0	0 - 5
14	Technical products	0.1 – 0.5	0 - 5
15	Aromatherapy and organic products	0.1 – 0.5	100

[a] Traditional perfumery products contained more natural oils than modern ones.
[b] Mainly mint oils.

According to the United Nation's COMTRADE database, global exports and imports of essential oils stood at US$ 4 B in 2015. Essential oils imports remained steady between 2010 and 2016 at an average of 200 M tons, except in 2011 with 194 M tons (Figure 1.16). Spending rose by an annual average of 4 % between 2012 and 2015. As listed by COMTRADE, the top ten import markets in 2015 were the United States of America (US$988 M), France (US$380 M), Germany (US$323 M), the United Kingdom (US$326 M), China (US$229 M), India (US$161 M), Japan (US$156 M), Ireland (US$146 M), Switzerland (US$138 M), Spain (US$136 M), Singapore (US$132 M) and Canada (US$118 M) [41].

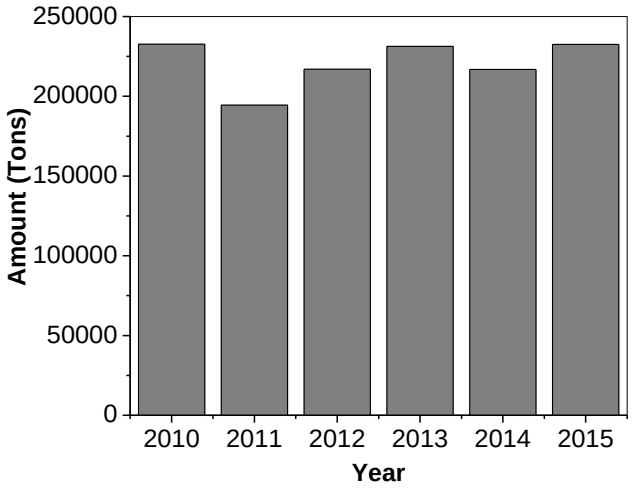

Figure 1.16 Global annual imports of essential oils, resinoids and terpenic by-products [41].

Exports of essential oils, resinoids and terpenic products were in 2010 and 2011 around 211 M tons of essential oils, and reached and average of 255 M tons between 2012 and 2015 (Figure 1.17). According to COMTRADE database, the top ten essential oils exporting countries in 2015 were China (US$796 M), United States of America (US$598 M), India (US$572 M), France (US$355 M), Brazil (US$256 M), United Kingdom (US$243 M), Argentina (US$224 M), Germany (US$178 M), Mexico (US$137 M) and Italy (US$132 M) [41].

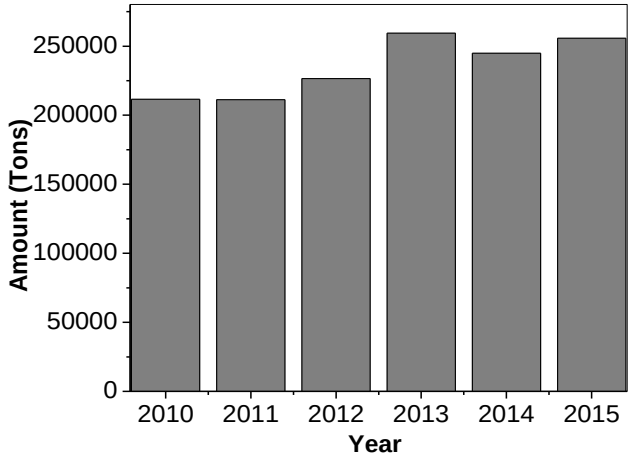

Figure 1.17 Global annual exports of essential oils, resinoids and terpenic by-products [41].

1.13 Kinetics of heterogeneous catalytic reactions

The mechanism of a catalyzed reaction can be described by the sequence of elementary reaction steps, including adsorption, surface diffusion, chemical transformations of adsorbed species, and desorption, and it is the basis for deriving the kinetics of the reaction. It is assumed that for each individual elementary step the transition-state theory is valid [4].

1.14 Reaction rate models

The rate at which a given chemical reaction is performed can be stated in several ways. It can be expressed as the rate of disappearance of the reactants or as the rate of formation of the products [42]. Consider the reaction (1.1):

$$aA + bB \leftrightarrow cC + dD \qquad (1.1)$$

With A, B: reagents; C, D: products and a, b, c, d: stoichiometric coefficients.

The numerical value of the reaction rate, $-r_A$, is defined as the number of moles of A that reacts (disappears) per unit time per unit volume ($mol/dm^3 \cdot s$).

In heterogeneous reaction systems, the reaction rate is usually expressed in measures other than volume, such as reaction surface area or catalyst weight. Thus, in the case of a gas-solid catalytic reaction, the dimensions of this velocity, $-r'_A$, are the number of moles of A which reacted per unit time per unit mass of catalyst ($mol/s \cdot g_{catalyst}$). If an experiment is carried out in a batch reactor, where the reaction is carried out at a constant volume, the reactants are mixed at time t = 0 and the concentration of one of the reagents C_A is measured at different times t, the reaction rate can be determined from the slope of a plot C_A vs time [42].

If r_A is the rate of formation of A per unit volume ($mol/s \cdot mL$), the reaction rate is defined as:

$$r_A = \frac{dC_A}{dt} \qquad (1.2)$$

This definition is valid only for a batch reactor of constant volume [42].

Knowledge of the rate of a catalytic reaction and its selectivity as a function of the process conditions and reactant concentrations is essential for the application of the catalyst in a commercial reactor. More specifically, the kinetics of the reaction are required in the form of a mathematical rate expression that can be used to reliably translate laboratory and pilot scale data into the design of a commercial scale unit. That rate, or kinetic expression tells how the reaction rate varies with process conditions such as temperature, pressure, and composition, and preferably also with a measure of the volumetric concentration of catalytic sites. The importance of a reaction's kinetics is that the rate and selectivity of a reaction determine the size of the catalytic reactor for a given overall production rate. Without a reliable means to predict the reaction rate, the reactor design could be highly speculative [4].

1.15 Esterification reaction and reaction mechanism

Esters can be formed by the reaction of a carboxylic acid with an alcohol forming the ester and water molecules. This esterification (reversible) reaction, also called the intermolecular dehydration reaction, is a very important and a common type of reaction in the chemical industry [43]. The general esterification reaction is shown below, reaction (1.2):

$$\text{Acid} + \text{Alcohol} \leftrightarrow \text{Ester} + \text{Water} \qquad (1.2)$$

The reaction mechanism for the formation of esters from carboxylic acids and alcohols in the presence of acidic catalyst was presented by Lilja *et al*. (2002). The reaction is initiated by the transfer of a proton from the catalyst to the carboxylic acid, Figure 1.18. The proton becomes attached to one of the lone pairs on the oxygen which is double-bonded to the carbon. The transfer of the proton to the oxygen gives it a positive charge. This results in a fair amount of positive charge on the carbon atom. Then, the positive charge on the carbon atom is attacked by the hydroxyl group of the alcohol molecule. After that, a molecule of water is lost from the ion. Finally, the catalyst is recovered by the transfer of proton from the ion to the catalyst surface [43]. The donation of a proton is commonly assumed to be a fast step, while the nucleophilic substitution is usually assumed to be

slow followed by fast steps resulting in the formation of ester and water and the recovery of the catalyst [43].

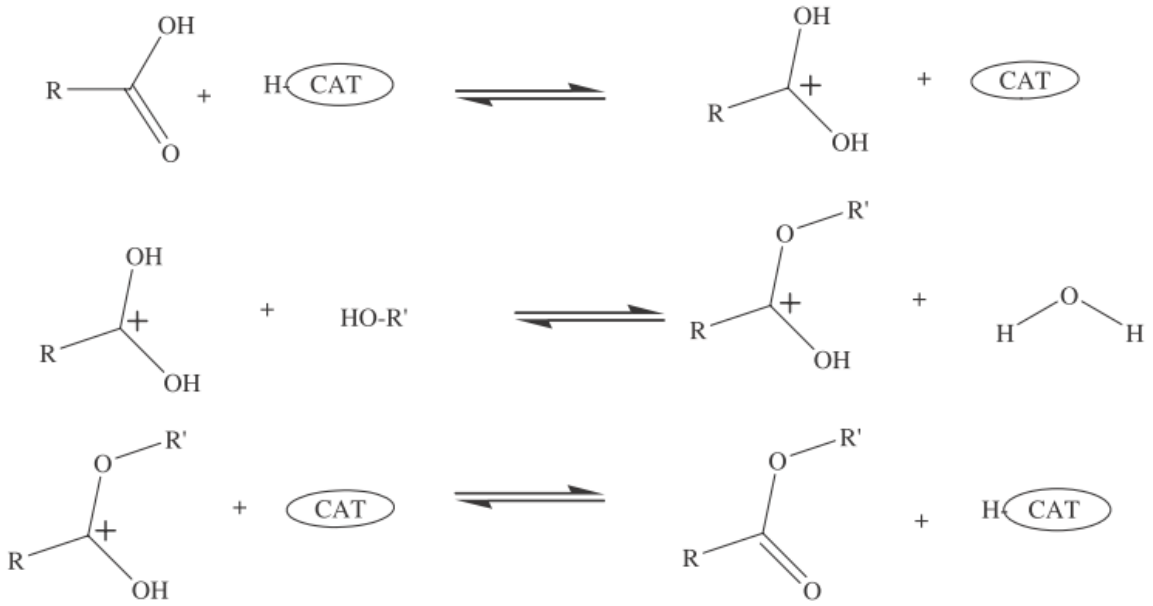

Figure 1.18 Reaction mechanism for the formation of esters from carboxylic acids and alcohols in the presence of acidic catalyst [43].

Liu *et al.* present a mechanism for an acid catalyzed esterification (Figure 1.19). The catalysts essentially promote the protonation of the carbonyl oxygen on the carboxylic group (step 1-2), thereby activating nucleophilic attack by an alcohol to form a tetrahedral intermediate (step 3-4). Disproportionation of this intermediate complex ultimately yields the ester (step 5-6) [44].

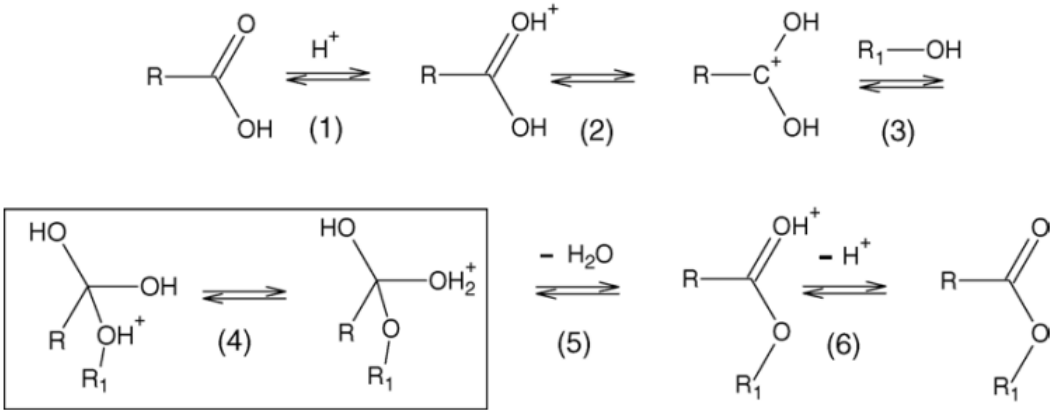

Figure 1.19 Mechanistic route of acid catalyzed esterification [44].

Costa *et al.* present a mechanism of the acetylation of alcohols with acetic anhydride (Fig. 1.20). It involves protonation of acetic anhydride followed by the formation of the acetyl cation, which attacks an alcohol molecule to give the ester after proton elimination [33].

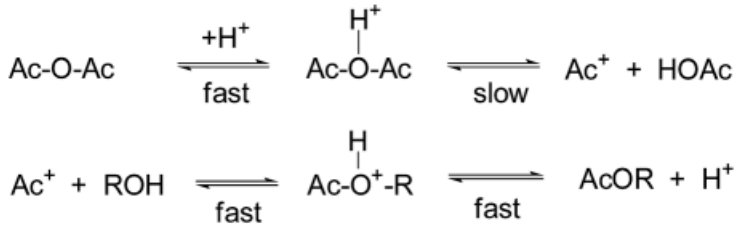

Figure 1.20 Mechanistic scheme of the acetylation of alcohols with acetic anhydride [33].

1.15.1 Pseudo-homogeneous reaction rates

Consider once again reaction (1.1):

$$aA + bB \leftrightarrow cC + dD \quad (1.1)$$

With A, B: reagents; C, D: products and a, b, c, d: stoichiometric coefficients.

The chemical reaction equation will then just be written as Eq. (1.3):

$$r'_A = -k'_1 \left(C_A{}^a C_B{}^b - \frac{1}{Kc} C_C{}^c C_D{}^d \right) \qquad (1.3)$$

where,

$$K_C = \frac{k'_1}{k'_{-1}} = \frac{C_{Ce}{}^c C_{De}{}^d}{C_{Ae}{}^a C_{Be}{}^b} \qquad (1.4)$$

r'_A is the reaction rate in terms of the amount of catalyst (m_{cat}), k'_1 is the forward reaction rate, C_{ie} is the concentration of the ith component at equilibrium and K_C is the equilibrium constant based on concentration of the reagents in the liquid mixture. For an esterification reaction, A, B, C and D represent alcohol, acetic acid, ester and water respectively. With the determination of the equilibrium constant based on the liquid phase concentration it is implied that the liquid mixture is ideal, and that the volume of the liquid mixture is constant [45].

When considering most reactions catalyzed by a heterogeneous catalyst the reaction on the catalyst surface is more complex than a normal elementary reaction equation and the

mechanisms are not so easily reducible to achieve a pseudo homogeneous rate equation. This is even truer for a resin catalyst, where the additional gel phase comes into play. Particularly, pseudohomogeneous models are commonly used for describing ion-exchange resin catalyzed esterification reactions [45].

1.15.2 Langmuir – Hinshelwood – Hougen –Watson kinetics

The Langmuir – Hinshelwood – Hougen – Watson (LHHW) approach is based on the Langmuir model describing the surface of a catalyst as an array of equivalent sites which do not interact either before or after chemisorption. Further, for derivation of rate equations, it is assumed that both reactants and products are equilibrated with surface species that react on the surface in a rate-determining step. Surface coverages are correlated with partial pressures or concentrations in the fluid phase by means of Langmuir adsorption isotherms. Despite that the Langmuir model is unrealistic, the LHHW kinetics approach has proved valuable for modeling heterogeneous catalytic reactions for reactor and process design [4].

As an example for a typical LHHW rate equation consider reaction (1.3).

$$A + B \leftrightarrow C \qquad (1.3)$$

$$r = \frac{k_{rds} N_T K_i \left(P_A P_B - P_C / K_{eq}\right)}{\left(1 + K_A P_A + K_B P_B + K_B P_B + K_C P_C + \sum_j K_j P_j\right)^n} \qquad (1.5)$$

$$\mathrm{r} = \frac{\text{rate factor x driving force}}{\text{inhibition term}} \qquad (1.6)$$

The numerator is a product of the rate constant of the k_{rds}, the concentration of active sites N_T, adsorption equilibrium constants K_i, and the driving force for the reaction ($P_A P_B - P_C/K_{eq}$). The latter is a measure of how far the overall reaction is from thermodynamic equilibrium. The overall equilibrium constant K_{eq}, can be calculated from thermodynamics. For the LHHW model, K_{eq} is equal to [4][46]:

$$K_{eq} = K_{eqa}\frac{K_{acid}K_{alcohol}}{K_{ester}K_{water}} \qquad (1.7)$$

$$K_{eqa} = \frac{x_{ester}x_{water}}{x_{acid}x_{alcohol}}\frac{\gamma_{ester}\gamma_{water}}{x_{acid}x_{alcohol}} = K_{eqx}K_{eq\gamma} \qquad (1.8)$$

x_i is mole fraction of the ith component, γ_i is the activity coefficient of the ith component K_{eqa} is the esterification reaction equilibrium constant K_{eq} is the overall equilibrium constant.

The denominator is an inhibition term which takes into account the competitive adsorption of reactants and products [4].

1.16 Research questions

Colombia has great diversity of natural resources that can be transformed into high value added products. Turpentine oil is obtained as a by-product of wood industry, which contains α- and β-pinene as main components. These monoterpenes can be transformed by various reactions into other useful products. Nopyl acetate is an artificial fragrance compound with a fruity odor of fresh wood that is not present in nature and is used in the preparation of soaps, detergents, creams, lotions and perfumes. It is prepared by the carbonyl-ene reaction of β-pinene and paraformaldehyde with subsequent acetylation of the intermediary nopol with acetic anhydride. Esterification reactions require the addition of a catalyst to obtain significant ester yields. Despite a high catalytic activity, homogenous catalysts are corrosive, exhibit undesired secondary reactions and a difficult reaction mixture separation. These problems can be overcome by the use of heterogeneous catalysts. Amberlyst-15 ion exchange resin is non-toxic, reusable, non – corrosive, as well as an effective catalyst for esterification reactions. Tin modified silicas (MCM-41, SBA-15, SiO_2) could be attractive alternatives for obtaining voluminous organic molecules like nopol. It has been found that Sn-MCM-41 and Sn-SBA-15 are adequate materials for the synthesis of nopol because their properties and acidity that also in required in the esterification of this alcohol with acetic acid. Furthermore, SiO_2 is a not expensive support.

Recently, environmental and economic considerations have promoted innovation processes towards the use of cleaner technologies. Therefore, there is a great challenge of using heterogeneous catalysts that can perform under mild reaction conditions, for example at low temperatures and pressures, while avoiding the use of harmful substances such as amines and chlorinated compounds.

- As the esterification reaction in the absence of a catalyst is slow and a reversible reaction, a catalyst is needed.
- A hydrothermally stable material is required for esterification reactions, as water is one of the products.
- The reaction kinetics is essential for the esterification reaction system characterization.
- The acid catalyst Sn-SBA-15, whose support is a mesoporous material would avoid mobility restriction of reactants and products. The structural characteristics of SBA-15 as support (higher pore volume, thicker pore walls, higher hydrothermal stability) would be most adequate than MCM-41 for the esterification reaction. SiO_2 is an economical support to evaluate catalytic activity for the esterification reaction of nopol.
- Ion exchange resins are the most common heterogeneous catalysts used for esterification reactions. Amberlyst-15 would be an efficient catalyst for the esterification of nopol, due to its high selectivity, suitability for continuous operation in columns, ease of recovery by filtration and negligible waste generation or disposal problems.
- Fundamental understanding of the reaction mechanism and kinetics are essential for system designs and optimization of catalytic chemical processes. LHHW and pseudohomogeneous type kinetic expressions could adequately represent experimental data for nopol esterification reactions.

1.17 Objectives

1.17.1 General:

Synthesize nopyl acetate by nopol esterification over heterogeneous catalysts.

1.17.2 Specifics:

1.17.2.1 Synthesis and characterization of Sn-MCM-41, Sn-SBA-15 and Sn-SiO_2 catalysts.

1.17.2.2 Effect determination of various reaction conditions (temperature, initial molar ratio of reactants, catalyst concentration) on nopol disappearance rate and on nopyl acetate formation rate using Sn-MCM-41, Sn-SBA-15, Sn-SiO_2 and Amberlyst-15.

1.17.2.3 Comparison of catalytic activity reached with *p*-toluenesulfonic acid (*p*-TSA) and the heterogeneous catalysts Amberlyst-15, Sn-MCM-41, Sn-SBA-15 and Sn-SiO_2

1.17.2.4 Evaluation of nopyl acetate production using β-pinene as substrate instead of nopol with Sn-MCM-41, Sn-SBA-15, Sn-SiO_2, Amberlyst-15.

1.17.2.5 Examination of the heterogeneity of the catalyst for best nopyl acetate under the conditions for obtaining the highest reaction rate.

1.17.2.6 Study the reaction kinetics for nopyl acetate production with the catalyst exhibiting the best nopyl acetate production.

1.17.2.7 Propose mechanisms for nopol esterification with acetic acid over the best material for nopyl acetate production.

1.18 Publications and participation in events

1.18.1 International publications

O. Arbelaez, L. Correa, R.Y. Parapat, K. Knemeyer, F. Bustamante, A.L. Villa, M. Schwarze. "Pd@Al_2O_3 - Catalyzed Hydrogenation of Allylbenzene to Propylbenzene in Methanol and Aqueous Micellar Solutions". Chemical Engineering Technology 38, 12, p. 2291–2298, 2015.

http://onlinelibrary.wiley.com/doi/10.1002/ceat.201500316/epdf

1.18.2 Submissions to international conferences

L.F. Correa, A.L Villa. “Acid: alcohol ratio effect on nopol esterification over Amberlyst-15 as catalyst”. XXIV Iberoamerican Congress on Catalysis (CICat). Medellín (Colombia) 2014. Submission: extended abstract. Participation: poster.

L.F. Correa, A.L Villa. “Nopyl acetate synthesis in presence of Amberlyst-15”. XXVII. Interamerican & Colombian Chemical Engineering Congress. Cartagena (Colombia), 2014. Submission: extended abstract. Acceptance: oral.

L.F. Correa, A.L Villa. “Catalyst loading effect on nopyl acetate synthesis over Amberlyst-15”. 24th North American Catalysis Society Meeting (NAM). Pittsburgh (USA), 2015. Submission: abstract. Participation: poster.

L.F. Correa, A.L Villa. “Esterification of nopol catalyzed by tin–containing mesoporous materials”. 18th International Zeolite Conference. Río de Janeiro (Brazil), 2016. Submission: abstract. Acceptance: oral. Participation: poster.

L.F. Correa, A.L Villa. “Esterificación de nopol con ácido acético sobre Amberlyst-15 y ácido *p*-toluensulfónico”. XXV Iberoamerican Congress on Catalysis (CICat). Montevideo (Uruguay) 2016. Submission: extended abstract. Participation: poster.

L.F. Correa, A.L Villa. “Esterification of nopol catalyzed by tin–containing mesoporous materials”. XXII Latin American Congress of Chemical Engineering Students. Medellín (Colombia), 2016. Submission: extended abstract. Participation: oral.

L.F. Correa, A.L Villa. “Nopyl acetate synthesis over tin-containing mesoporous materials”. 25th North American Catalysis Society Meeting (NAM). Denver (USA), 2017. Submission: abstract. Participation: oral.

1.18.3 Submissions to national conferences

L.F. Correa, A.L Villa. “Obtention of nopyl acetate by esterification of nopol with acetic acid over Amberlyst-15”. VIII Colombian Symposium on Catalysis (SiCCat). Armenia (Colombia), 2013. Submission: abstract. Acceptance: oral. Participation: poster.

L.F. Correa, A.L Villa. “Nopyl acetate synthesis over Amberlyst-15 catalyst”. XII Colombian Congress of Phytochemistry. Cartagena (Colombia), 2014. Submission: abstract. Acceptance: oral.

L.F. Correa, A.L Villa. “Esterification of nopol with acetic acid on Amberlyst-15 using different solvents”. IX Colombian Symposium on Catalysis (SiCCat). Cali (Colombia), 2015. Submission: abstract. Acceptance: oral.

1.18.4 Financial support

For the development of this thesis, financial support from Comité para el Desarrollo de la Investigación (CODI) of Universidad de Antioquia (UdeA) was granted through project MDC11-1-12. Logistic and financial support was provided by Environmental Catalysis Research Group of UdeA. Through Deutscher Akademischer Austauschdienst (DAAD) an internship to Technische Universität Berlin in 2013 was carried out. An internship at Massachusetts Institute of Technology (MIT) was supported logistically by Professor Yuriy Román-Leshkov and financially by the Fulbright Foreign Student Program 2015.

1.19 Thesis structure

This thesis is divided into three chapters. Chapter 1 presents general information on essential oils, mainly terpenes, and the challenges to obtain them; also the esterification reaction, the type of catalysts that have been used for this reaction and the problem related to the synthesis of nopyl acetate are topics of this chapter. The objectives of the research, as well as a brief explanation of the research are presented in Chapter 1.

Chapters 2 and 3 contain the main results of the research carried out. Chapters 2 and 3 begin with an introduction, followed by theoretical information of the techniques, data treatment and procedures used, then the results and their discussion are presented, ending finally with partial conclusions.

Chapter 2 describes synthesis procedures and various characterization techniques used for the catalysts obtained. Results and discussion of these techniques such as BET, SEM, TEM, AA, NH_3 -TPD, TPR, FTIR, UV –Vis, Raman, XRD and TGA are presented.

Chapter 3 contains some fundamentals of esterification reaction kinetics, catalyst type and loading, acid: alcohol molar ratio and solvent effect on nopyl acetate synthesis, chromatographic analysis conditions and catalyst heterogeneity test procedures. Results and discussion about the effect of particle size and stirring rate on reaction kinetic and catalytic activity with different acetylating agents are presented.

Conclusions, recommendations, suggestions and annexes are found in the final part of this manuscript.

CHAPTER 2

CHAPTER 2. SYNTHESIS AND CHARACTERIZATION OF CATALYSTS

2.1 Introduction

Chapter 2 presents the synthesis and characterization of Sn-MCM-41, Sn-SBA-15 and Sn-SiO_2 heterogeneous catalysts obtained by incipient wetness impregnation using $SnCl_2 \cdot 2H_2O$ as precursor at room temperature. Physicochemical properties of the materials were determined by surface area BET, SEM, AA of Sn, NH_3-TPD, FTIR, UV-vis, Raman, XRD, TGA, TEM and TPR. As the esterification reaction in the absence of a catalyst is slow and the reaction is reversible with water as one of the by-products, a hydrothermal stable material is required as catalyst. Sn-SBA-15 is an acid catalyst, with a mesoporous support that would avoid mobility restriction of reactants and products. Additionally, Sn-MCM-41 has been found to be a suitable mesoporous material for nopol production. The use of Sn supported on SiO_2 is an economical option, as well as Amberlyst-15, since it is a non-corrosive, non-hazardous, environmentally benign ion exchange resin, easy to recover through filtration, which does not lead to waste or disposal problems.

2.2 Generalities

The esterification reaction is a liquid-phase process, where the limiting conversion of the reactants is determined by equilibrium. Typically esterification reactions are very slow; it requires several days to attain the equilibrium in the absence of catalyst. Therefore, the reaction is enhanced with an added catalyst. Mineral acids, such as H_2SO_4, HCl and HI, and strong organic acids, such as HCOOH, can be utilized as homogeneous catalysts. The disadvantage with homogeneous catalysts is their miscibility with the reaction medium, which causes separation problems. Furthermore, equipment corrosion can occur at high catalyst concentrations. Therefore, heterogeneous catalysts, such as ion-exchange materials containing sulphonic acid groups (–SO_3) and mesoporous silicas are used in esterification reactions [47], [48].

2.2.1 Amberlyst-15

Amberlyst-15 is one of the polymeric cation-exchange resins with sulfonic acid functionality used as heterogeneous catalyst in non-aqueous as well as aqueous media. Amberlyst-15 holds various advantages such as nontoxicity, reusability, non-corrosive, chemical and physical stability, environmental compatibility; it is inexpensive and commercial availability. Amberlyst-15 is a brown-grey solid, which physical properties are shown in Table 2.1. Because the unique properties of Amberlyst-15, it is used as a powerful catalyst for various organic transformations as other heterogeneous reusable acid catalysts for various selective transformations of simple and complex molecules [49]-[50].

Table 2.1 Amberlyst-15 physical properties [49].

Appearance	Opaque spheres
Standard ionic form	H^+
Acidity (mmol/g)	4.7
Moisture (%)	52-57
Surface area (m^2/g)	53
Pore diameter (Å)	300
Total pore volume (mL/g)	0.4
Maximum operating temperature (°C)	120

Amberlyst-15 is a macro reticular polystyrene based ion exchange resin with strongly acidic sulfonic group (Figure 2.1). Thus, it serves as an excellent source of strong acid. It has been used in various acid catalyzed reactions. It is easy to measure, safe to use, and readily removed at the end of the reaction. An additional advantage is that the catalyst can be regenerated and can be used several times [49].

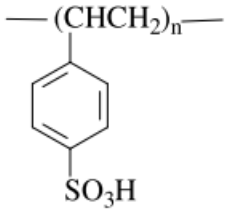

Figure 2.1 Amberlyst-15 resin chemical structure.

Amberlyst-15 is a powerful and selective acid catalyst for esterification reactions. Petrini *et al.* reported a mild and selective methyl esterification of aliphatic carboxylic acids using Amberlyst-15 in methanol at room temperature in excellent yield. No racemisation, epimerization and ketalization products have been observed with this method. Excellent results are obtained in the esterification of bile acids. However, aromatic carboxylic acid such as 5-methylfuroic acid and conjugated carboxylic acid such as trans-aconitic acid do not react with methanol at room temperature. They can be transformed into esters only by refluxing the mixture for a long time [49].

Amberlyst-15 has also been used for production of biodiesel (BD). Talukder and coauthors reported that palm fatty acid distillate (PFAD), a byproduct from the palm oil refinery process, has been utilized as an alternative feedstock for biodiesel production via Amberlyst-15 catalyzed esterification. The BD yield obtained using Amberlyst-15 was 97 % [49].

2.2.2 MCM-41

Ordered mesoporous material MCM-41 was firstly prepared in 1992. It was considered to have great potential use in fields such as catalysis, adsorption and separation. The incorporation of heteroatom such as aluminum into the inorganic framework generated active sites in the framework and made the material being applicable in petroleum processing. Generally, this kind of material was synthesized under hydrothermal conditions with particle sizes of hundreds of nanometers or larger. As a result, the material usually possessed long one-dimensional pores that was not in favor of the molecular's exiting [51].

The acidity of MCM-41 can be varied or increased from [52]:

• Proper selection of aluminum sources and methods of preparation.

• The incorporation of different heteroatoms besides aluminum (like Ga, B, Fe among others).

• Addition of acidic groups (-$AlCl_2$, -HSO_3) and / or chemical loading of extra-strong acids, among others.

This material exhibits a highly ordered hexagonal array of unidimensional cylindrical pores with a narrow pore size distribution, although the walls are amorphous (Figure 2.2). The pore sizes usually vary between 2 and 10 nm depending on the alkylammonium surfactant chain length, the presence of organic additives, or post-treatments. The pore wall thickness is usually between 0.7 and 1.1 nm. MCM-41-type mesoporous silicas are highly porous and commonly show BET (Brunauer-Emmett-Teller) surface areas exceeding 1000 $m^2 \cdot g^{-1}$ and pore volumes up to 1 $cm^3 \cdot g^{-1}$. The N_2 sorption isotherm measured for MCM-41 is distinctive, being a type IV isotherm which is generally observed for mesoporous materials, but with an unusually sharp capillary condensation step. The long-range ordering of MCM-41 can be evidenced using XRD, where Bragg reflections can be detected at low 2θ angles. The only reflections observed are due to the ordered hexagonal array of parallel pore walls and can be indexed as a hexagonal *p6mm* structure. No reflections at higher 2θ are observed. Subsequent developments proved that ordered mesoporous materials could also be formed in an acidic medium, or by using neutral amines, non-ionic surfactants, or block copolymers as the SDAs (structure directing agents). In addition, heteroatoms, such as Al or Ti, could be incorporated into the mesostructured silicate framework, as is done with zeolitic frameworks, and surface functionalization was achieved by incorporating organic and organometallic groups [53].

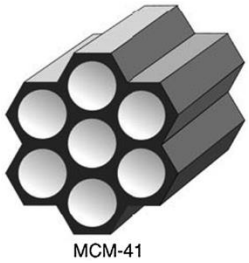

Figure 2.2 The structure of mesoporous silica MCM-41 [54].

2.2.3 SBA-15

Major progress in the preparation of mesoporous silicas was made by Zhao *et al*. in 1998 who used poly(ethylene oxide)-poly(propylene oxide)-poly(ethylene oxide) triblock copolymers (Pluronic-type) for the synthesis under acidic conditions of a large-pore material called SBA-15 and other related materials. These syntheses were based on the use of organic silica sources such as TEOS or tetramethoxysilane (TMOS) in combination

with diluted acidic aqueous solution of pluronic-type triblock copolymer (<7 wt. % in water, ideally 2.5 wt. %) such as P_{123} (EO_{20}-PO_{70}-EO_{20}, EO = ethylene oxide, PO = propylene oxide) and F_{127} (EO_{106}-PO_{70}-EO_{106}) [53].

The use of triblock copolymers leads to a considerable expansion in accessible range of pore sizes. In most cases, mesoporous silicas obtained with triblock copolymers possess uniform large pores with dimensions well above 5 nm in diameter and thick walls. The latter provided high thermal stability and improved the hydrothermal stability when compared with mesoporous silicas synthesized with low-molecular-weight ionic surfactants [54]. Hexagonally ordered SBA-15 can be prepared with pore sizes between 4.5 nm and 15 nm with wall thicknesses of 3.0 to 6.5 nm (Figure 2.3). SBA-15 usually exhibits a large surface area (ca. 800–1000 $m^2\ g^{-1}$) and pore volumes up to 1.5 $cm^3\ g^{-1}$ [53].

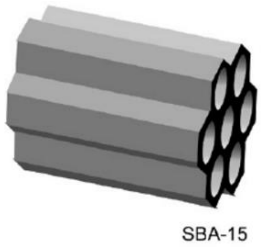

Figure 2.3 The structure of mesoporous silica SBA-15 [54].

SBA-15 silica, being more or less the large pore equivalent to MCM-41, is of growing interest for a wide range of applications (e.g., selective sorbent, support for catalysts and biomolecules, nanoreactor), and is therefore the subject of increasing numbers of studies. Originally, SBA-15 was thought to be a large-pore equivalent of MCM-41 mesoporous silica with unconnected mesoporous cylindrical channels. However, several studies have shown that the pore size distribution of the hexagonal SBA-15 is rather bimodal, in which the larger, hexagonally ordered structural pores are connected by smaller pores (micropores) located inside the silica walls The presence of complementary porosity in the walls of SBA-15-type silicas is one of the fundamental differences from the smaller-pore MCM-41-type systems, and it is of major importance for further development of block copolymer-directed silicas [53].

The microporosity of the material can be varied in different ways [55]:

- The source of silicon (eg TEOS, TMOS, sodium silicate, sodium metasilicate).
- The chain length of the copolymer block polymer used as structurant.
- Method of heating (conventional hydrothermal heating or microwave heating).
- Synthesis temperature and time.
- The molar ratio H^+/Si (pH).
- The silicon/surfactant ratio.
- The addition of co-solvent (ethanol) and other additives.

It is not easy to understand how each factor influences microporosity, because the factors are not usually independent.

2.2.4 SiO_2

Silica (SiO_2) is a commonly occurring compound in nature. Various crystalline and non-crystalline silica minerals of inorganic and bio-genic origin are known. Depending on temperature, pressure, composition of the precursor phases, among other factors, several different crystalline modifications are formed. Quartz is the most abundant and well-known polymorph. Silica occurs as meter-sized quartz crystals or as amorphous masses made up of submicroscopic crystallites having different microstructures or growth fabrics. In addition, synthetic polymorphs have been produced for which no natural counterparts exist. In industry, quartz sand and silica rocks are widely used as raw materials for production of glass, ceramics, and silicon. Single crystals of quartz are grown artificially for application as resonator crystals in clocks, communication technology, and computer electronics [56].

2.2.4.1 Occurrence and geochemistry

Silica, silicon dioxide, SiO_2, is the major constituent of rock-forming minerals in magmatic and metamorphic rocks. It is also an important component of sediments and soils. Bound as silicates it accounts for ca. 75 wt % of the Earth's crust. Free silica predominantly occurs as quartz, which makes up 12–14 wt % of the lithosphere [56].

2.2.4.2 Silica fume

Silica fume is a very fine powder consisting of noncrystalline silica spheres with an average diameter of ca. 0.1 μm. It forms at temperatures of about 2050 K as a byproduct of the reduction of quartz in electric arc furnaces for the production of silicon and ferrosilicon. The silica vapor is condensed and collected to prevent its emission. Silica fume is mainly used as an ad-mixture in cement, concrete, and mortars to improve strength and durability. Due to the small particle size and the large surface area (up to 30 m^2/g), it acts both as a microfiller that reduces the porosity and as a pozzolan which reacts with the calcium hydroxide from the cement [56].

2.2.4.3 Silica gel

Silica gel has the nominal chemical formula $SiO_2 \cdot H_2O$ and is a solid, amorphous form of hydrous silicon dioxide distinguished by its microporosity and hydroxylated surface. The structure of silica gel is an interconnected random array of ultimate polymerized silicate particles, called micelles, which are spheroidal and 2–10 nm in diameter (resulting in high surface areas of ca. 300–1000 m^2/g SiO_2). The properties of silica gel are a result of the silica micelles, their state of aggregation, and the chemistry of the micelle surface [56].

The high surface area of silica gel (~ 400 m^2/g) makes it an attractive solid for using it in catalytic processes [57]. Silica itself does not catalyze many reactions of commercial significance. Silica aluminas have acidic catalytic properties best exemplified in catalytic cracking. Silica gel is also used as a support in olefin polymerization [56].

2.2.5 Material characterization techniques

2.2.5.1 X-Ray Diffraction (XRD)

X-Ray Diffraction and Diffusion X-ray diffraction (XRD, sometimes also called WAXS: wide-angle X-ray scattering) is one of the most important techniques for catalyst characterization. For most catalysts XRD is limited to powder pattern identification of crystalline phases. For zeolites, and catalysts with good crystallinity, long range order exists, and XRD can give a complete description of their structure. In all cases, the

possible presence of amorphous phases should be taken into account in interpretation [58].

X-rays interact within matter. When a beam of X-rays impinges on a material it is scattered in various directions by the electron clouds of the atoms. Interference can occur if the wavelength of the X-rays is comparable to the separation between the atoms. An ordered array of scattering centres (such as atoms or ions in a crystalline solid), can give rise to interference maxima and minima. The wavelengths of X-rays used in X-ray diffraction experiments therefore typically lie between 0.6 and 1.9 Å [58].

Both MCM-41 and SBA-15 consist of a hexagonal arrangement of mesopores with an XRD pattern characterized by a peak projecting around 2θ = 2.6° and 0.7°, respectively. The mathematical models that govern the relationship between these peaks for the spacing between planes are shown in Equation (2.1), where the right side of the expression corresponds to the Bragg law (λ = 2d (sin θ)) [38].

$$\frac{1}{d^2} = \frac{4}{3}\left(\frac{h^2 + hk + k^2}{a^2}\right) + \frac{l^2}{c^2} = \frac{4\,sen^2\theta}{\lambda} \qquad (2.1)$$

With:

d: interplanar spacing for each combination of hkl, usually in Å or nm.

a, c: cell parameters, units of Å or nm.

h, k, l: Miller indices corresponding to the characteristic planes.

λ = wavelength of the incident X-ray beam, ~ 0.154 nm for a Cu lamp.

Θ = angle of incidence

2.2.5.2 BET surface area

The specific surface area is a physicochemical property of interest in the characterization of materials MCM-41 and SBA-15. Usually the areas for this type of materials are in the order of 700 to 1500 m^2/ g. The determination of the surface area described in this chapter was based on the theory developed by Stephen Brunauer, Paul Hugh Emmett and Edward Teller, called the BET method [59].

By adsorption and nitrogen capillary condensation in mesoporous materials with adsorption isotherm type IV, the pore size distribution is determined. However, for the last mentioned calculation, it is essential to have data throughout the range of relative pressures and to determine the isotherms of nitrogen adsorption and desorption. In particular, BET area analyses are determined by the nitrogen adsorption at five relative pressure points, which fulfill the BET equation, Equation (2.2), under the following assumptions: i) the gas molecules are adsorbed physically on the surface of the solid in multilayers, ii) there is no interaction between the adsorption of each layer, and iii) Langmuir theory can be applied to each layer. Normally this equation is valid in a range of relative pressures between 0.05 and 0.30 [60].

$$\frac{x}{V(1-x)} = \frac{(C-1)x}{C V_m} + \frac{1}{C V_m} \qquad (2.2)$$

Where the relative pressure is $x = P / P_o$, P is the partial pressure of nitrogen, P_o is the saturation pressure at the analysis temperature, V (cm^3) is the volume of the adsorbate at a given P value, V_m is the volume of the monolayer per amount of sample (cm^3/g), C is the BET constant that is related to the adsorption energy and (CV_m) is the adsorption capacity of a monolayer [60].

2.2.5.3 Atomic absorption

Optical atomic spectral analysis is the detection (qualitative analysis) and/or determination (quantitative analysis) of the concentrations of metal elements in a sample within the spectral range from 100 nm to 1 mm, using the characteristic line spectra of free atoms in the gaseous state [61].

A sample is introduced and atomized in the absorption cell in liquid or solid form (depending on atomizers) to accomplish the excitation process. If a liquid solution is required, elements are extracted by liquid reagents from solid materials. The liquid sample in the absorption cell is atomized, with thermal means (flame or graphite furnace) or chemical means (hydride or mercury vapor generator) used to excite the atoms. Flame produced by an air-acetylene mixture (2100 - 2400 °C) is used for most metal elements

(such as calcium or zinc) that do not form refractory compounds, which cannot be ionized or atomized at this temperature range. A hotter nitrous oxide-acetylene flame (2600-2800 °C) is used for elements (such as silicon or aluminum) forming refractory compounds (silicon dioxide or aluminum dioxide). A graphite furnace atomizer provides a wider range of temperatures (2100 - 2900 °C) and handles liquid or solid samples [62].

Not all elements are detected by atomic absorption. Elements with wavelengths of resonance lines below 190 nanometers, nonmetals (such as hydrogen, carbon, nitrogen, and oxygen), and noble gases are volatile, easily absorbed by air, and immediately lost at temperatures greater than 2100 °C they disappear before excitation. Elements that form very strong refractory compounds have extremely high melting points (greater than 2900 °C). Because these compounds cannot be atomized by flame or furnace, no atoms can be excited [62].

2.2.5.4 Scanning electron microscopy

SEM is a powerful magnifying device that uses an electron beam to form an image of the surface of an object. The image is characterized by great depth of field and shadowing, as well as a three-dimensional appearance, which gives the viewer clarity and perspective [63]. The scanning electron microscope has numerous applications in metallurgy, geology, electronics, medicine, and biology. SEM images are of value in industry for both quality control and research. It allows one to look at a surface rather than through it. In its basic emission modes, it can be used to study particles more than ten micrometers in diameter. Crystalline and amorphous structures can be studied. The SEM can be used on metallic, organic, and inorganic surfaces that are either smooth or rough [63].

2.2.5.5 Ammonia temperature-programmed desorption (NH_3-TPD)

TPD analyses determine the number, and type strength of active sites available on the surface of a catalyst from measurement of the amount of gas desorbed at various temperatures. After the sample has been outgassed, reduced, or otherwise prepared, a steady stream of analysis gas flows through the sample and adsorbs on the active sites.

Programmed desorption begins by raising the temperature linearly with time while a steady stream of inert carrier gas flows through the sample.

At a certain temperature, the heat overcomes the activation energy; therefore, the bond between the adsorbate and adsorbent will break and the adsorbed species desorb. If different active metals are present, they usually desorb the adsorbed species at different temperature. These desorbed molecules enter the stream of inert carrier gas and are swept to the detector, which measures the gas concentrations. The volume of desorbed species, combined with the stoichiometry factor and the temperature at which pre-adsorbed species desorb, yields the number and strength of active sites.

Despite the fact that TPD is widely used because of its simplicity the main draw-backs of this technique have to be pointed out. TPD gives an average value of acid strength rather than a distribution. Results obtained by this technique are strongly affected by mass or heat transfer and diffusion.

- TPD enables only to distinguish the strength of active sites, but not their types.
- Desorption on weak sites is hindered by adsorbates on strong sites.
- During desorption, a readsorption may occur.
- Peaks overlap, so TPD can be used only to roughly distinguish the various acid site strengths.

TPD-NH_3 analyses allow the identification of the acid strength of catalytic sites. Signals below 400 °C are attributed to weak acid sites and above 400 °C to strong acid sites [64]; however, based on measurements of ammonia desorption energies directly associated with acid strength reported by various authors, Parmaliana *et al.* [65] proposed a distribution of weak, medium and high acid sites in the range 180-250 °C, 280-330 °C and 380-500 °C, respectively.

2.2.5.6 Infrared spectroscopy

Infrared spectroscopy is certainly one of the most important analytical techniques available to today's scientists. One of the great advantages of infrared spectroscopy is that virtually any sample in virtually any state may be studied. Liquids, solutions, pastes,

powders, films, fibres, gases and surfaces can all be examined with a judicious choice of sampling technique. As a consequence of the improved instrumentation, a variety of new sensitive techniques have now been developed in order to examine formerly intractable samples.

Infrared spectrometers have been commercially available since the 1940s. At that time, the instruments relied on prisms to act as dispersive elements, but by the mid 1950s, diffraction gratings had been introduced into dispersive machines. The most significant advances in infrared spectroscopy, however, have come about as a result of the introduction of Fourier-transform spectrometers. This type of instrument employs an interferometer and exploits the well-established mathematical process of Fourier-transformation. Fourier-transform infrared (FTIR) spectroscopy has dramatically improved the quality of infrared spectra and minimized the time required to obtain data. In addition, with constant improvements to computers, infrared spectroscopy has made further great strides.

Infrared spectroscopy is a technique based on the vibrations of the atoms of a molecule. An infrared spectrum is commonly obtained by passing infrared radiation through a sample and determining what fraction of the incident radiation is absorbed at a particular energy. The energy at which any peak in an absorption spectrum appears corresponds to the frequency of a vibration of a part of a sample molecule.

The visible part of the electromagnetic spectrum is, by definition, radiation visible to the human eye. Other detection systems reveal radiation beyond the visible regions of the spectrum and these are classified as radiowave, microwave, infrared, ultraviolet, X-ray and *γ*-ray. Infrared radiation is divided into three regions: near infrared (800 to 3000 nm), medium infrared (3000 to 25000 nm), and far infrared (25000 to 107 nm).

2.2.5.7 Ultraviolet–Visible spectroscopy

With UV/Vis spectroscopy is possible to investigate electron transfers between orbitals or bands of atoms, ions, and molecules in the gas phase as well as in liquids and solids. The spectral region of 250 to 500 nm is of special interest for in situ UV/Vis spectroscopy.

Investigations of solutions and crystals usually take place in transmission, whereas powder samples are often measured in diffuse reflections (DRS: diffuse reflectance spectroscopy). A significant advantage of UV/Vis spectroscopy lies in the individual detection of electron transfers without superimposition by neighboring vibrational bands. Unlike IR spectroscopy, where the use of Fourier transform techniques predominates, dispersive spectrometers are almost exclusively applied for UV/Vis spectroscopy because of the large band widths. Important applications of UV/Vis spectroscopy in heterogeneous catalysis are *in situ* investigations of the synthesis of solid catalysts, support interactions, and for the modification of solid catalysts during calcination and poisoning [66].

2.2.5.8 Raman spectroscopy

Raman spectroscopy is a spectroscopic technique based on inelastic scattering of monochromatic light, usually from a laser source. Inelastic scattering means that the frequency of photons in monochromatic light changes upon interaction with a sample. Photons of the laser light are absorbed by the sample and then reemitted. Frequency of the reemitted photons is shifted up or down in comparison with original monochromatic frequency, which is called the Raman effect. This shift provides information about vibrational, rotational and other low frequency transitions in molecules. Raman spectroscopy can be used to study solid, liquid and gaseous samples [67].

2.2.5.9 Thermogravimetric analysis (TGA)

Conventional thermal analysis techniques include differential scanning calorimetry, differential thermal analysis (DTA), thermogravimetric analysis (TGA), dynamic mechanical analysis, thermomechanical analysis, microthermal analysis and dielectric thermal analysis. Thermal analysis of a material can be either destructive or non-destructive, but in almost all cases subtle and dramatic changes accompany the introduction of thermal energy. Thermal analysis can offer advantages over other analytical techniques including: variability with respect to application of thermal energy (step-wise, cyclic, continuous, and so on), small sample size, the material can be in any ‘solid’ form – gel, liquid, glass, solid, ease of variability and control of sample preparation,

ease and variability of atmosphere, it is relatively rapid, and instrumentation is moderately priced. Most often, thermal analysis data are used in conjunction with results from other techniques such as those based on pyrolysis, infrared spectroscopy and nuclear magnetic resonance (NMR) spectroscopy [68].

Thermogravimetric analysis is a technique in which the mass of a substance is monitored as a function of temperature or time as the sample specimen is subjected to a controlled temperature program in a controlled atmosphere.

2.3 Experimental

2.3.1 MCM-41 synthesis

The synthesis procedure of MCM-41 was based on the method reported by Grün *et al* [69]. 2.2 g of myristyltrimethylammonium bromide (MTABr, Aldrich, 99 %) was dissolved in 120 mL of deionized water and 10.6 mL of ammonium hydroxide (EM Science, 28-30 %), followed by the slow addition of 10 g of tetraethyl orthosilicate TEOS (Acros Organics, 98 %). The mixture was stirred for 1 h, then the white precipitate was filtered and washed with 100 mL of deionized water. After drying at 373 K for 12 h, the sample was calcined at 823 K in air for 5 h to remove the template.

2.3.2 SBA-15 synthesis

Mesoporous silica SBA-15 was synthesized according to the reported procedure [70]. In a typical synthesis, 2 g of amphiphilic triblock copolymer, poly (ethylene glycol)-block-poly (propylene glycol)-block-poly (ethylene glycol) with an average molecular weight of 5800 (Aldrich), was dispersed in 15 g of water and 60 g of 2 M HCl solution while stirring, followed by the addition of 4.25 g of tetraethyl orthosilicate TEOS (Acros Organics, 98 %) to the homogeneous solution. This gel was continuously stirred at 313 K for 24 h, and finally crystallized in a teflon-lined autoclave at 373 K for 2 days. After crystallization, the solid product was centrifuged, filtered, washed with deionized water, and dried in air at room temperature. The material was calcined in air at 823 K for 24 h to decompose the triblock copolymer and to obtain a white powder (SBA-15).

2.3.3 SiO_2 synthesis

SiO_2 was synthesized according to Gonzalez *et al.* [71]. 13.7 mL of ethanol was added to 20 mL of TEOS continuously stirred during 1 h at 45 °C, followed by the slow addition of 12.74 mL of H_2O-CH_3COOH (acetic acid –water) solution (pH = 5). The mixture was stirred under reflux conditions during 24 h at 45 °C. The temperature was raised slowly to 80 °C and was kept for 1 h. The obtained gel was dried in a rotary evaporator at 70 °C for 3 h to remove the solvent and dried in an oven at 100°C for 2 h. Finally the material was calcined in a muffle at 673 K for 4 h at 0.5 °C/min.

2.3.4 Synthesis of Sn-MCM–41, Sn-SBA-15, Sn-SiO_2 by incipient wetness impregnation

Sn-containing materials were synthesized by incipient wetness impregnation under inert atmosphere using gaseous N_2 and at room temperature [72]. 3 mL of $SnCl_2 \cdot 2H_2O$ solution in ethyl acetate (28.7 μmol Sn mL^{-1}) was added dropwise to the support (2 g) and mixed. The wet solid was allowed to dry at room temperature for 24 h and calcined at 550 °C for 5 h. Theoretical tin concentration in the synthesized materials was 0.51 % w/w, concentration that was adequate for obtaining high nopol yields [73].

2.3.5 Characterization

To identify the phases of synthesized materials, X-ray diffraction (XRD) analysis was performed on a BRUKER model D8 ADVANCE diffractometer with DaVinci Geometry. Samples were prepared by pulverizing the material in an agate mortar and reducing them to a 38 μm (400 mesh) particle size. The selected specimen of each sample was inserted in a polymethylmethacrylate sample holder by the front filling technique. The analysis conditions were a 40 kV voltage, 30 mA current, 0.6 mm divergence aperture, 2.5° primary Soller apertures, 0.014247° 2ɵ sampling, $0.5 \leq 2ɵ \leq 10°$ measuring range, CuKα1 radiation, nickel filter, lineal LynxEye detector, continuous scanning type and 2°/min sampling time.

The complete BET surface area analysis was determined on an ASAP2010 equipment. The metal content in the solid samples was determined by atomic absorption

spectrometry (AAS) on Philips PU9200 equipment. Programmed temperature ammonia desorption analysis (TPD-NH_3) was performed on a Micromeritics Autochem 2920 instrument; sample pretreatment took place using Argon (50 mL/min) at a heating rate of 10 °C/min to 550 °C, this temperature was kept for 30 min. Subsequently, samples were cooled by convection at 40 °C and saturated with ammonia (0.3 % NH_3/He, 50 mL/min) for 90 min. The physisorbed dispersed ammonia was desorbed with He (30 mL/min) at 40 °C for 1 h, then the sample was heated at 10 °C/min to 800 °C. The Gaussian deconvolution of the peaks was performed with Microcal Origin 6.0 software. SEM analysis was performed on a JEOL model JSM-6490LV. TEM (transmission electron microscopy) micrographs were obtained from a Tecnai F20 Super Twin TMP equipped with a field emission source, resolution of 0.1 nm in 200 Kv, maximum magnification in TEM 1.0 MX, GATAN US 1000XP-P camera. IR analysis was performed in an Agilent Technologies CARY 630 Fourier transform infrared model coupled to a diamond sampling accessory ATR (Attenuated Total Reflectance); the analysis conditions were 64 scanning signals, 0.6 mm spatial interval and 4 cm^{-1} resolution with a Happ Genzel apodization. Thermogravimetric analyses were performed on a TA Instruments model Q500, the samples were heated under air atmosphere at a rate of 10 °C/min to 800 °C, and then they were left at constant temperature for 10 min.

2.4 Results: Sn-MCM-41, Sn-SBA-15, Sn-SiO_2 synthesis and characterization

2.4.1 X-ray diffraction (XRD)

Figures 2.4 and 2.5 show the XRD patterns of the MCM-41 and Sn-MCM-41, SBA-15 and Sn-SBA-15 materials, respectively. The MCM-41 materials synthesized present the characteristic reflection (1 0 0), guaranteeing the presence of a regular system of one-dimensional and hexagonal pore. On the other hand, SBA-15 materials exhibit well-defined diffraction peaks indexed in (1 0 0), (1 1 0) and (2 0 0), which are consistent with the original SBA-15 report [38]. It should be noted that the incorporation of tin generates a displacement to the right of the characteristic peaks of the supports and is due to the location of the tin species in the materials prepared by incipient wetness impregnation. Figure 2.6 shows that not defined XRD peaks were obtained neither for SiO_2 nor Sn-SiO_2. Performing a high angle (2θ = 10 – 80 °) XRD analysis (Figure 2.7) to tin supported

materials, reveals peaks at 2θ = 23° (Sn-MCM-41, Sn-SBA-15) and 27.3° (Sn-SiO_2) which are of amorphous silica. Any of the samples display peaks related with the presence of nano SnO_2 particles (peaks at 2θ = 33.9 and 52.1°) [74].

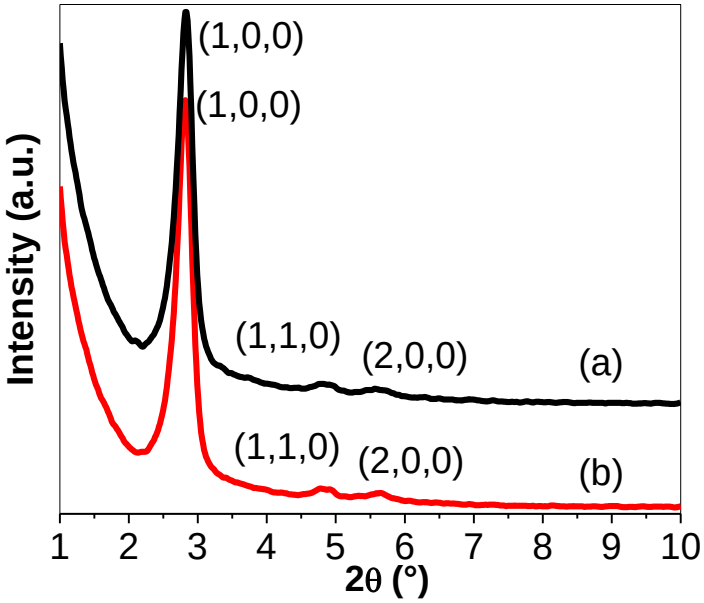

Figure 2.4 X-ray diffraction patterns of (a) MCM-41, (b) Sn-MCM-41.

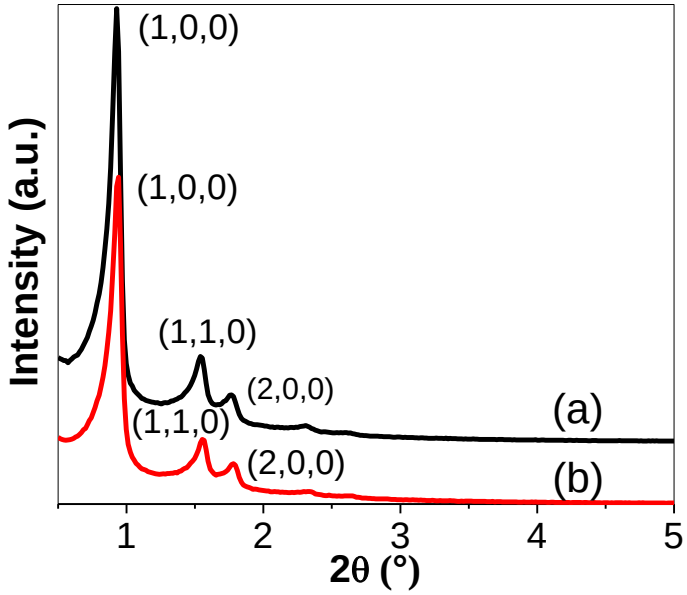

Figure 2.5 X-ray diffraction patterns of (a) SBA-15, (b) Sn-SBA-15.

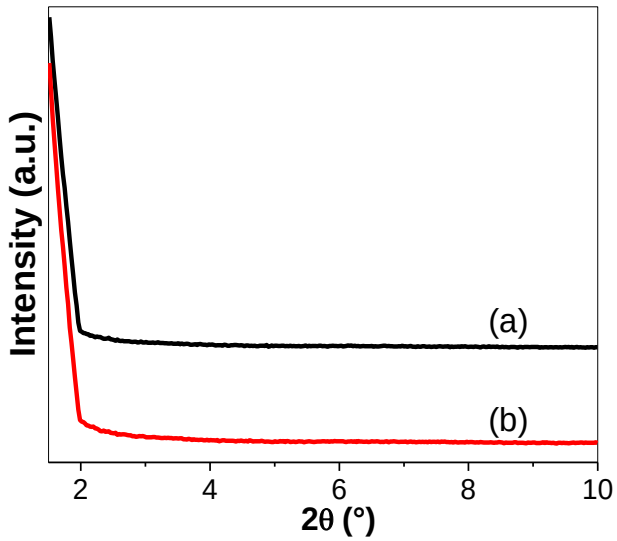

Figure 2.6 X-ray diffraction patterns of (a) SiO_2, (b) Sn-SiO_2.

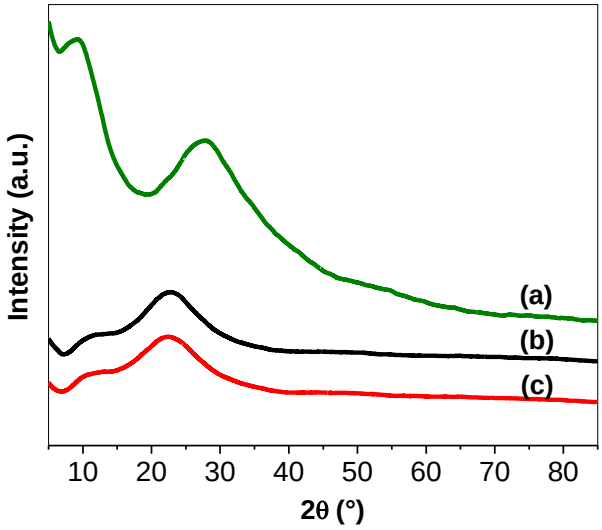

Figure 2.7 X-ray diffraction patterns in the region 10–80° 2θ of (a) Sn-SiO_2, Sn-MCM-41, (c) Sn-SBA-15.

2.4.1.1 Crystalline domain size

Results of the crystalline domain sizes in the highest intensity peaks of MCM-41 and SBA-15 materials are shown below (Table 2.2). In the case of SiO_2 materials, no defined peaks were obtained in the XRD patterns. The values were obtained using Equation (2.3).

$$T = 0.94\ \lambda_{Cu} / d_{100} \cos(\theta) \qquad (2.3)$$

With d_{100}: full width at half maximum (FWHM).

θ: 2θ peak angle.

λ_{Cu}: wavelength used in the XRD experiment.

Table 2.2 Material crystalline domain size

Materials	T (crystalline domain size) x 10^{-4} nm
MCM-41 Sn-MCM-41	9.10
SBA-15	1.90
Sn-SBA-15	1.97

No variation in the crystalline domain size was observed in MCM-41 and SBA-15 after Sn incorporation.

2.4.2 Sn content

The content of Sn in the synthesized materials was determined by atomic absorption. Table 2.3 shows that Sn deposition in Sn-SBA-15 and Sn-MCM-41 was similar and slightly higher than in Sn-SiO_2.

Table 2.3 Sn atomic absorption of synthesized catalysts

Material	mol Si/mol Sn	Sn (wt%) nominal	Sn (wt%) experimental
Sn-MCM-41	506.8	0.51	0.39
Sn-SBA-15	494.1	0.51	0.40
Sn-SiO_2	640	0.51	0.31

2.4.3 Scanning electron microscopy

SEM micrographs of SBA-15 and Sn-SBA-15 have many domains in the form of loops that add to a microstructure similar to wheat. Samples incorporated with tin have a similar morphology. SEM images of MCM-41 and Sn-MCM-41 exhibit a morphology with the appearance of small rolls, characteristic of these materials (Figure 2.8) [21]. Silica gel particles appear as spheres exhibiting a rough surface with porous morphological structures. After tin incorporation, these particles seem to lose their spherical shape due to additional crushing during the incipient wetness impregnation procedure.

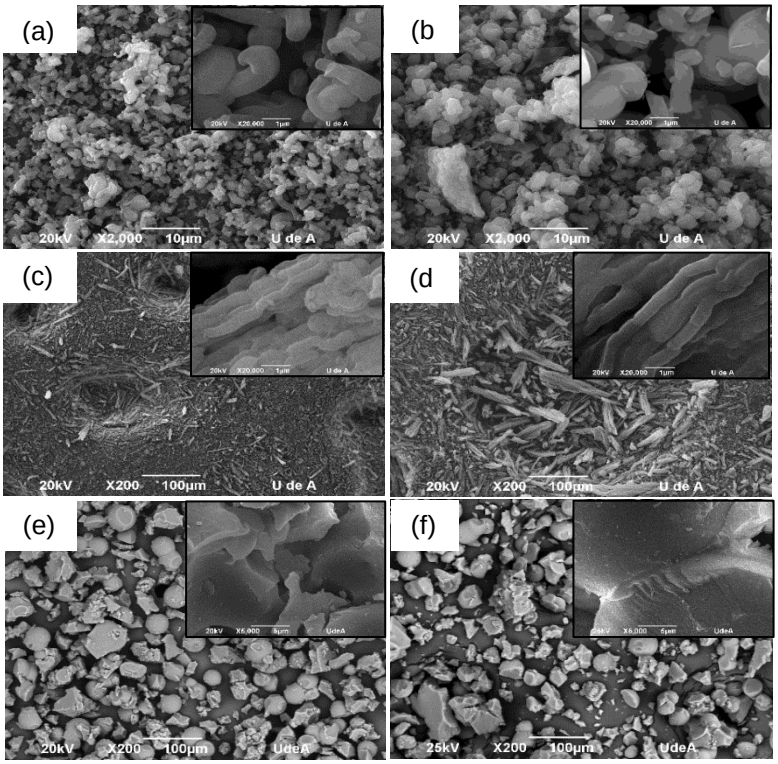

Figure 2.8 Scanning electron microscopy (SEM) of (a) MCM-41, (b) Sn-MCM-41, (c) SBA-15 and (d) Sn-SBA-15, (e) SiO_2 and (f) Sn-SiO_2.

2.4.4 Transmission electron microscopy (TEM)

TEM images of samples are shown in Figure 2.9. For MCM-41 (a), Sn-MCM-41 (b), SBA-14 (c) and Sn-SBA-15 (d), ordered channel arrays of parallel lines are observed clearly along the direction of the pore arrangement. This shows that the samples have highly ordered long-range structure confirming that the hexagonal pore structure of MCM-41 and SBA-15 was robust enough to survive the tin incorporation process and so offers a good matrix to support highly dispersed tin species. SiO_2 nanoparticles keep their amorphous feature before and after tin impregnation (Figure 2.9 e, f) [75], [76].

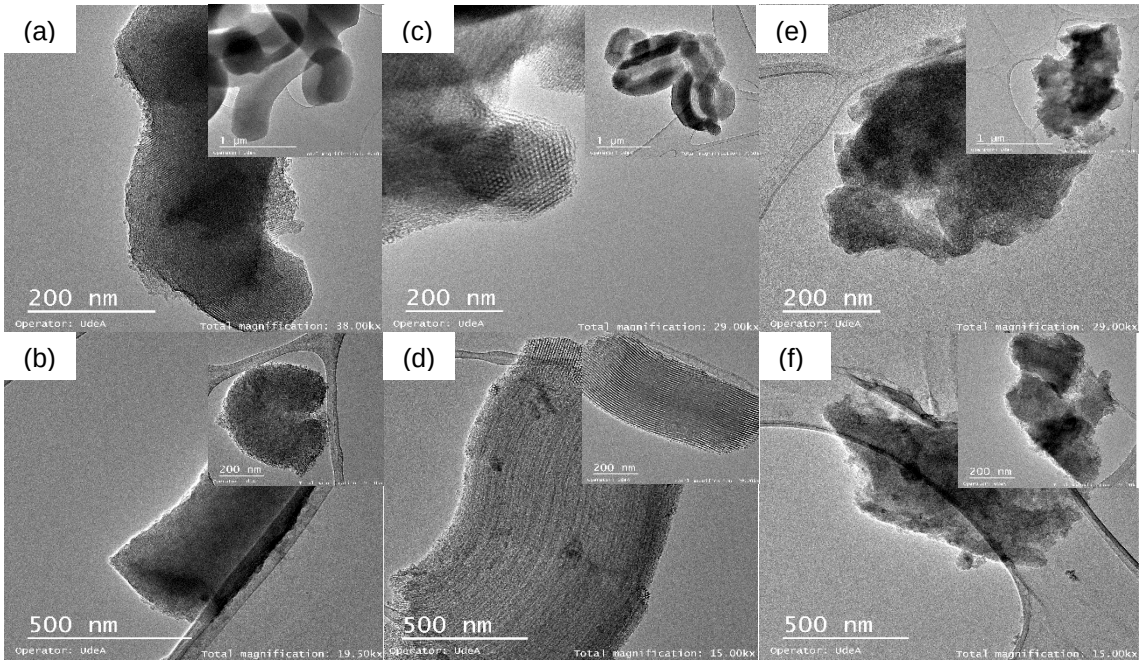

Figure 2.9 Transmission electron microscopy (TEM) of (a) MCM-41, (b) Sn-MCM-41, (c) SBA-15 and (d) Sn-SBA-15, (e) SiO_2 and (f) Sn-SiO_2.

2.4.5 N_2 adsorption/desorption analysis

2.4.5.1 BET surface area and pore volume

The post synthesis modification of MCM-41, SBA-15 and SiO_2 by impregnation leads to loss of surface area, Table 2.4, as reported by Shah *et al.* [70]. MCM-41 materials register a loss of 20 m^2/g after tin incorporation, SBA-15 materials 60 m^2/g and SiO_2 materials 70.2 m^2/g. It is evident that tin incorporation decreases total pore volume in each material.

Table 2.4 Structural properties of synthesized materials

Material	BET surface area (m^2/g)	Total pore vol. (cm^3/g)	Pore width (nm)
MCM-41	596	0.334	1.2
Sn-MCM-41	576	0.211	1.6
SBA-15	531	0.275	6.5
Sn-SBA-15	470	0.243	
SiO_2	434	0.162	1.3
Sn-SiO_2	364	0.124	

2.4.5.2 N_2 adsorption/desorption isotherms

The adsorption-desorption isotherms of N_2 of all materials adjust to a Type IV isotherm (Figure 2.10 - 2.12), characteristic in solids with mesopores according to the IUPAC classification. In the MCM-41 and SBA-15 materials, a H1 type hysteresis is presented [77]. The SiO_2 materials exhibit a hysteresis usually associated with the filling and emptying of mesopores by capillary condensation. The hysteresis is of type H2, common in many inorganic oxides gels that possess a complex porous structure consisting of pore interconnected networks of different size and form [78]. The isotherms of Amberlyst-15 resin (Figure 2.13) are of type I, where the adsorbed quantity is supposed to quickly increase for low pressures, reaching a limit value or plateau when the relative pressures are close to 1. This type of isotherm is characteristic of microporous materials, where the adsorbent–adsorbate interactions are favoured in micropores [79].

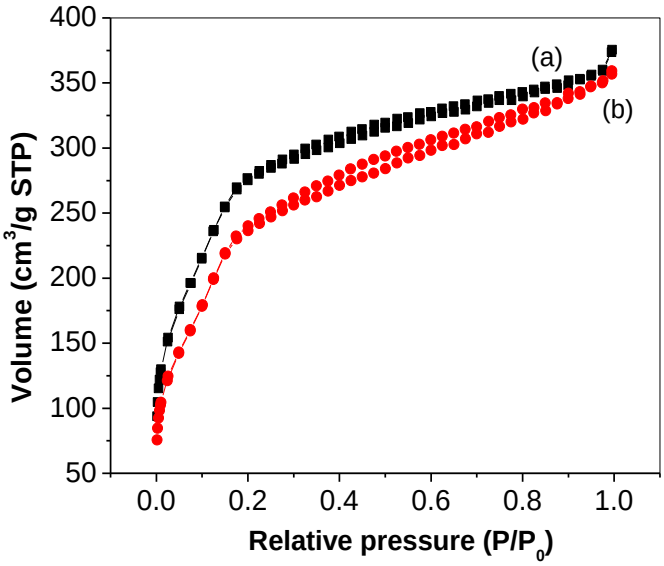

Figure 2.10 N_2 adsorption-desorption isotherm (a) MCM-41 and (b) Sn-MCM-41.

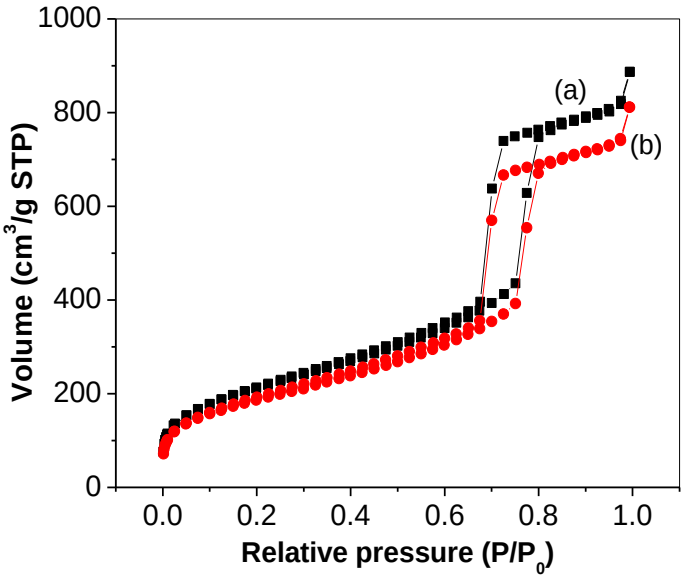

Figure 2.11 N_2 adsorption-desorption isotherm (a) SBA-15 and (b) Sn-SBA-15.

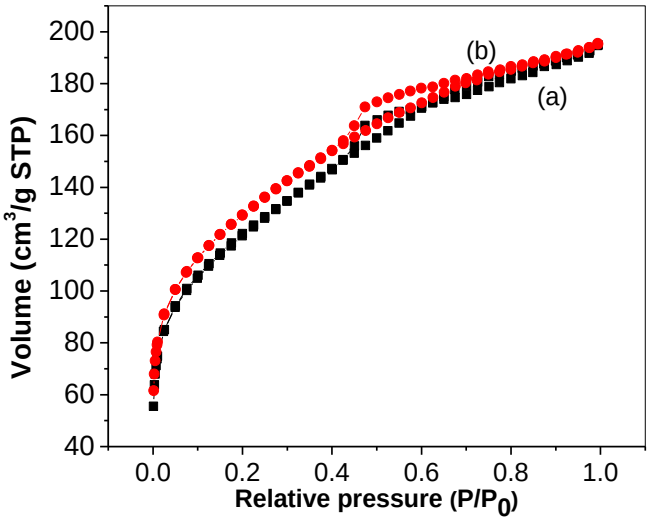

Figure 2.12 N_2 adsorption – desorption isotherm (a) SiO_2 and (b) Sn-SiO_2.

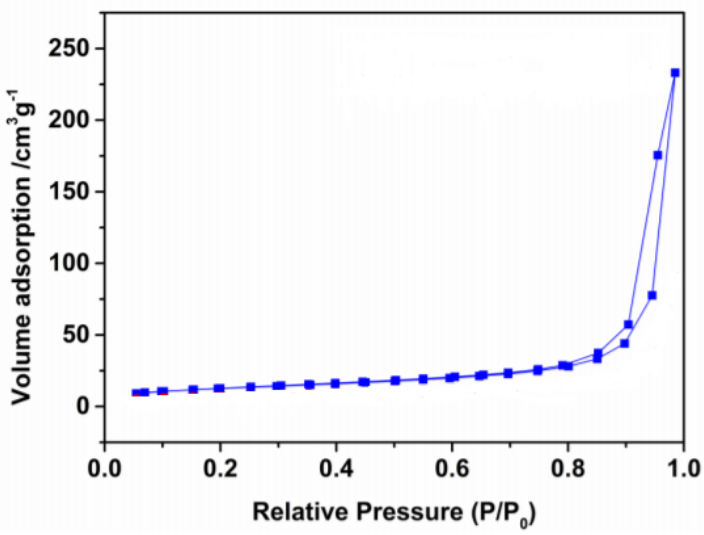

Figure 2.13 N_2 adsorption – desorption isotherm of Amberlyst-15 resin [80].

2.4.6 Infrared spectroscopy

The signal at 1635 cm^{-1} for all materials corresponds to the presence of H_2O and hydroxyl groups (Figure 2.14). At wavenumbers below 1300 cm^{-1}, the vibrations are attributed to silicate layers and equilibrium charge cations. There is no displacement of the Sn-O-Sn bond signal, 1050 cm^{-1}, at low wavenumber values, confirming tin was not incorporated into the catalyst structure [81]. SiO_2 materials stand out for having a lower band intensity at this wavenumber compared to MCM-41 and SBA-15 materials. The signal at 960 cm^{-1} in all materials is attributed to the Si–O stretching vibrations of Si–OH groups present at defect sites [82]. Particularly, the intensity of this band decreases with tin incorporation.

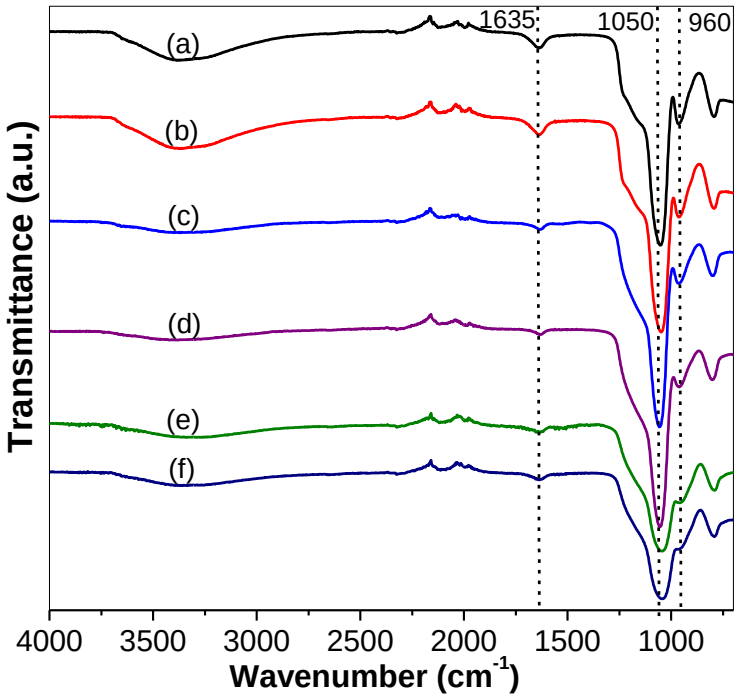

Figure 2.14 Infrared spectroscopy patterns of (a) MCM-41, (b) Sn-MCM-41, (c) SBA-15, (d) Sn-SBA-15, (e) SiO_2 and (f) Sn-SiO_2.

2.4.7 Ultraviolet–visible spectroscopy

All materials exhibit a strong UV-vis absorption band in the 200-290 nm region, Figure 2.15. However, with tin incorporation, there is a slight shift to the right of the band, which corresponds to Sn-O-Sn polymeric species in hexagonal coordination [83]. Shah *et al.* also reported for Sn-impregnated SBA-15 an absorption band at 250 nm similar to the one obtained in Figure 2.15 attributed to the presence of small amounts of hexa-coordinated tin species [88].

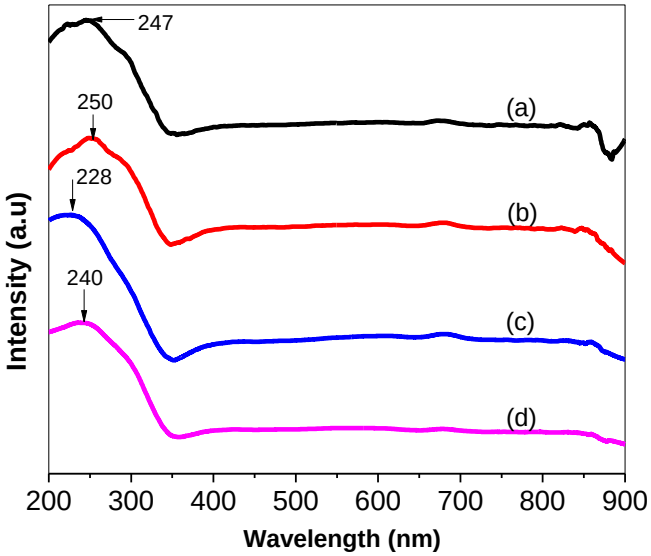

Figure 2.15 UV-vis analysis de (a) MCM-41, (b) Sn-MCM-41, (c) SBA-15 y (d) Sn-SBA-15.

Figure 2.16 shows the UV-vis spectrum of SiO_2 and Sn-SiO_2. The major SiO_2 absorption bands are located at wavelengths of 267 nm and 775 nm. When Sn is incorporated in SiO_2 the UV-vis spectrum of SiO_2 is modified, since the band at 267 nm disappears.

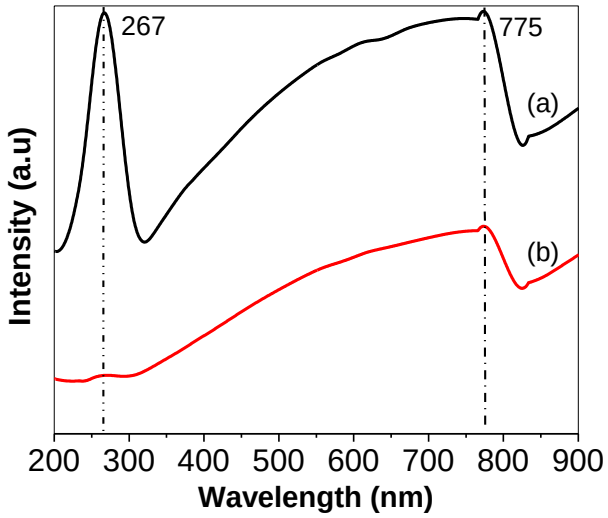

Figure 2.16 UV-vis pattern of (a) SiO_2, (b) Sn-SiO_2.

2.4.8 Temperature-programmed desorption of ammonia (NH_3-TPD)

Total acidity values in Table 2.5 were obtained as mmol of NH_3 per gram of catalyst from the calibration curve equation (2.4).

$$y = 3.3204x - 0.0023 \qquad (2.4)$$

with y: NH_3 volume, x: area under the curve.

MCM-41 exhibits a peak at 260 °C (Figure 2.17) indicating the presence of weak acid sites and Sn-MCM-41 shows a peak at 362 °C corresponding to sites of medium acidity, in addition, a peak at 577 °C in both materials reveals the presence of high acid sites [65].

SBA-15 exhibits a peak at 90 °C and Sn-SBA-15 at 110 °C (Figure 2.17) corresponding to very weak sites, and peaks below 180 °C are identified as physisorbed ammonia in very weak acid sites. In addition, a peak is presented at 625 °C in SBA-15 and another at 660 °C in Sn-SBA-15 that verify the presence of high acid sites [65].

SiO_2 and Sn-SiO_2 exhibit a peak at 89 °C (Figure 2.17) of very weak acid sites; additionally, a peak at 550 °C in SiO_2 and another at 620 °C in Sn-SiO_2 correspond to sites of high acidity [65].

The addition of tin to MCM-41 and SBA-15 supports does not significantly enhance total acidity values (Table 2.5). On the other hand, after tin impregnation, SiO_2 support experiences a 37.5 % acidity increase (0.25 to 0.40 mmol NH_3/g cat.). This suggests that the acidity increase is mainly associated to the type of support.

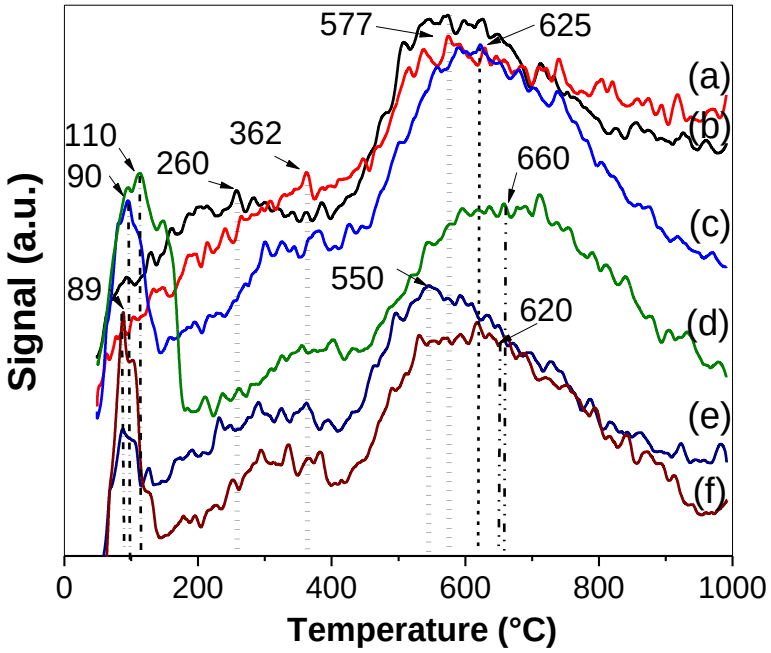

Figure 2.17 Temperature programmed desorption (NH_3-TPD) of (a) MCM-41,(b) Sn-MCM-41, (c) SBA-15, (d) Sn-SBA-15, (e) SiO_2 and (f) Sn-SiO_2.

Table 2.5 Total acidity of synthesized materials

Material	Total acidity (mmol NH_3/g cat.)
MCM-41	0.14
Sn-MCM-41	0.15
SBA-15	0.30
Sn-SBA-15	0.34
SiO_2	0.25
Sn-SiO_2	0.40

2.4.9 Hydrogen temperature-programmed reduction (TPR-H_2)

The H_2-TPR analysis (Figure 2.18) of the materials Sn-MCM-41 and Sn-SBA-15 shows a peak at 890 °C corresponding to SnOx species and two other peaks at 215 and 525 °C attributed to the presence of thin SnOx films. For the other materials (MCM-41, SBA-15, SiO_2 and Sn-SiO_2), no defined profiles were obtained.

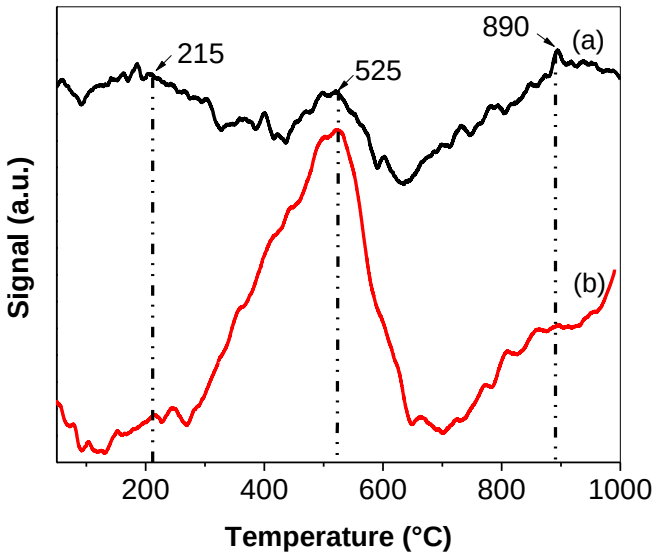

Figure 2.18 Hydrogen temperature programmed reduction (TPR-H_2) of (a) Sn-MCM-41 and (b) Sn-SBA-15.

2.4.10 Raman spectroscopy

The Raman spectrum of SiO_2, MCM-41 and Sn-SiO_2 show a band at 600 and 603 cm^{-1}, Figure 2.19. Brinker *et. al.* reported that amorphous silicas show a signal at 608 cm^{-1} which is indicative of cyclic trisiloxanes (3-membered rings) [84]. These species are preferably formed by dehydrating the surface of the amorphous silica [85]. In the frequency range 300-1400 cm^{-1}, the vibration bands at 798 cm^{-1} (Sn-MCM-41), 805 cm^{-1} (SBA-15, Sn-SBA-15, SiO_2, Sn-SiO_2) are associated with Si–O–Si asymmetric stretching modes and the bands at 980 cm^{-1} (Sn-SBA-15), 985 cm^{-1} (SBA-15), 983 cm^{-1} (Sn-MCM-41) are associated with Si–O–Si symmetric stretching modes [83]. Samples exhibit bands around 480-516 cm^{-1} which are attributed to Si-Si vibration mode [86]. All materials show an intense band around 500 cm^{-1}, which is attributed to cyclic tetrasiloxane rings (D1 defect mode) [87]. No peak corresponding to Sn oxides was observed, which should be present at 29.8, 33.2 cm^{-1} (corresponding to SnO), and 26.5, 36.0 cm^{-1} (assigned to SnO_2) [88].

In the case of MCM-41 materials, the bands at 1260, 1326 and 1388 cm^{-1} disappear with the incorporation of Sn, but a signal at 980 cm^{-1} appears. Sn-SBA-15 shows a new band at 1331 cm^{-1}, with respect to its support.

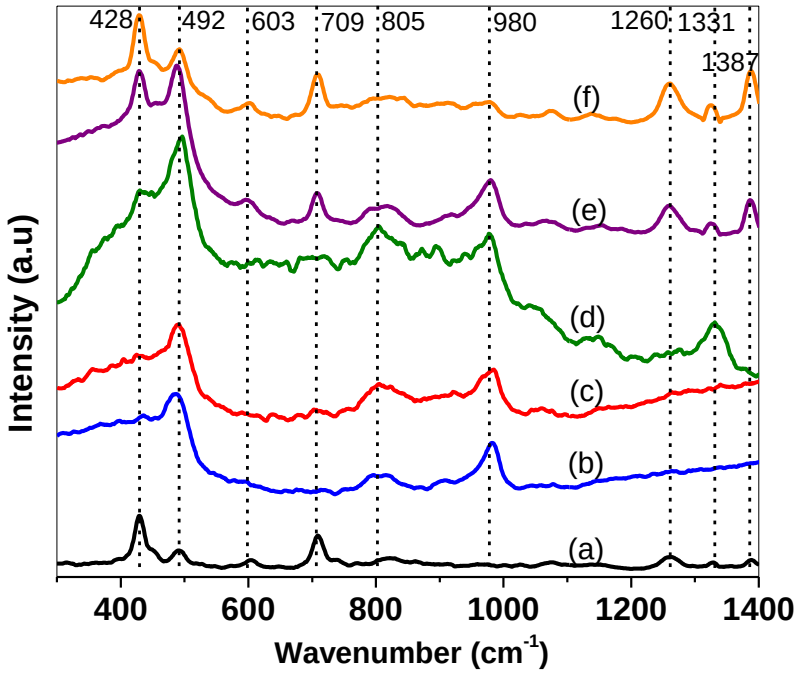

Figure 2.19 Raman analysis of (a) MCM-41, (b) Sn-MCM-41, (c) SBA-15, (d) Sn-SBA-15, (e) SiO_2 and (f) Sn-SiO_2.

2.4.11 Thermogravimetric analysis

The thermogravimetric profiles reveal a loss of weight of the materials due to physisorbed water at temperatures below 300 °C. In MCM-41, the temperature at which the first weight loss occurs (21.69 %) is shown in Figure 2.20, where a peak is highlighted at 49.27 °C, and the second occurs at 770 °C. In the case of Sn-MCM-41, the first weight loss (27.69 %) is recorded at 59.98 °C and the second loss (1.83 %) at 770 °C (Figure 2.21). SBA-15 presented the first weight loss (5.82 %) at 30.34 °C and subsequently a loss of 0.33 % at 770 °C (Figure 2.22). Finally, Sn-SBA-15 presents a pattern similar to its support, since the first loss (6.61 %) occurs at 39.1 °C and then loses 1.18 % at 780 °C (Figure 2.23). All the materials present a second loss that arises from 600 °C and is attributed to the oxidation of organic residue. The weight gain presented in the profiles can be

attributed to the readsorption of some compound present in the medium. In the case of SiO_2, a first weight loss (13.66 %) is registered at 50 °C and a second weight loss (3.45 %) appears at 425 °C (Figure 2.24). For Sn-SiO_2, the first weight loss (16.11 %) is observed at 52 °C and a second weight loss (3.07 %) at 530 °C (Figure 2.25). It is evident that MCM-41 and Sn-MCM-41 materials have a higher affinity for water than SBA-15, Sn-SBA-15, SiO_2 and Sn-SiO_2 since the percentages of water loss are higher. In turn, tin incorporated supports have higher affinity to water than their supports. It is desirable to work with materials having hydrophobic characteristics to avoid interactions with water molecules which may be present in the reaction medium and thus prevent it from inhibiting the production of the desired products.

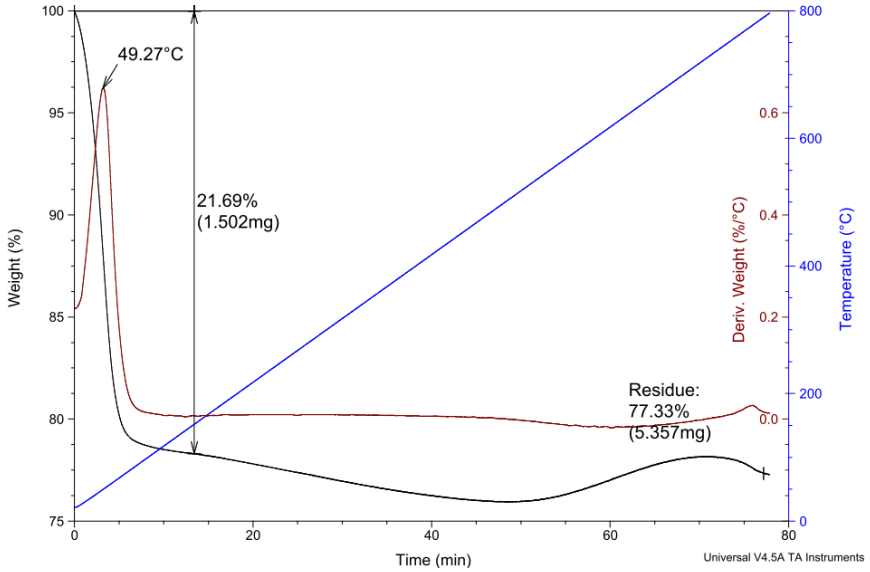

Figure 2.20 TGA analysis of MCM-41.

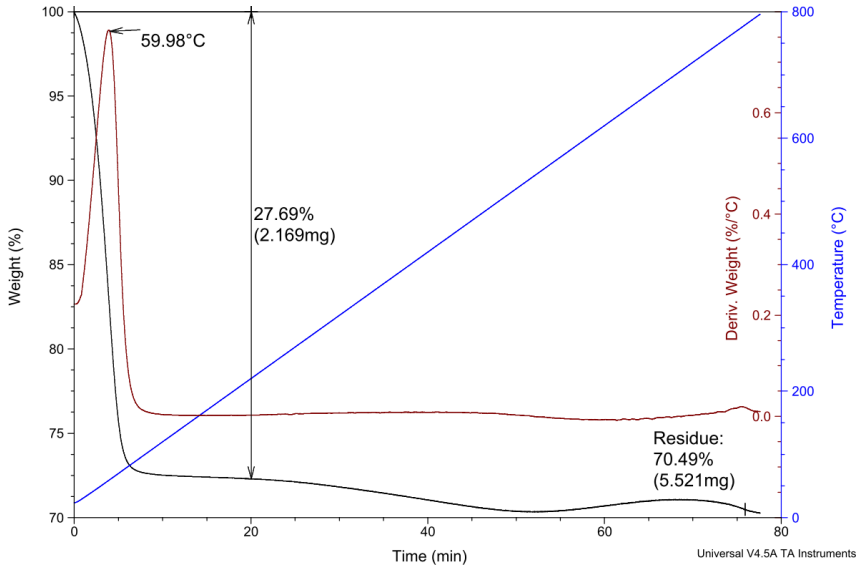

Figure 2.21 TGA analysis of Sn-MCM-41.

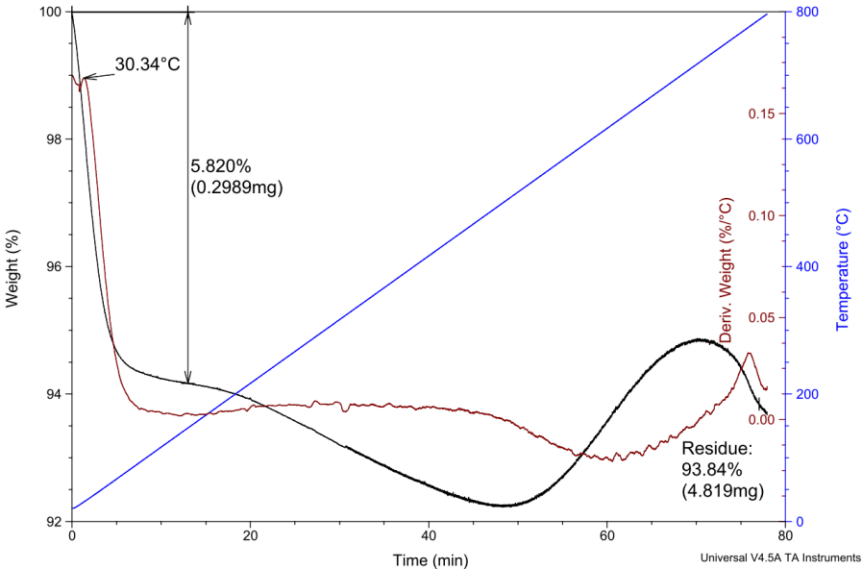

Figure 2.22 TGA analysis of SBA-15.

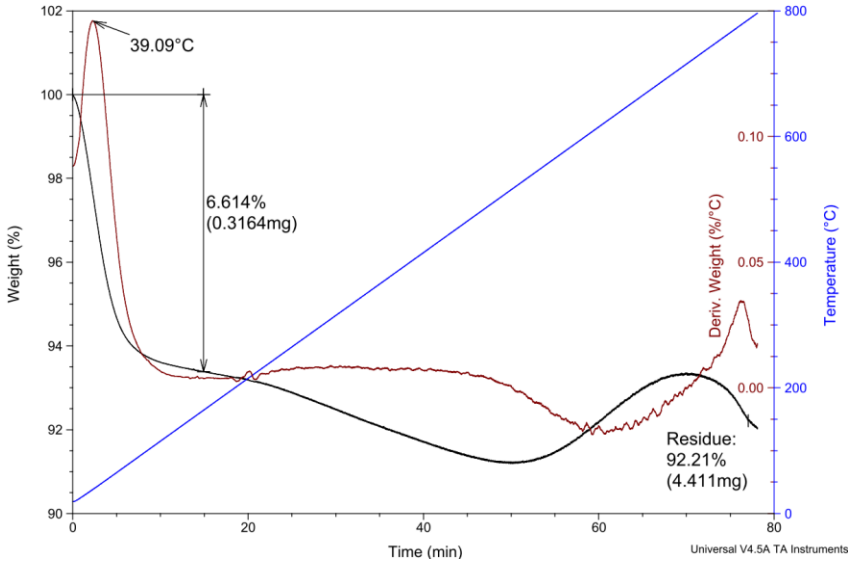

Figure 2.23 TGA analysis of Sn-SBA-15.

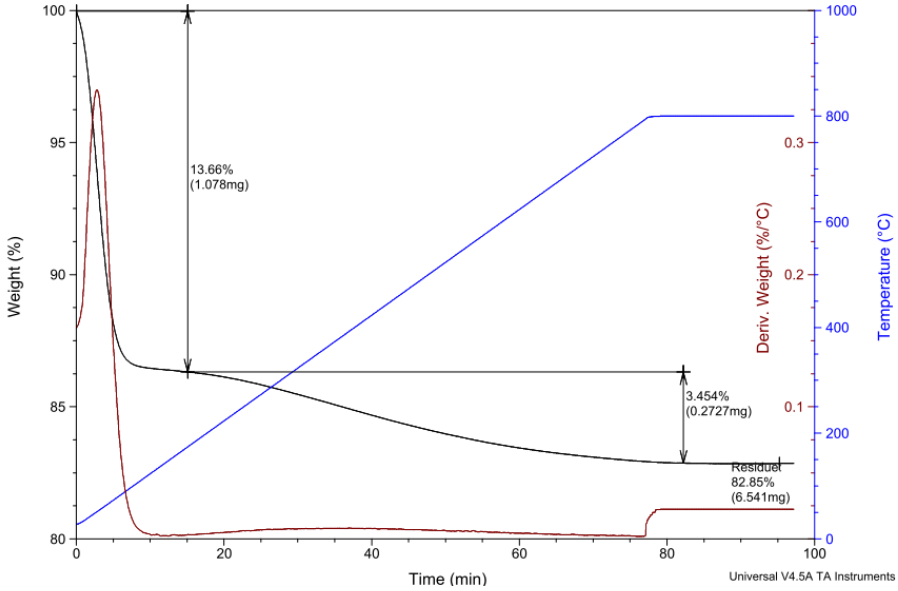

Figure 2.24 TGA analysis of SiO_2.

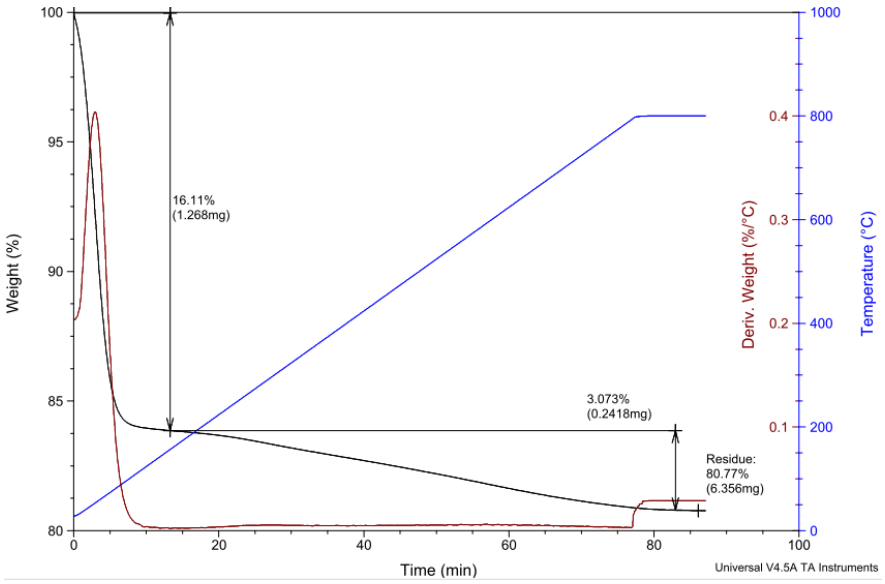

Figure 2.25 TGA analysis of Sn-SiO_2.

2.4.12 Chapter conclusions

Mesoporous silicas synthesized by incipient wetness impregnation have ordered hexagonal mesostructures and high surface area (470–596 m^2/g). SiO_2 synthesis by sol-gel method is a practical procedure that allows obtaining a suitable material as support. The adsorption and desorption isotherms of all synthesized materials are type IV, typical of mesoporous materials. SEM micrographs indicate that SBA-15 and Sn-SBA-15 exhibit a characteristic morphology of SBA-15 materials, represented in domains in the form of loops that are added to a microstructure, similar to wheat. According to XRD patterns, Sn-MCM-41 and Sn-SBA-15 retain their structure (the characteristic hexagonal features of the parent MCM-41 and SBA-15) after impregnation with $SnCl_2•2H_2O$. Silica gel particles appear as spheres exhibiting a rough surface with porous morphological structures. TPD-NH_3 analyses showed that MCM-41 and SBA-15 materials exhibit medium, weak and very weak acid sites, whereas SiO_2 materials display very weak and high acid sites. MCM-41 displays least amount of acid sites (0.14 mmol NH_3/ g cat.) whilst Sn-SiO_2 presents the highest amount (0.40 mmol NH_3/ g cat.). UV-vis patterns of Sn-MCM-41 and Sn-SBA-15 indicate the presence of Sn-O-Sn polymer species in hexagonal coordination. In SiO_2 and Sn-SiO_2 the absence of the 267 nm band in Sn-SiO_2 is attributed to the incorporation of Sn species. Raman spectrum of SBA-15 and SiO_2 materials

reveals vibration bands with Si-O-Si asymmetric stretching modes and for SBA-15 and MCM-41 materials Si-O-Si symmetric stretching modes. According to the thermogravimetric analysis (TGA), tin incorporated materials have higher affinity to water than their supports, thus Sn-SBA-15 (least total weight loss of 7.79 %) exhibits most desirable hydrophobic characteristics, avoiding interactions with water molecules present in the reaction medium.

CHAPTER 3

CHAPTER 3. NOPYL ACETATE SYNTHESIS

3.1 Introduction

In this chapter the activity of the synthesized materials in terms of conversion, selectivity, and / or initial reaction rates is presented. The conditions required for kinetic studies, the effect of particle size and stirring rate on catalyst activity was evaluated. Heterogeneity of prepared materials was analyzed and reaction mechanisms are proposed and discussed.

3.2 Experimental

3.2.1 Blank reactions

Esterification reaction using no catalysts were performed in a 25 mL three-neck round-bottom flask, coupled to a condenser. 10 mL of nopol/toluene solution (0.25 M) was used with acetic acid (99.5 % Merck) at a 1:2, 1:1 and 2:1 acid: alcohol molar ratio. The reaction mixture was heated at 80 °C and stirred at 750 rpm. Samples were analyzed by GC.

3.2.2 Catalytic activity evaluation

The esterification reaction was performed in a 25 mL three-neck round-bottom flask, coupled to a condenser. Catalyst and nopol/toluene solution (0.25 M) were loaded into the reactor, which was magnetically stirred and heated to the desired temperature. Acetic acid (99.5 % Merck) was finally added. Samples were collected at specified reaction times (1, 2, 8 and 24 h) and analyzed by gas chromatography (GC).

3.2.2.1 Effect of reaction parameters on the esterification of nopol

3.2.2.1.1 Acid: alcohol molar ratio effect

The effect of acid to alcohol molar ratio was studied by varying the molar ratio (1:2, 1:1 2:1) at the following reaction conditions: 20 mL of nopol/toluene solution (0.25 M), 80 °C, catalyst (Amberlyst-15) loading 1.25, 2.5, 5 and 6.25 mg/mL and stirring speed of 750 rpm.

3.2.2.1.2 Effect of catalyst loading

Study of effect of catalyst loading on nopyl acetate yield was performed over Amberlyst-15, Sn-MCM-41 and Sn-SBA-15. In the case of Amberlyst-15, the catalyst loading was set at 1.25, 2.5, 3.7 and 6.1 mg/mL (20 mL of nopol/toluene solution (0.25 M), 80 °C and stirring speed of 750 rpm).

3.2.2.1.3 Effect of catalyst type

In this study, four heterogeneous catalysts (Amberlyst-15, Sn-MCM-41, Sn-SBA-15, Sn-SiO_2) and one homogeneous catalyst (*p*-toluenesulfonic acid, *p*-TSA) were tested in the esterification of nopol with acetic acid at 50, 80 °C, 750 rpm, acetic acid: nopol molar ratio = 2:1, nopol/ n-hexane, toluene 0.25 M (10 mL), 3.75 mg catalyst/mL.

3.2.2.1.4 Effect of solvent

The effect of different solvents on the conversion of nopol was evaluated using acetonitrile, ethanol, ethyl acetate, toluene, n-hexane, and holding other reaction parameters constant (50 – 80 °C, 750 rpm, nopol/solvent 0.25 M (20 mL), acetic acid 99.5 %, Amberlyst-15 (3.7 mg/mL)). Table 3.1 displays physicochemical properties of the solvents tested, reaction temperatures were chosen according to boiling points of solvents. Amberlyst-15 ion exchange resin has been a reference material with respect to literature reports, and therefore was used to perform these reactions.

Table 3.1 Physical and chemical properties of solvents used [89].

Property/ solvent	Acetonitrile	Ethyl acetate	Ethanol	n-Hexane	Toluene
P_b (°C)	82	77	79	69	111
Solubility in H_2O (%) @ 20°C	∞	8.5	∞	0.014	0.05
Ɛ @ 20°C	37.5	6.02	22.4	1.9	2.38
Polarity	Aprotic dipolar	Aprotic non-polar	Protic	Aprotic non-polar	Aprotic non-polar

P_b: boiling point, Ɛ: dielectric constant

3.2.2.2 Esterification of nopol with acetic anhydride

The esterification reaction was performed in a 25 mL three-neck round-bottom flask, coupled to a condenser. Catalyst loading was fixed at 3.7 mg/mL, 10 mL of nopol/toluene solution (0.25 M) was used with acetic anhydride (98.5 %, Merck) at a 3:1 acid – anhydride: alcohol ratio. The reaction mixture was heated at 80 °C and stirred at 750 rpm. Samples were analyzed by GC.

3.2.2.3 Heterogeneity tests

Heterogeneity tests are proof of catalyst heterogeneous nature by establishing if active species leach or not under reaction tested conditions. For heterogeneity studies, the following procedures were followed:

Test 1. The suspension of catalyst in a mixture of solvent and nopol was stirred for 20 minutes. After removal of the catalyst, acetic acid was added to the filtrate and the reaction mixture was analyzed after one hour of reaction. If products are obtained, there may be leaching of the active species.

Test 2. The suspension of catalyst in the mixture of acetic acid and solvent was stirred for 20 minutes. After removal of the catalyst, nopol was added to the filtrate and the reaction mixture was analyzed after one hour of reaction. If products are obtained, there may be leaching of the active species.

Test 3. The reaction was carried out to obtain a conversion lower than 10 %, after separating the solid, the liquid was analyzed. The reaction continued for more than one hour. If the activity increased, there may be leaching of the active species.

Test 4. Catalyst reuse. The recovered catalyst was reused as many times as possible, under equivalent reaction conditions to those used with the fresh catalyst. The catalyst was washed with acetone and dried in an oven. If the catalyst activity decreases after each reaction, catalyst deactivation may be possible through another mechanism different to leaching.

3.2.3 Experiments to determine the kinetics of the esterification of nopol with acetic acid

The esterification reaction was performed in a 25 mL three-neck round-bottom flask, coupled to a condenser (Figure 3.1). Catalyst loading was fixed at 3.7 mg/mL; 10 mL of nopol/toluene solution (0.25 M) was used with acetic acid (99.5 %) at a 1:1 acid: alcohol molar ratio. The reaction mixture was heated at 50 °C and stirred at 1000 rpm using a Heidolph magnetic stirrer with temperature controlled hot plate. Amberlyst-15 was used as catalyst because it displays the highest nopol conversion and its nopyl acetate selectivity increased with time.

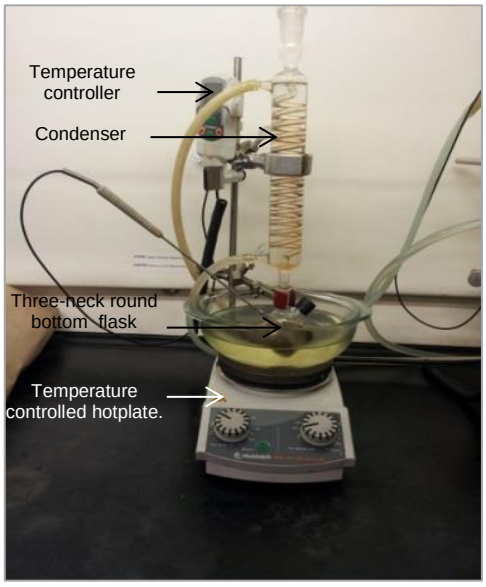

Figure 3.1 Reaction setup.

Catalyst and nopol/toluene solution (0.25 M) were loaded into the reactor, which was heated to the desired temperature. Acetic acid was added finally. This was taken as the starting time of the reaction (zero time) for a run. For kinetic measurements, samples of the reaction mixture were collected at specified reaction times (1, 2, 8 and 24 h) and analyzed by gas chromatography.

For an esterification reaction,

$$A + B \leftrightarrow E + W \qquad (1.1)$$

the reaction rate equation can be written as,

$$-r_B = -\frac{dC_B}{dt} = C_{B0}\frac{dX_B}{dt} = k_1 C_A C_B - k_2 C_E C_W = k_1 C_{B0}^2 (1 - X_B)^2 - k_2 (C_{B0} X_B)^2 \qquad (3.1)$$

In equilibrium, $-r_B = 0$, the equilibrium constant is expressed by,

$$K = \frac{C_{Ee} C_{We}}{C_{Ae} C_{Be}} = \frac{X_{Be}^2}{(1 - X_{Be})^2} \qquad (3.2)$$

3.2.3.1 Tests to determine the effect of particle size on the initial reaction rate

The equations for determining the initial reaction rates of nopol and nopyl acetate at average particle sizes of 40, 49, 58 and 76.5 *μ*m were found from plots of concentration (M) of nopol and nopyl acetate vs reaction time (min). The reaction rates found correspond to the slopes of the equations in units of mmol/(g.s).

If r_A is the rate of formation of A per unit volume (mol/s•mL), the reaction rate is defined as:

$$r_A = \frac{dC_A}{dt} \qquad (1.16)$$

This definition is valid only for a batch reactor of constant volume [42].

These reactions were performed at the conditions displaying highest catalytic performance over Amberlyst-15: 10 mL of nopol-toluene solution (0.25 M), acid: alcohol molar ratio of 2:1, 80 °C, catalyst loading 3.7 mg/mL and stirring at 750 rpm.

3.2.3.2 Tests to determine the effect of stirring on the initial reaction rate

The effect of the stirring rate on the conversion of acetic acid and nopol was determined, plotting the concentration of acetic acid and nopol with respect to time and the equation that best represented the data for each stirring speed was determined.

The slopes were obtained from the linear regression in mmol/(g.s) at the following reaction conditions: 10 mL nopol/ toluene solution (0.25 M), acid: alcohol molar ratio 2: 1,

80 °C, 500, 750 and 1000 rpm, catalyst loading 3.7 mg/mL and average particle size of 42 μm.

3.2.4 Chromatographic method

The reaction samples collected at different reaction times (0, 60, 120, 480, 540, 1440 min) were analyzed on an Agilent 7890A / MSD gas chromatograph equipped with a FID detector and DB-1 capillary column (30 m x 0.320 mm x 0.25 μm). He (1 mL / min) was used as entrainment gas and a split ratio of 25: 1. The oven was maintained at 70 °C for 3 min and then the temperature was raised to 180 °C at 10 °C/min for 1 minute. The quantification of nopyl acetate, acetic acid and nopol was performed by multipoint calibration using dodecane as internal standard. Compound retention times are shown in Table 3.2.

Table 3.2 Retention times of the compounds of interest

Compound	Retention time, min
Dodecane	10.564
Nopol	11.519
Nopyl acetate	13.412

The conversion of acetic acid (A.A) and nopol was determined with Equation (3.3) and the selectivity to nopyl acetate (nop. ac.) with Equation (3.4).

$$\text{Conversion (\%)} = \frac{(C_i - C_f)_{reagent}}{(C_i)_{reagent}} * 100\ \% \qquad (3.3)$$

$$\text{Selectivity (\%)} = \frac{(C_f)_{nop.\ ac.}}{(C_i - C_f)_{nopol}} * 100\ \% \qquad (3.4)$$

C_i: initial concentration, C_f: final concentration

3.2.5 Flow diagram of experimental procedures

Figure 3.2 displays a flow diagram with the experimental procedures carried out to study the nopol esterification.

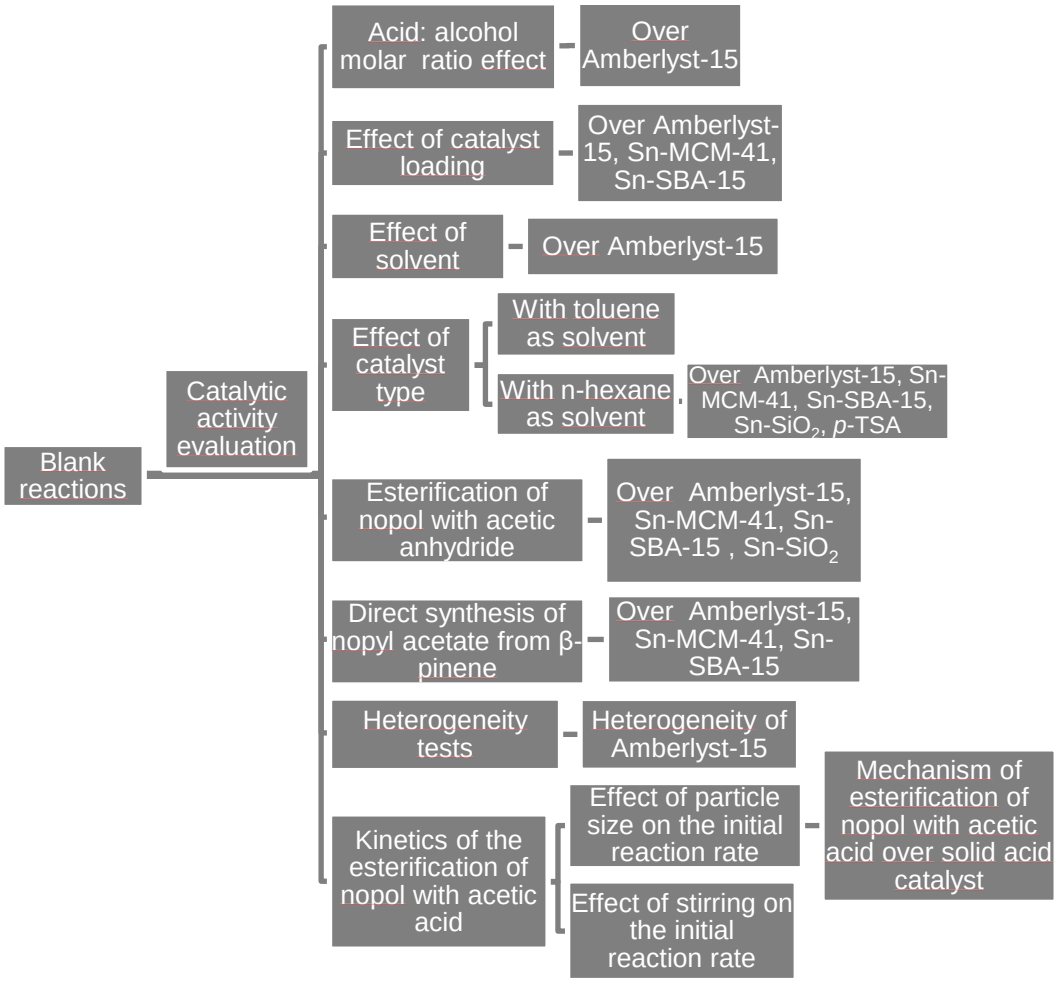

Figure 3.2 Flow diagram of experimental procedures.

3.3 Results

3.3.1 Blank reactions

The results of catalytic activity in the esterification reaction of nopol with acetic acid without using catalyst are shown in Table 3.3.

It is evident that no production of nopyl acetate is present, probably due to the formation of side products analyzed by mass spectrometry, such as 1,3,5 – cycloheptatriene, bicyclo (3,1,1) heptan – 2 – one, 6, 6 – dimethyl -, 1(R) and spiro (4,4) none – 1,3 – diene, 1,2 –dimethyl (Figure 3.3).

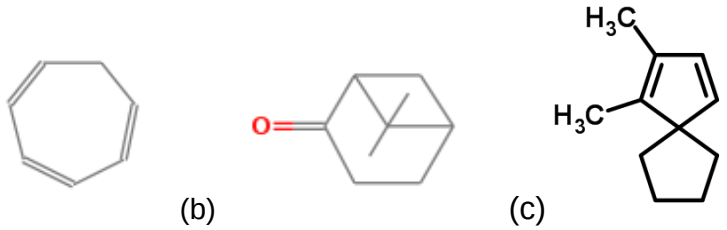

(a) (b) (c)

Figure 3.3. Nopyl acetate production side products. (a) 1,3,5 – cycloheptatriene, (b) bicyclo (3,1,1) heptan – 2 – one, 6, 6 – dimethyl -, 1(R), (c) 1,2 –dimethyl spiro (4,4) none – 1,3 – diene.

The effect of the acid: alcohol molar ratio on the reaction is decisive, since no activity was obtained at a 1:2 molar ratio and at a 1:1 molar ratio values are lower with respect to the 2:1 ratio.

Table 3.3 Blank reactions at different acid: alcohol molar ratios

Acid:alcohol	t (min)	X_{AA}	X_{nopol}	$S_{nop.\ ac.}$
1:2	30	39	0.0	0.0
	60	32.2	0.0	0.0
	90	40.3	0.0	0.0
	120	40.1	0.0	0.0
	480	85.5	3.0	0.0
	1440	96.3	0.0	0.0
1:1	0	31.8	7.0	0.0
	30	28.1	8.4	0.0
	90	31.4	5.9	0.0
	120	29.9	5.9	0.0
	480	31.0	3.8	0.0
	1440	35.0	4.2	0.0
2:1	30	4.0	12.8	0.0
	60	8.3	11.4	0.0
	90	8.3	11.4	0.0
	120	3.7	6.4	0.0
	480	6.5	8.2	0.0
	1440	20.6	7.0	0.0

Conversion (X), selectivity (S). Reaction conditions: 80 °C, 750 rpm, nopol/toluene solution 0.25 M (20 mL), acetic acid (99.5 %).

3.3.2 Acid: alcohol molar ratio effect

At 1:1, 1:2 and 2:1 acid: alcohol molar ratio, nopol conversion is similar varying between 25 –100 % at different reaction times (Figure 3.4). With the increase in acetic acid to nopol mole ratio from 1:1 to 2:1, the selectivity increased for all reaction times except at 30 min, as expected based on the Le Châtelier principle, the increase of the amount of one of the reactants enhances the production of the ester [90]. Yang *et al*. also found that an appropriate excess of acid rather than alcohol appears to favor ester selectivity using Amberlyst-15 in the esterification of acrylic acid with 1,4 butanediol [91]. The selectivity to nopyl acetate reached 8.2 % in the presence of Amberlyst-15 catalyst for an acetic acid to nopol mole ratio equal to 2:1 and a reaction time of 90 and 120 min. Mazotti *et al.* suggested that the change in the reaction rate with change in the acid to alcohol mole ratio is a consequence of the selective sorption of the reactants on the resin. It has been found that the initial reaction rate of esterification reactions over cation exchange resins have a maximum respect to the acid to alcohol mole ratio. It was reported that initial rates depended on the acid to alcohol mole ratio according to the overall alcohol concentration, the overall acid concentration, and the reaction temperature [92].

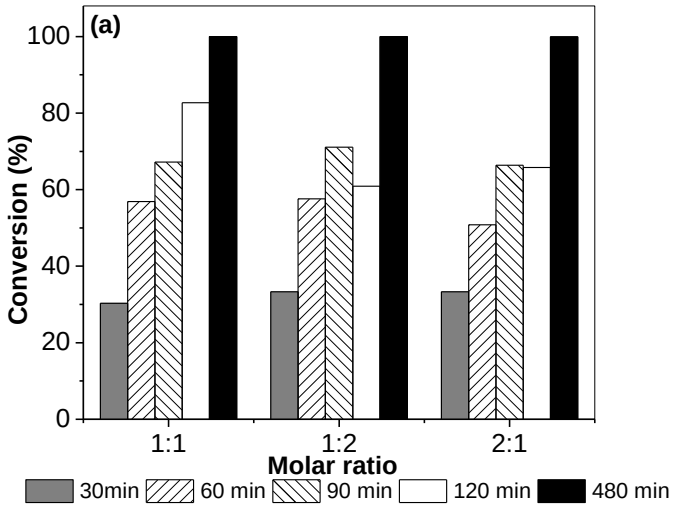

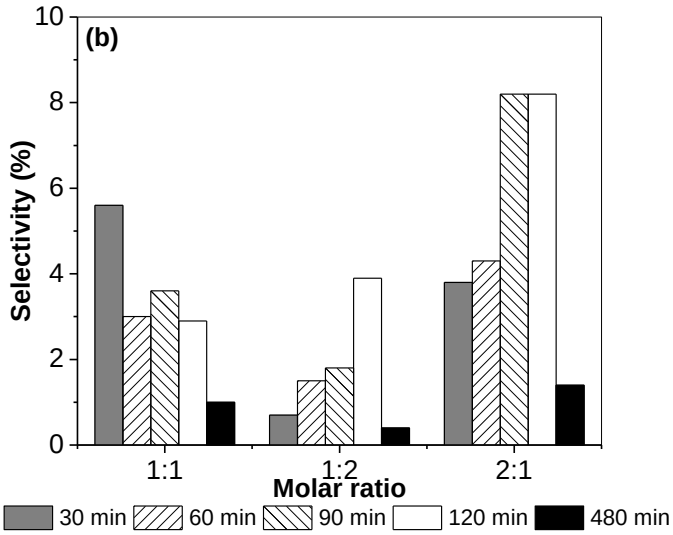

Figure 3.4 Nopol conversion (a), nopyl acetate selectivity (b) in acid: alcohol molar ratio effect. Reaction conditions: 80 °C, 750 rpm, nopol/solvent solution 0.25 M (20 mL), acetic acid, Amberlyst-15 (6.1 mg/mL).

3.3.3 Effect of catalyst loading

The effect of catalyst concentration on the esterification reaction was evaluated over Amberlyst-15, Sn-MCM-41 and Sn-SBA-15, for establishing a specific concentration that allows to obtain the highest ester selectivity.

3.3.3.1 Amberlyst-15

Using a 6.1 mg/mL catalyst loading (Table 3.4), nopol conversion (50.8 %) and nopyl acetate selectivity (4.3 %) increase to 65.8 % and 8.2 %, respectively from 60 to 120 min. With 3.7 mg/mL, low product selectivity (1 %) is obtained at 1440 min, suggesting that the reaction reaches its end at 480 min with remaining catalyst loadings. The reaction is low with 3.6 and 4.9 mg/mL catalyst concentration, thus requiring more time to reach an alcohol conversion over 50 %. The most significant nopol conversion (66.4 %) and ester selectivity (8.2 %) resulted with 6.1 mg/mL of catalyst at 90 min. Catalyst loading notoriously affects alcohol conversion and ester production due to an availability increase of H^+ ions provided by the resin. Nevertheless, an amount of active catalyst sites higher than those required by the

reactant molecules leads to a selectivity lowering, as seen with 7.3 and 8.5 mg/mL of material.

Table 3.4 Conversion of nopol and nopyl acetate selectivity using Amberlyst-15

Amberlyst-15 (mg/mL)	Time (min)	X nop (%)	S nop. ac. (%)
3.7	60	40.9	4.6
	120	49.3	3.7
	480	90.7	6.3
	540	n.d	n.d
	1440	98.2	1.0
4.9	60	39.6	1.5
	120	76.3	3
	480	100	1
	540	n.d	n.d
	1440	100	0
6.1	60	50.8	4.3
	120	65.8	8.2
	480	99.9	1.4
	540	n.d	n.d
	1440	100	0
7.3	60	56.6	4.7
	120	84.1	4.7
	480	98.6	0.6
	540	n.d	n.d
	1440	100	0
8.5	60	70.5	5.25
	120	94.2	3.75
	480	100	0
	540	n.d	n.d
	1440	100	0

Reaction conditions: 80 °C, 750 rpm, nopol/ toluene solution 0.25 M (20 mL), acetic acid (99.5%), acid: alcohol = 2:1, Amberlyst-15 (3.7 – 8.5 mg/mL), n.d: no data.

3.3.3.2 Sn-SBA-15

The catalytic activity in nopol esterification is shown in Table 3.5 using different amounts of Sn-SBA-15 catalyst.

Highest conversions of nopol (11.8 - 16.2 %) are achieved using 3.7 and 4.9 mg/mL of Sn-SBA-15, while best selectivities (4.6 - 7.5 %) are displayed with 3.7 to 6.1 mg/mL of material.

Table 3.5 Esterification of nopol over Sn-SBA-15. Conversion of acetic acid, nopol and nopyl acetate selectivity.

Sn-SBA-15 (mg/mL)	Time (min)	XAA (%)	X nopol (%)	S nop. ac. (%)
2.4	60	3.1	0.0	0.0
	120	0.0	3.6	0.0
	480	23.6	4.3	1.5
	540	n.d	n.d	n.d
	1440	66.0	0.0	0.0
3.7	60	4.8	15.2	0.2
	120	4.1	11.8	0.7
	480	5.4	4.8	7.5
	540	n.d	n.d	n.d
	1440	14.5	10.5	5.2
4.9	60	7.6	16.2	0.0
	120	2.8	15.6	1.5
	480	1.8	12.0	3.4
	540	n.d	n.d	n.d
	1440	37.8	0.0	0.0
6.1	60	40.6	0.0	0.0
	120	42.4	10.2	2.0
	480	n.d	n.d	n.d
	540	57.8	11.4	4.6
	1440	82.5	0.0	0.0

Reaction conditions: 80 °C, 750 rpm, nopol/toluene solution 0.25 M (20 mL), acetic acid (99.5 %), acid: alcohol = 2:1, n.d: no data.

3.3.3.3 Sn-MCM-41

The catalytic activity in nopol esterification over Sn-MCM-41 as catalyst is shown in Table 3.6.

It is noteworthy that when 2.4 mg/mL of material is used there is no product formation and no conversion of nopol, probably due to the low amount of catalyst used. The highest conversion of nopol (13.9 %) is observed at 480 min using 3.7 mg/mL of catalyst, while the best selectivities (21 – 25 %) are obtained with 3.7 and 6.1 mg/mL of material.

Table 3.6 Acetic acid and nopol conversion, nopyl acetate selectivity in the nopol esterification over Sn-MCM-41

Sn-MCM-41 (mg/mL)	t (min)	X_{AA} (%)	X_{nopol} (%)	$S_{nop.\ ac.}$ (%)
2.4	60	20.7	0.0	0.0
	120	25.0	0.0	0.0
	480	33.3	0.0	0.0
	540	n.d	n.d	n.d
	1440	57.9	0.0	0.0
3.7	60	18.0	0.0	0.0
	120	24.5	1.6	0.0
	480	42.1	13.9	2.7
	540	n.d	n.d	n.d
	1440	64.0	3.1	21.2
4.9	60	20.2	0.0	0.0
	120	22.8	0.9	0.0
	480	43.2	2.1	14.2
	540	n.d	n.d	n.d
	1440	59.2	0.0	0.0
6.1	60	42.7	0.0	0.0
	120	43.6	9.3	2.1
	480	n.d	n.d	n.d
	540	52.7	2.2	24.9
	1440	73.7	8.3	9.7

Reaction conditions: 80 °C, 750 rpm, nopol/ toluene solution 0.25 M (20 mL), acetic acid (99.5 %), acid: alcohol = 2:1, n.d: no data.

For all materials, catalyst concentration increase causes a conversion rise. In the case of Amberlyst-15 such behavior is expected because the number of resin functional groups increases, and this will cause the growing of the reaction rates. At longer reaction times,

the influence of thermodynamic limitations will be dominant and the effect of catalyst concentration on reaction rates is expected to become less pronounced [92].

3.3.4 Effect of solvent

Amberlyst-15 was used in presence of different solvents for nopol esterification with acetic acid due to the high conversion obtained with this catalyst. Highest nopol conversion (98.2 %) was obtained using toluene, followed by ethyl acetate (53.1 %) (Figure 3.5). Ester selectivity decreases in the following order: n-hexane (50 °C) > ethyl acetate (70 °C) > toluene (80 °C) > ethanol (60 °C) > acetonitrile (65 °C). At 120 min a high selectivity (10.3 %) over n-hexane is noticeable, though a low nopol conversion (5.8 %) is observed at these reaction conditions. Thus, ester production is favored by the use of non-polar solvents such as n-hexane, toluene and ethyl acetate.

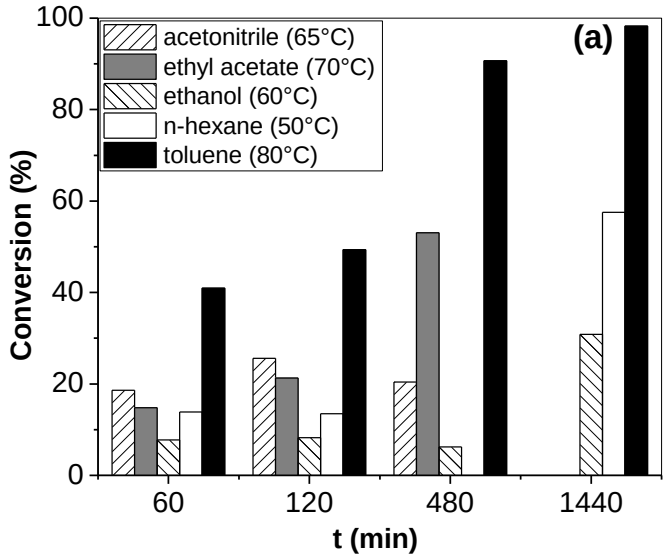

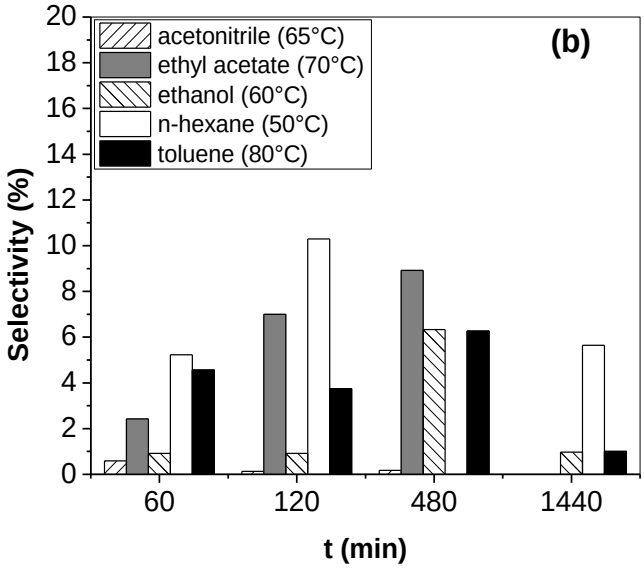

Figure 3.5 (a) Nopol conversion and (b) nopyl acetate selectivity using different solvents over Amberlyst-15. Reaction conditions: 50 - 80°C, 750 rpm, nopol/solvent 0.25 M (20 mL), acetic acid 99.5 %, Amberlyst-15.

3.3.4.1 Nopol esterification using toluene and n-hexane as solvents

According to previous results, working with toluene yields best nopol conversions and with n-hexane best ester selectivities (Figure 3.5). Therefore, different volumetric toluene:n-hexane ratios (50:50, 30:70 and 70:30) were tested in the esterification of nopol using Amberlyst-15 aiming to achieve better catalytic performance.

Figure 3.6 shows the catalytic results in the reaction using toluene and n-hexane separately as solvents.

It is observed that the higher conversion of nopol and selectivity to nopyl acetate in the presence of toluene is reached at 1440 min of reaction. High conversion values were observed at all reaction times (40.9 - 90.7 %).

Conversion to nopol (Figure 3.6) using n-hexane is low (5.8 %) at 480 min. However, the selectivity to the ester at this time is high (55.7 %). It is noticeable that n-hexane favors nopyl acetate selectivity and toluene, nopol conversion. Apolar aprotic nature of both solvents induces a greater substrate transformation. High ester selectivity over n-

hexane can be due not only to its apolar aprotic nature but also to low solubility (0.01 %, 20 °C) in this solvent of the water produced in the esterification reaction.

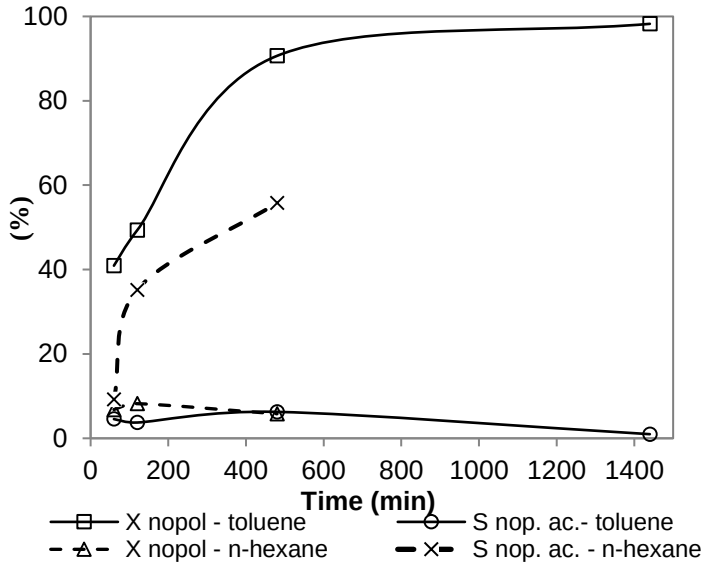

Figure 3.6 Amberlyst-15 activity using toluene and n-hexane as solvent. Reaction conditions: nopol/ n-hexane, nopol/ toluene solution 0.25 M (20 mL), acetic acid (99.5 %), 50 °C (using n-hexane), 80 °C (using toluene), 750 rpm, Amberlyst-15 (3.75 mg/mL).

Figure 3.7 shows the activity of Amberlyst-15 in the esterification reaction using toluene / n-hexane as solvent at different volumetric ratios at 960 min.

The conversion of nopol does not exceed 32.9 % at the three toluene: n-hexane volumetric ratios of 50:50, 30:70 and 70:30. The highest selectivity to nopyl acetate (14.3 %) is obtained with the 30:70 ratio as a result of the presence of a greater amount of n-hexane in the reaction medium. Increase in nopol conversion in presence of n-hexane is evident by adding toluene, since it went from 8.2 % to 32.9 %.

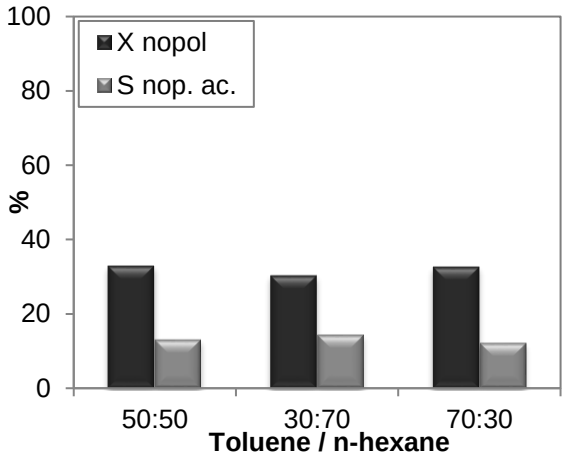

Figure 3.7 Amberlyst-15 activity in the esterification of nopol using different ratios of toluene: n-hexane as solvent. Reaction conditions: Amberlyst-15 (75 mg), nopol/ toluene 0.25 M (20 mL), acetic acid (99.5 %), 80 °C, 750 rpm, 960 min.

3.3.5 Catalyst effect on the esterification of nopol

3.3.5.1 Preliminary catalyst evaluation

The catalytic activity over Amberlyst-15 (A-15), Sn-MCM-41, Sn-SBA-15 catalysts is shown in Figures 3.8 (a, b) and 3.9.

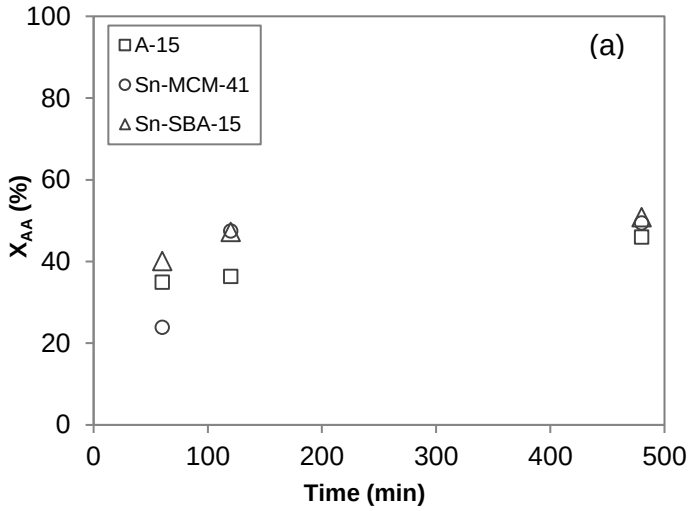

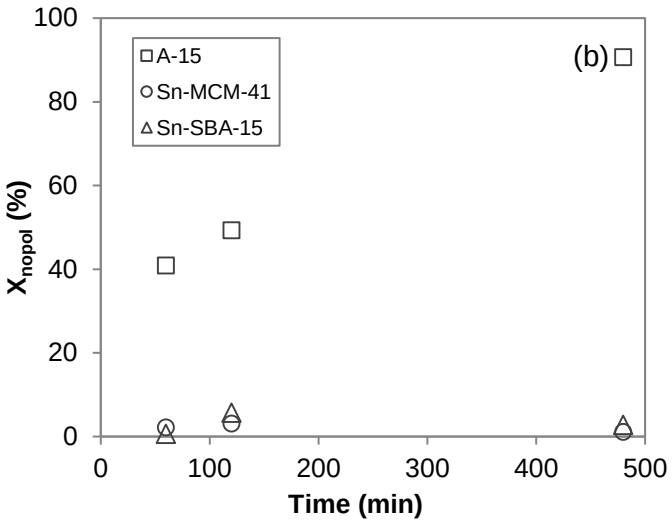

Figure 3.8 (a) Acetic acid (AA), and (b) nopol conversion over solid heterogeneous catalysts. Reaction conditions: 750 rpm, 80 °C, nopol/toluene solution 0.25 M (20 mL), acetic acid 99.5 %, catalyst (3.75 mg/mL).

A similar acetic acid conversion at all reaction times in the presence of Sn-MCM-41 and Sn-SBA-15 are observed in Figure 3.8 (a). Undoubtedly, the highest conversion (50.9 %) is reached at 480 min with Sn-SBA-15.

The conversion of nopol (Figure 3.8 (b)) is low over mesoporous materials Sn-MCM-41 and Sn-SBA-15 (0.6 - 5.7 %). However, conversion is high (98.2 %) over Amberlyst-15.

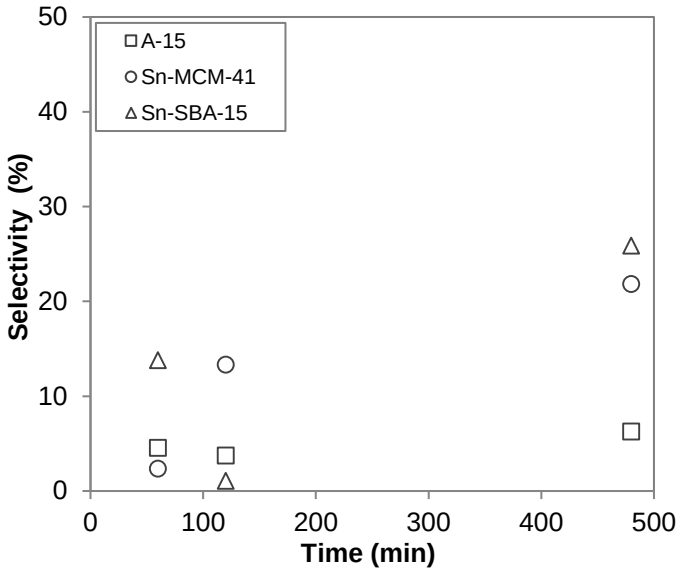

Figure 3.9 Selectivity to nopyl acetate over solid heterogeneous catalysts. Reaction conditions: 750 rpm, 80 °C, nopol/ toluene solution 0.25 M (20 mL), acetic acid 99.5 %, catalyst (3.75 mg/mL).

At 480 min, selectivity to nopyl acetate reached 25.9 % over Sn-SBA-15, followed by Sn-MCM-41 with 21.8 % and Amberlyst-15 with 6.3 % (Figure 3.9). Both Sn-SBA-15 and Amberlyst-15 experienced a decrease at 120 min, possibly due to a displacement in the equilibrium toward the reagents. A high surface area of Sn-SBA-15 (470.5 m^2/g) and Sn-MCM-41 (575.8 m^2/g) with Sn active species induce a better ester selectivity compared to Amberlyst-15. Interestingly, Amberlyst-15 with highest acidity value (4.7 mmol NH_3/g cat.) displays exceedingly much higher nopol conversion (98.2 %) than silicious materials (0.6 -0.57 %).

3.3.5.2 Catalyst performance using toluene as solvent

Catalytic activity of Sn-MCM-41 (575.8 m^2/g), Sn-SBA-15 (470.5 m^2/g), Sn-SiO_2 (363.6 m^2/g) and Amberlyst-15 (53 m^2/g) in the esterification reaction using toluene as solvent at an acid: alcohol molar ratio of 2:1 (Figure 3.10) and 6:1 (Figure 3.11) is presented.

Highest acetic acid and nopol conversion was obtained over Amberlyst-15 (46 and 91 %), Sn-SiO_2 (33.4 and 6 %), followed by Sn-MCM-41 (21.4 and 2.4 %) and Sn-SBA-15 (5.4 and 4.8 %). Nopyl acetate selectivity over Sn-MCM-41 (576 m^2/g) displayed 17.8 %. Mesoporous structure and high surface area contribute to the diffusion of reactant

molecules. The highest pore volume of Amberlyst-15 (0.4 cm^3/g) compared with Sn-MCM-41 (0.15 cm^3/g) and Sn-SBA-15 (0.34 cm^3/g), seems to give a better substrate-catalyst interaction.

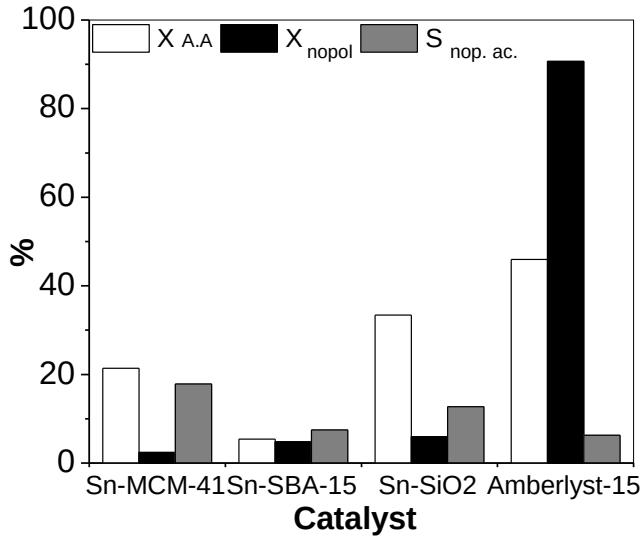

Figure 3.10 Catalyst effect on the esterification of nopol in presence of toluene. Reaction conditions: 80 °C, 750 rpm, nopol/toluene solution 0.25 M (20 mL), acetic acid (99.5 %), acid : alcohol = 2:1, catalyst (3.7 mg/mL), reaction time 480 min.

Clearly, the increase of the acid: alcohol molar ratio to 6:1 enhances product selectivity (Figure 3.11). Nopol conversion in presence of acetic acid is highest over Sn-SBA-15 (19 %), followed by 15 % without catalyst, Sn-SiO_2 (7 %) and Sn-MCM-41 (10 %). Best ester selectivity in presence of acetic acid was obtained over Sn-MCM-41 and blank reaction (100 %), followed by Sn-SiO_2 (83 %) and Sn-SBA-15 (78 %).

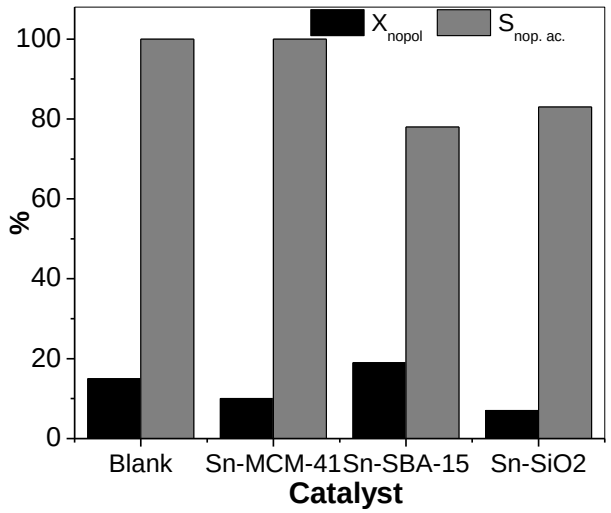

Figure 3.11 Catalyst effect on the esterification of nopol with acetic acid increase. Reaction conditions: 80 °C, 750 rpm, nopol/toluene solution 0.25 M (20 mL), acetic acid (98.5 %), acid: alcohol = 6:1, catalyst (3.7 mg/mL).

3.3.5.3 Catalyst performance using n-hexane as solvent

These tests were performed in presence of n-hexane, as it has shown to promote higher ester selectivities compared to toluene.

Performance of the heterogeneous catalysts Sn-MCM-41, Sn-SBA-15, Sn-SiO_2, Amberlyst-15 and the homogeneous catalyst *p*-toluenesulfonic acid (*p*-TSA) in the esterification reaction using n-hexane as solvent is presented in Figure 3.12.

From the heterogeneous catalysts evaluated, Amberlyst-15 showed the highest nopol conversion (57.6 %) followed by Sn-SiO_2 (19.1 %), Sn-MCM-41 (12 %) and Sn-SBA-15 (10.3 %). However the homogeneous catalyst (*p*-TSA) predominates with a value of 99.7 %. By comparing the performance of the sulfonic acids *p*-TSA and Amberlyst-15, the best catalytic activity of *p*-TSA can be attributed to a higher density of acid sites per gram, as it is 5.25 mmol/g and in Amberlyst-15 4.7 mmol/g [93]. Comparing the esterification rate with each sulfonic acid per acid site reveals it is somewhat similar, 8.82 x10-4 s^{-1} (*p*-TSA) and 6.90 x 10^{-4} s^{-1} (Amberlyst-15).

The selectivity to the ester over the heterogeneous catalysts reaches a maximum of 15.2 % with Sn-SBA-15, followed by Sn-MCM-41 (12 %), Amberlyst-15 (9 %) and Sn-SiO_2 (8.6 %). There is not doubt that the best performance is displayed by the *p*-TSA, exhibiting a selectivity of 45.6 %.

Conventionally, esterification reactions are industrially performed under batch conditions in homogeneous liquid phase catalyzed by strong Brønsted acids, such as sulfuric acid, hydrochloric acid or ortophosphoric acid [94]. Based on this statement and the results acquired under the reaction conditions performed, Brønsted acid type materials (Amberlyst-15 and *p*-TSA), are suitable catalysts in the nopol esterification reaction.

Over *p*-TSA the greater selectivity is reached at 60 min, which differs from Sn-MCM-41 and Sn-SBA-15 in which case the selectivity tends to increase with time. Particularly Sn-SiO_2 and Amberlyst-15 exhibits highest selectivity (9 and 8.6 %) at 120 min, however it subsequently decreases (5.6 and 8 %) at 1440 min.

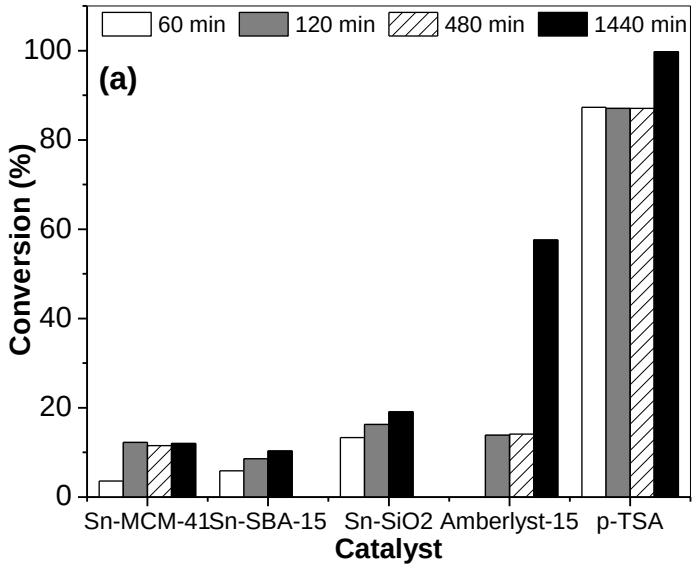

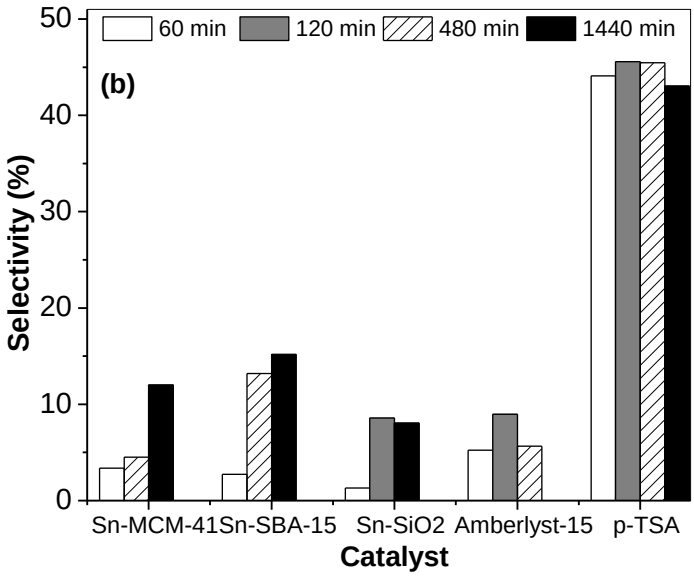

Figure 3.12 Catalyst effect on the esterification of nopol in presence of n-hexane. Reaction conditions: 50 ° C, 750 rpm, acid: alcohol = 2:1, nopol/ n-hexane 0.25 M (10 mL), acetic acid, catalyst (3.75 mg/mL).

3.3.6 Esterification of nopol with acetic anhydride

The use of acetic anhydride as acetylating agent in the esterification of nopol is more suitable than acetic acid, considering it can enhance the reaction toward the ester whilst removing the by-product water by reacting to produce acetic acid: $Ac_2O + H_2O \rightarrow 2HOAc$ [92].

Catalytic activity and ester selectivity of tin incorporated materials (Sn-MCM-41, Sn-SBA-15, Sn-SiO_2) and Amberlyst-15 in the esterification reaction with acetic anhydride (Figure 3.13, Table 3.7) is presented.

In presence of acetic anhydride substrate conversion over Sn-SiO_2 reaches 75 % at 60 min compared to 58 % in absence of catalyst, 48 % over Sn-MCM-41 and 45 % using Sn-SBA-15. Interestingly, with MCM-41 nopol conversion reaches 68.3 % at 60 min which indicates that tin incoporation not necessarily contributes to a higher catalytic activity with this material. Amberlyst-15 and Sn-SiO_2 favor highest nopol conversion, 99.5 and 97.6 % respectively. Tin incorporation in SiO_2 enhances nopol conversion from 60 to 75 % at 60 min.

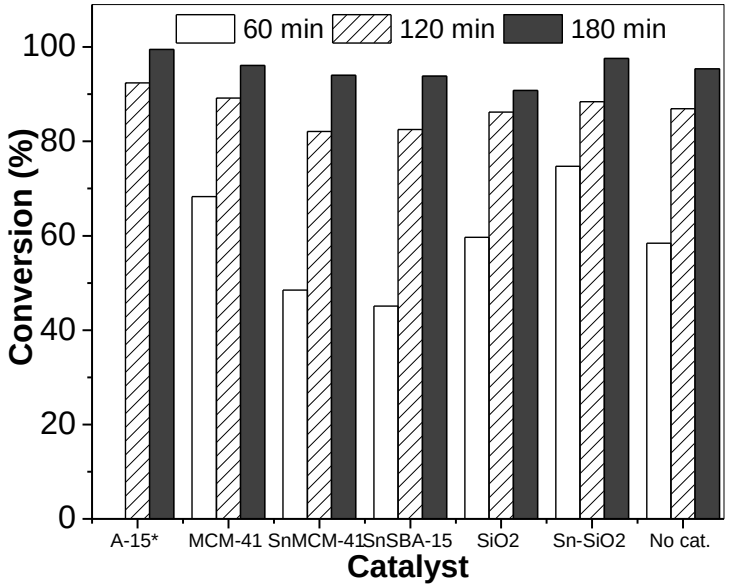

Figure 3.13 Nopol esterification using acetic anhydride. Reaction conditions: 70 °C*, 80 °C, 750 rpm, nopol/toluene solution 0.25 M (10 mL), acetic anhydride (98.5 %), anhydride: alcohol = 3:1, catalyst (3.7 mg/mL).

According to Table 3.7, nopyl acetate selectivity is above 98 % at 60 min through 180 min over all materials except with MCM-41, even without catalyst. In contrast with SiO_2 materials that exhibit 100 % ester selectivity, absence of tin species in MCM-41 implicates a 94.7 % maximum selectivity only.

Table 3.7 Nopyl acetate selectivity using acetic anhydride as esterifying agent

Catalyst	Time (min)	$S_{nop.\ ac.}$ (%)
Amberlyst-15	60	-
	120	92.4
	180	99.5
MCM-41	60	93.3
	120	91.0
	180	94.7
Sn-MCM-41	60	100
	120	100
	180	100
Sn-SBA-15	60	100
	120	100
	180	100

SiO_2	60	100
	120	100
	180	100
$Sn\text{-}SiO_2$	60	100
	120	100
	180	100
None	60	100
	120	100
	180	98.4

Reaction conditions: 70 °C, 80 °C, 750 rpm, nopol/toluene solution 0.25 M (10 mL), acetic anhydride (98.5 %), anhydride : alcohol = 3:1, catalyst (3.7 mg/mL).

3.3.7 Reactions of nopyl acetate under esterification conditions

To establish the possible side reactions of nopyl acetate under esterification reaction conditions, tests were carried out in presence and absence of acetic acid and catalyst.

Figure 3.14 shows that at 60 min of reaction, conversion of nopyl acetate amounts to 26 % and afterwards reaches 99.9 % at 1440 min. The ester is undoubtedly transformed into another product(s). However, there is concern about acetic acid as it has a low conversion (0.8 -14.1 %) during the reaction; probably nopyl acetate is transformed because of the temperature effect.

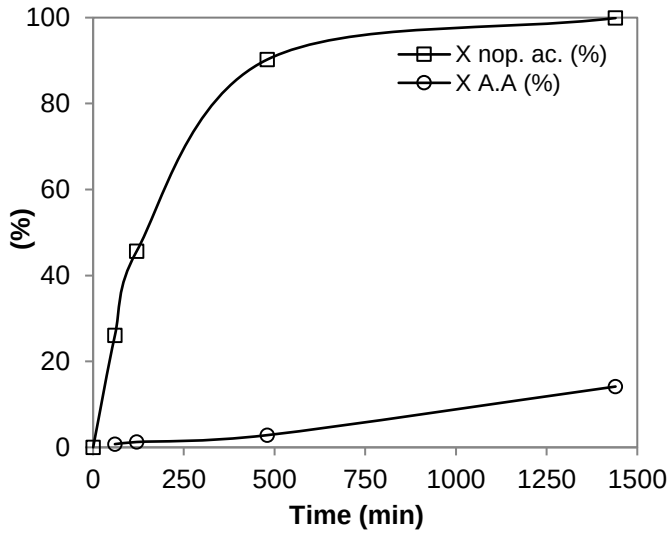

Figure 3.14 Reaction of nopyl acetate with acetic acid over Amberlyst-15. Reaction conditions: Amberlyst-15 (3.75 mg/mL), nopyl acetate/toluene 0.25 M (20 mL), acetic acid (99.5 %), 80 °C, 750 rpm.

Figure 3.15 reveals that there is no conversion of nopyl acetate in the presence of acetic acid alone, thus highlighting the catalyst role in the reaction. It is clear that there is conversion of nopyl acetate in presence of Amberlyst-15 and without acetic acid. Necessarily, this effect indicates that acetic acid does not promote the conversion of nopyl acetate into other products.

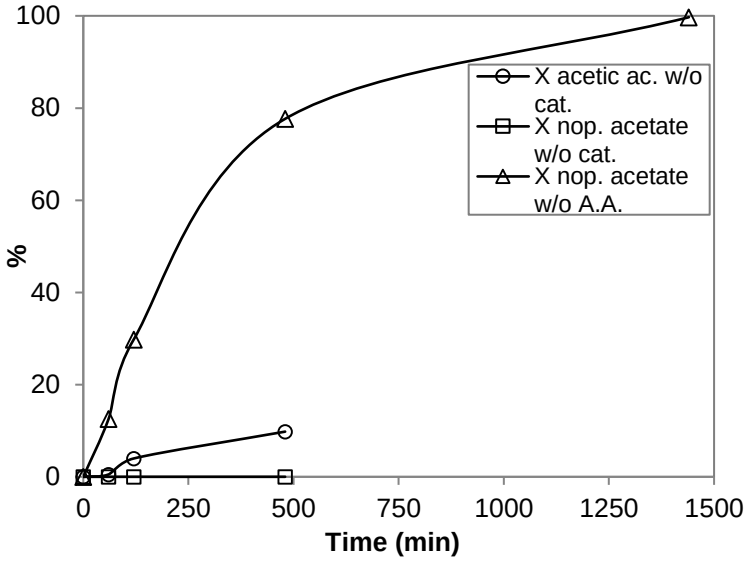

Figure 3.15 Reaction of nopyl acetate without (w/o) catalyst or acetic acid (A.A). Reaction conditions: nopyl acetate/toluene solution 0.25 M (20 mL), acetic acid (A.A) (99.5 %), 80 °C, 750 rpm.

3.3.8 Direct synthesis of nopyl acetate from β-pinene

Nopyl acetate is prepared in industry by the reaction of β-pinene and paraformaldehyde with subsequent esterification of the intermediary nopol with acetic acid [95]. In the following section, the direct synthesis from β-pinene is evaluated in presence of Amberlyst-15, Sn-MCM-41 and Sn-SBA-15 catalysts (Figures 3.16, 3.17). Particularly, Sn-MCM-41 and Sn-SBA-15 have been reported to be highly active for the selective synthesis of nopol by Prins condensation of β-pinene and paraformaldehyde [19].

In Figure 3.16 a similar trend is observed in the conversion of acetic acid at all reaction times using Sn-MCM-41 and Sn-SBA-15. With both materials, maximum conversions were achieved from 42.7 to 43.3 %. Over Amberlyst-15, the conversion of acetic acid (6 -12.8 %) is low during the first 120 minutes, however from 480 min it rises near 50 %.

Conversion of β-pinene (Figure 3.16) in the presence of Amberlyst-15 gradually increases with time, obtaining at the end the highest conversion value (84.4 %) of the three experiments performed. Sn-MCM-41 and Sn-SBA-15 showed similar behavior, although slightly higher conversion values were recorded over Sn-SBA-15 (44.6 -68.4 %). Undoubtedly, the advantage of using mesoporous catalysts over Amberlyst-15 lies in the fact that lower reaction times are required to reach conversions above 50 %.

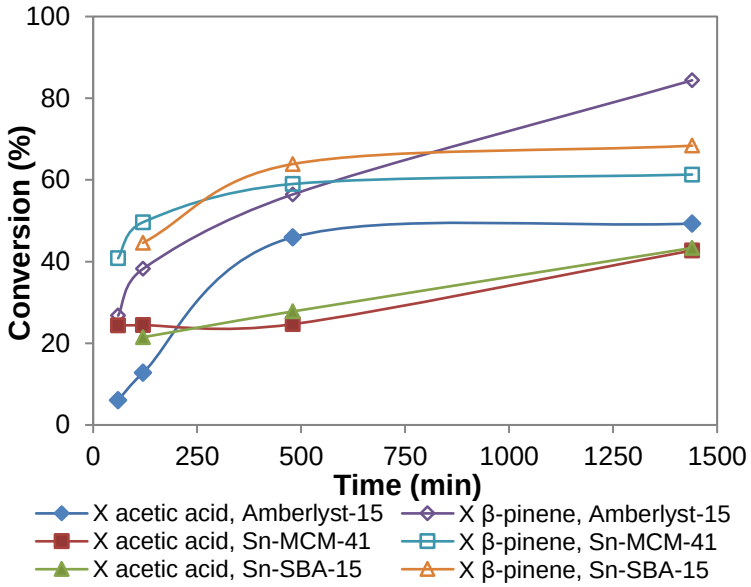

Figure 3.16 Conversion (X) of acetic acid and β–pinene in the direct synthesis of nopyl acetate. Reaction conditions: 750 rpm, β-pinene/toluene 0.25 M (20 mL), (HCHO) x: β-pinene molar ratio = 2:1, acetic acid (99.5 %), catalyst (3.75 mg/mL).

Selectivity to nopol increases with time over Sn-MCM-41 and Sn-SBA-15 reaching at the end of the reaction 89 % and 87.2 % respectively (Figure 3.17). Amberlyst-15 shows a steady tendency until 480 min with an average value of 2.3 %. After this, selectivity decreases dramatically to 0.8 % at 1440 min. Selectivity to nopyl acetate (Figure 3.17) has a tendency to increase with time when using the three materials, despite very low values. Sn-MCM-41 and Sn-SBA-15 present similarities at 1440 min (0.7 and 0.61 %) and at the same reaction time Amberlyst-15 exhibits 1.8 % ester selectivity.

At the reaction conditions for direct synthesis of nopyl acetate from β-pinene and paraformaldehyde over tin incorporated materials, Sn-MCM-41 and Sn-SBA-15, nopol production is favored. Despite low values among the three catalysts Amberlyst-15 slightly favored more nopyl acetate formation. Nevertheless, results clearly show that this reaction is not suitable for nopyl acetate synthesis over the catalysts worked with; indicating probably that the acetic acid requirement needs to be higher, considering the small amounts of nopol being produced during the reaction.

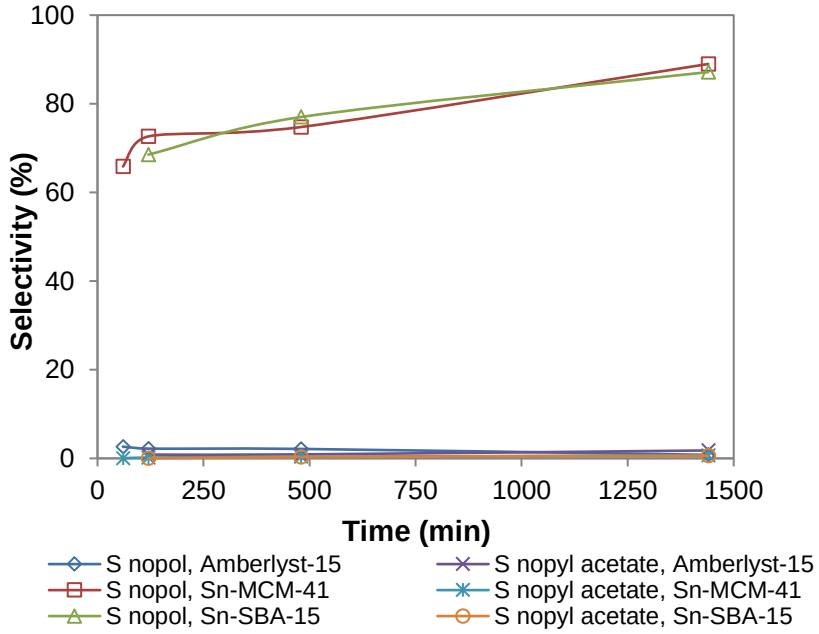

Figure 3.17 Selectivity (S) to nopol and nopyl acetate in the direct synthesis of nopyl acetate. Reaction conditions: 750 rpm, β- pinene/toluene 0.25 M (20 mL), (HCHO) x: β-pinene molar ratio = 2:1, acetic acid (99.5 %), catalyst (3.75 mg/mL).

3.3.9 Amberlyst-15 heterogeneity evaluation

3.3.9.1 Heterogeneity of Amberlyst-15

According to mass transfer diffusion experiments using n-hexane as solvent, Amberlyst-15 displays most consistent values and highest nopol and nopyl acetate reaction rates. Table 3.8 shows the results obtained from the three heterogeneity tests performed over Amberlyst-15 catalyst.

Table 3.8 Amberlyst-15 heterogeneity tests in the esterification of nopol with acetic acid

Time (min)	C nopol (M) / Test		
	1	2	3
0	0.302	0.302	0.191
30	n.d	n.d	0.207
60	0.301	0.307	n.d
80	n.d	n.d	0.273

Reaction conditions: 50 °C, 750 rpm, nopol/n-hexane solution 0.25 M (10 mL), acetic acid (99.5 %), catalyst (37.5 mg/mL). n.d: no data.

In test 1 the initial concentration of nopol/ n-hexane solution was 0.3 M. By removing the catalyst from the reaction medium and adding acetic acid to react for 1 h, it did not change the concentration of the substrate, inferring that no conversion took place.

Likewise, in test 2, nopol was added to the reaction medium after removal of the catalyst and no substrate conversion was present, since the concentration did not vary (0.302-0.307 M).

In the third and last heterogeneity test, an initial concentration of 0.191 M was used. Removal of the catalyst and allowing the reaction to react for 80 min showed an equilibrium shift towards the substrate, implying an increase in concentration of nopol (0.273 M).

3.3.9.2 Amberlyst-15 catalyst reusability

Amberlyst-15 was used as fresh catalyst in the reaction, separated by decantation, washed three times with acetone under continuous stirring and dried in an oven at 80 ° C overnight. It was used in the esterification of nopol with acetic acid with a fresh reaction mixture under the following reaction conditions: 0.25 M nopol/n-hexane solution, nopol: acetic acid molar ratio equal to 2:1, 3.75 mg / mL catalyst and a temperature of 50 °C. The procedure was repeated after the first reuse. The results obtained (Table 3.9) indicate that the catalyst is not reusable, since there is loss of catalytic activity during the four cycles.

Table 3.9 Amberlyst-15 reusability tests in the esterification of nopol with acetic acid

Entry	Time (min)	Conversion (%)	Selectivity (%)
Fresh	60	21.0	3.1
	120	25.9	4.7
	480	42.8	5.2
	1440	72.4	5.5
1	60	6.9	6.1
	120	n.d.	n.d.
	480	9.3	18.1
	1440	30.8	11.7
2	60	n.d.	n.d
	120	n.d.	n.d.
	480	20.8	4.9
	1440	8.2	40
3	60	0.7	100
	120	n.d.	n.d.
	480	n.d.	n.d.
	1440	14.8	21.7
4	60	0	0
	120	0	0
	480	16.2	8
	1440	12.6	29

Reaction conditions: 50 °C, 750 rpm, acid/alcohol = 2:1, Amberlyst-15 (3.75 mg/mL), n.d: no data.

3.3.10 Sn-SiO_2 catalyst reusability

Reusability of Sn-SiO_2 in the esterification of nopol with acetic anhydride are shown in Table 3.10. The catalyst does not lose catalytic activity until the first reuse. Only during the second and third reuse there is a decrease in the conversion of nopol from 72 % to 56 - 61 % at 60 min of reaction. For all cycles, at 120 and 180 min, the conversion of nopol or ester selectivity does not decrease.

Table 3.10 Reusability of Sn-SiO_2 in the esterification of nopol with acetic anhydride

Catalyst	Time (min)	Conversion (%)	Selectivity (%)
SiO_2	60	59.7	100
SiO_2	120	86.2	100
SiO_2	180	90.8	100
Sn-SiO_2	60	74.7	100
Sn-SiO_2	120	88.4	100
Sn-SiO_2	180	97.6	100
1st reuse	60	72.3	100
1st reuse	120	88.9	100
1st reuse	180	96.2	100
2nd reuse	60	55.7	100
2nd reuse	120	85.2	100
2nd reuse	180	93.9	100
3rd reuse	60	60.6	100
3rd reuse	120	86.5	100
3rd reuse	180	95.3	100

Reaction conditions: 80 °C, 750 rpm, nopol/toluene solution 0.25 M (10 mL), 7.5 mmol acetic anhydride (98.5 %), catalyst (37.5 mg), catalyst was washed three times with acetone and dried after every reuse.

3.3.11 Effect of particle size on the initial reaction rate

In order to determine the absence of internal diffusion problems during the catalytic reaction, the initial reaction rate of nopol and nopyl acetate with various average catalyst particle sizes (40, 49, 58 and 76.5 μm) was determined. Toluene and n-hexane were used as solvents due to the good catalytic performance observed in the esterification reaction.

3.3.11.1 Using toluene as solvent

When the diffusion restrictions within the catalyst particle were evaluated in the range of 40 to 76.5 μm, at a constant stirring speed of 750 rpm (Table 3.11 - 3.12), the results indicate that the initial rate of transformation of nopol varies less when the particle size is in the range of 49 and 58 μm. Equations of substrate and product concentration with respect to time were adjusted to polynomials for each average particle size and they were of 2, 3 and 4 order.

Table 3.11 Equations used to determine initial reaction rates at different Amberlyst-15 particle sizes

Average particle size (μm)	Nopol	Nopyl acetate
40	$C = -1\cdot10^{-9}t^3 + 3\cdot10^{-6}t^2 - 0.0015t + 0.1751$	$C = 7\cdot10^{-13}t^4 - 1\cdot10^{-9}t^3 - 2\cdot10^{-8}t^2 + 0.0002t + 0.0007$
49	$C = 6\cdot10^{-12}t^4 - 1\cdot10^{-8}t^3 + 9\cdot10^{6}t^2 - 0.0022t + 0.2112$	$C = -1\cdot10^{-6}t^2 + 0.0003t + 0.0011$
58	$C = 1\cdot10^{-11}t^4 - 2\cdot10^{-8}t^3 + 1\cdot10^{-5}t^2 - 0.0024t + 0.2028$	$C = 5\cdot10^{-9}t^3 - 4\cdot10^{-6}t^2 + 0.0005t + 6\cdot10^{-15}$
76.5	$C = 4\cdot10^{-12}t^4 - 9\cdot10^{-9}t^3 + 6\cdot10^{-6}t^2 - 0.0017t + 0.1961$	$C = 2\cdot10^{-10}t^3 - 5\cdot10^{-7}t^2 + 0.0002t - 3\cdot10^{-5}$

C**:** nopol concentration (M)**,** t**:** reaction time (min), R^2 =1.

Table 3.12 Nopol initial disappearance reaction rate and nopyl acetate formation rate at different Amberlyst-15 particle sizes

Mesh (ASTM)	Average particle size (μm)	$-r_{nopol,0}$ (mmol/g*s)	$-r_{nop.\ ac.,0}$ (mmol/g*s)
325-400	40	0.401	0.053
270-325	49	0.587	0.080
230-270	58	0.641	0.134
170-230	76.5	0.454	0.053

Reaction conditions: Amberlyst-15 (3.75 mg/mL), nopol / toluene 0.25 M (20 mL), ácid: alcohol = 2:1, acetic acid (99.5 %), 80 °C, 750 rpm.

3.3.11.2 Using n-hexane as solvent

Tables 3.13 and 3.14 show the equations and initial reaction rates obtained at different particle sizes. For an average particle size of 58 - 76.5 μm, differences in the initial reaction rate may be neglected.

Table 3.13 Equations used to determine initial reaction rates at different Amberlyst-15 particle sizes using n-hexane (96 %)

Average particle size (μm)	Nopol	Nopyl acetate
49	$C = -3 \cdot 10^{-4}t + 0.2106$	$C = 4 \cdot 10^{-5}t + 0.0001$
58	$C = -3 \cdot 10^{-5}t + 0.2127$	$C = 8 \cdot 10^{-6}t + 0.0003$
76.5	$C = -3 \cdot 10^{-5}t + 0.2096$	$C = 7 \cdot 10^{-6}t + 0.0002$

C: nopol, nopyl acetate concentration (M), t: time (min).

Table 3.14 Initial reaction rates at different Amberlyst-15 particle sizes using n-hexane (96 %)

Material	Average particle size (μm)	$-r_{nopol,0}$ (µmol/g·s)	$r_{nop.\ ac.,0}$ (µmol/g·s)
Amberlyst-15	49	1.372	0.183
	58	0.137	0.037
	76.5	0.137	0.032

Reaction conditions: 750 rpm, nopol/n-hexane 0.25 M (20 mL), acetic acid (99.5 %), Amberlyst-15 (3.75 mg/mL).

In Tables 3.15 and 3.16 the initial reaction rate values and the equations used to determine these values at different particle sizes of Sn-SBA-15 are presented.

Table 3.15 Equations used to determine r_{j0} at different particle sizes of Sn-SBA-15

Average particle size (μm)	Nopol	Nopyl acetate
49	$C = 0.0001t + 0.2397$	$C = 4 \cdot 10^{-6}t - 1 \cdot 10^{-7}$
58	$C = 0.0003t + 0.2301$	$C = 5 \cdot 10^{-6}t + 1 \cdot 10^{-5}$
76.5	$C = 0.0004t + 0.2410$	$C = 4 \cdot 10^{-6}t - 2 \cdot 10^{-5}$

C: nopol, nopyl acetate concentration (M), t: time (min).

Table 3.16 Initial reaction rates at different particle sizes of Sn-SBA-15 using n-hexane (96 %)

Material	Average particle size (μm)	$-r_{nopol,0}$ (μmol/g·s)	$r_{nop.\ ac.,0}$ (μmol/g·s)
Sn-SBA-15	49	0.457	0.018
	58	1.372	0.023
	76.5	1.829	0.018

Reaction conditions: 750 rpm, nopol/n-hexane solution 0.25 M (20 mL), acetic acid (99.5 %), Sn-SBA-15 (3.75 mg/mL).

3.3.12 Stirring speed effect on the initial reaction rates for nopol esterification

3.3.12.1 Using n-hexane as solvent

To determine the absence of external diffusion problems, the initial reaction rate of nopol and nopyl acetate was evaluated at stirring rates of 500, 750 and 1000 rpm.

In Tables 3.17 and 3.18 the equations used to determine the initial reaction rates and their values at different stirring speeds over Amberlyst-15 are presented.

Table 3.17 Equations used to determine r_{j0} at stirring speeds over Amberlyst-15

Stirring speed (rpm)	Nopol	Nopyl acetate
500	$C = -0.0001t + 0.2183$	$C = 1 \cdot 10^{-5}t + 8 \cdot 10^{-5}$
750	$C = -0.0001t + 0.2426$	$C = 1 \cdot 10^{-5}t - 0.0002$
1000	$C = -0.0001t + 0.2278$	$C = 3 \cdot 10^{-5}t - 0.0002$

C: nopol, nopyl acetate concentration (M), t: time (min).

Table 3.18 Initial reaction rates at different stirring speeds over Amberlyst-15 using n-hexane 95 %

Material	Stirring speed (rpm)	$-r_{nopol,0}$ (μmol/g·s)	$r_{nop.\ ac.,0}$ (μmol/g·s)
Amberlyst-15	500	0.457	0.046
	750	0.457	0.046
	1000	0.457	0.137

Reaction conditions: nopol/n-hexane solution 0.25 M (20 mL), acetic acid (99.5 %), Amberlyst-15 (3.75 mg/mL).

At 500 and 750 rpm there is no differences between reaction rates. Nopol esterification reaction over Amberlyst-15 is not external diffusion controlled at stirring speeds between 500 and 1000 rpm. In Tables 3.19 and 3.20 the equations used to determine the initial reaction rates and their values at different stirring speeds over Sn-MCM-41 are presented.

Table 3.19 Equations used to determine r_{j0} at different stirring speeds over Sn-MCM-41

Stirring speed (rpm)	Nopol	Nopyl acetate
500	$C = -8 \cdot 10^{-5}t + 0.2403$	$C = 4 \cdot 10^{-6}t + 3 \cdot 10^{-5}$
750	$C = -3 \cdot 10^{-4}t + 0.2486$	$C = 4 \cdot 10^{-6}t + 3 \cdot 10^{-5}$
1000	$C = -4 \cdot 10^{-4}t + 0.2297$	$C = 5 \cdot 10^{-6}t + 2 \cdot 10^{-5}$

C: nopol, nopyl acetate concentration (M), time (min).

Table 3.20 Initial reaction rates at different stirring speeds over Sn-MCM-41 using n-hexane 95 %

Material	**Stirring speed (rpm)**	**-r nopol,$_0$ (μmol/g·s)**	**r nop. ac.,$_0$ (μmol/g·s)**
Sn-MCM-41	500	0.366	0.018
	750	1.372	0.018
	1000	1.829	0.023

Reaction conditions: nopol/n-hexane solution 0.25 M (20 mL), acetic acid (99.5 %), Amberlyst-15 (3.75 mg/mL).

Highest initial reaction rates are achieved at 1000 rpm over Sn-MCM-41.

In Tables 3.21 and 3.22 the equations used to determine the initial reaction rates and their values at different stirring speeds over Sn-SBA-15 are presented.

Table 3.21 Equations used to determine r_{j0} at different stirring speeds over Sn-SBA-15

Stirring speed (rpm)	Nopol	Nopyl acetate
500	$C = -1 \cdot 10^{-4}t + 0.2198$	$C = 4 \cdot 10^{-6}t + 3 \cdot 10^{-5}$
750	$C = -2 \cdot 10^{-4}t + 0.2452$	$C = 4 \cdot 10^{-6}t + 5 \cdot 10^{-5}$
1000	$C = -8 \cdot 10^{-5}t + 0.2033$	$C = 2 \cdot 10^{-6}t - 4 \cdot 10^{-5}$

C: nopol, nopyl acetate concentration (M), t: time (min)

Table 3.22 Initial reaction rates at different stirring speeds over Sn-SBA-15 using n-hexane (95 %)

Material	Stirring speed (rpm)	$-r_{nopol,0}$ (μmol/g·s)	$r_{nop.\ ac.,0}$ (μmol/g·s)
Sn-SBA-15	500	0.457	0.018
	750	0.918	0.018
	1000	0.366	0.009

Reaction conditions: 750 rpm, nopol/n-hexane solution 0.25 M (20 mL), acetic acid (99.5 %), Amberlyst-15 (3.75 mg/mL).

At 750 rpm highest reaction rate is obtained over Sn-SBA-15.

3.3.13 Kinetics of the esterification of nopol with acetic acid

3.3.13.1 Reaction rate equation

A reaction rate equation was proposed, based on what has been reported in the literature for esterification reactions. Esterification reactions are known to be reversible and of second order [46].

$$A + B \leftrightarrow E + W \qquad (1.1)$$

with A: acid, B: alcohol, E: ester and W: water. Considering that $C_{A0} = C_{B0}$ y $C_{E0} = C_{W0} = 0$, the reaction rate equation can be written as,

$$-r_B = -\frac{dC_B}{dt} = C_{B0}\frac{dX_B}{dt} = k_1 C_A C_B - k_2 C_E C_W = k_1 C_{B0}^2 (1 - X_B)^2 - k_2 (C_{B0} X_B)^2 \qquad (3.1)$$

In equilibrium, $-r_B = 0$. Hence, from the above equations, conversion of B at equilibrium conditions can be determined by,

$$K = \frac{C_{Ee} C_{We}}{C_{Ae} C_{Be}} = \frac{X_{Be}^2}{(1 - X_{Be})^2} \qquad (3.2)$$

With C_{ie}, X_{ie}: concentration and conversion of i at equilibrium conditions.

And the equilibrium constant by,

$$K = \frac{k_1}{k_2} \tag{3.5}$$

Combining the above three equations into the equilibrium conversion terms yields,

$$\frac{dX_B}{dt} = k_1 C_{B0} \left[(1 - X_B)^2 - \left(\frac{1 - X_{Be}}{X_{Be}} \right)^2 X_B^2 \right] \tag{3.6}$$

With conversions measured in terms of X_{Be}, this can be indicated as a reversible pseudo second order reaction, which when integrated, results in:

$$\ln \left[\frac{X_{Be} - (2X_{Be} - 1)X_B}{X_{Be} - X_B} \right] = 2k_1 \left(\frac{1}{X_{Be}} - 1 \right) C_{B0} t \tag{3.7}$$

Figure 3.18 shows the experimental data collected at 323 K (50°C) used to plot the left-hand side of equation 3.7 versus time to get a straight line passing through the origin. From the slope of this line, the forward reaction rate constant (k_1) was found.

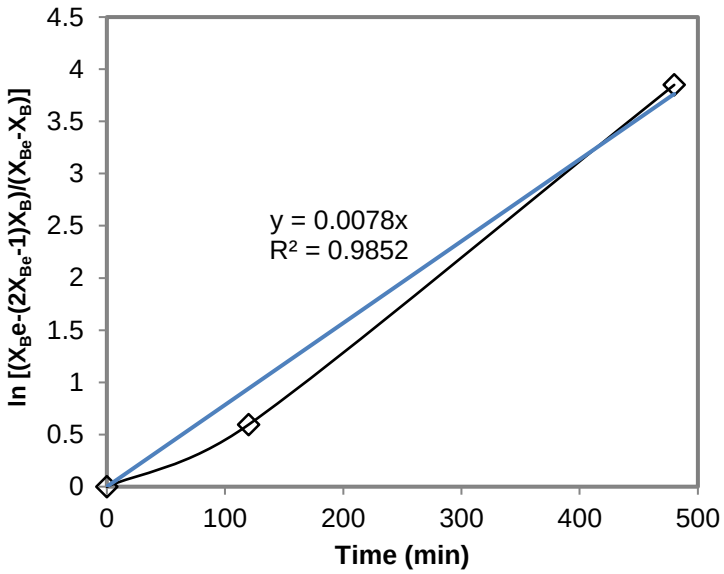

Figure 3.18 Experimental results obtained from equation 3.8. 50 °C, acid: alcohol molar ratio of 1:1, 1000 rpm, Amberlyst-15.

After reaching a stable conversion value, the equilibrium constant (K_c = 0.038) and the reaction rate constant (3.71 x 10^{-3} L.mol^{-1}.h^{-1}) were determined.

From equation (3.5) we can rewrite equation (3.1) in the following way,

$$r = k_1 (C_A C_B - \frac{1}{Kc} C_E C_W) \tag{3.8}$$

Substituting the values of k_1 and K_c in (3.8) the reaction rate equation of the nopol esterification reaction,

$$r = 3.71 \text{ x } 10^{-3}(C_A C_B - \frac{1}{0.038} C_E C_W) \qquad (3.9)$$

3.3.14 Mechanism of esterification of nopol with acetic acid over solid acid catalyst

After a broad search in the literature about esterification reaction kinetics, two mechanisms are proposed for the esterification reaction of nopol with acetic acid over a solid acid catalyst [43] [96].

3.3.14.1 Mechanism 1

The reaction is initiated by the transfer of a proton from the catalyst to the carboxylic acid (acetic acid) (Figure 3.19). The proton attaches to one of the free pairs on oxygen, which is double bonded to the carbon. The transfer of the proton to the oxygen gives it a positive charge. This results in a good amount of positive charge on the carbon atom (reaction step 3.11). Then, the positive charge on the carbon atom is attacked by the hydroxyl group of the alcohol molecule (nopol). Subsequently, a water molecule detaches itself from the ion (reaction step 3.12). Finally, the catalyst is recovered by transferring the proton from the ion to the catalyst surface (reaction step 3.13). This mechanism is represented by the following scheme given in Figure 3.19 [43]:

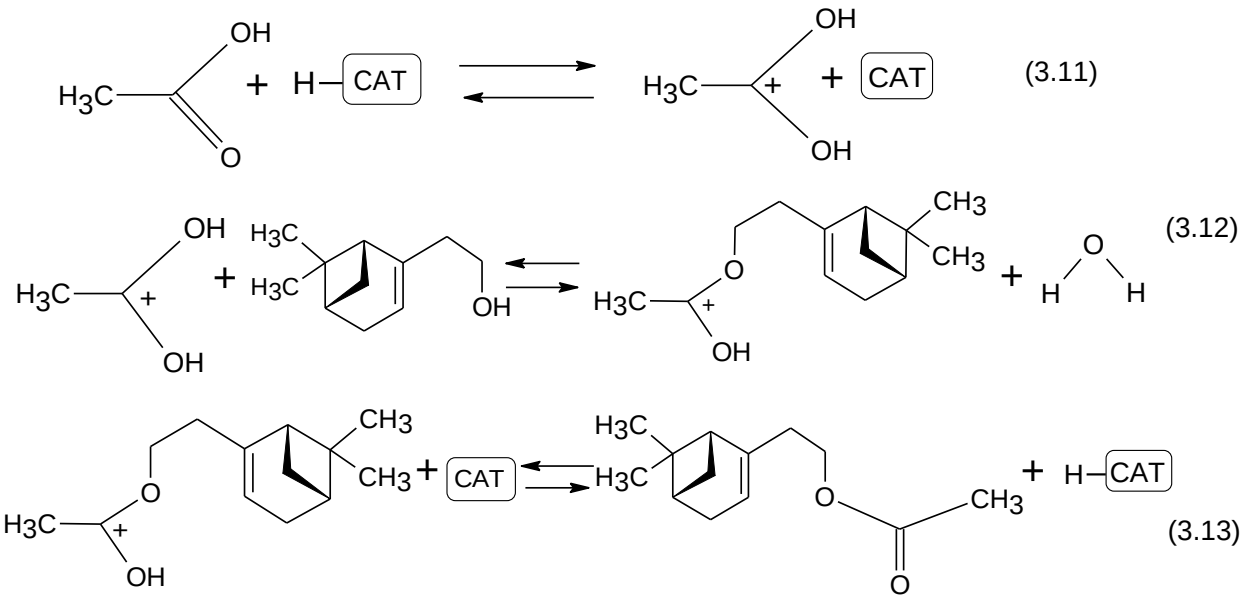

Figure 3.19 Mechanism of reaction for the synthesis of nopyl acetate [43].

3.3.14.2 Mechanism 2: bimolecular reaction [96]

1. It is easy for ketone oxygen to capture a hydrogen ion to form a protonated carbonyl substrate (Figure 3.20) (reaction step 3.14).

2. The substrate causes the carbon atom of the carboxyl to possess greater electropositivity, which leads to the attack of the nucleophile (nopol) to generate a tetrahedral intermediate (reaction step 3.15).

3-4. The transfer of a proton from one oxygen atom to another produces a secondary tetrahedral intermediate and converts the OH group into a good leaving group (reaction steps 3.16 - 3.17).

5. The oxygen-acyl bond is broken and one molecule of water is lost (reaction step 3.18).

6. The loss of a proton produces the ester product (reaction step 3.19).

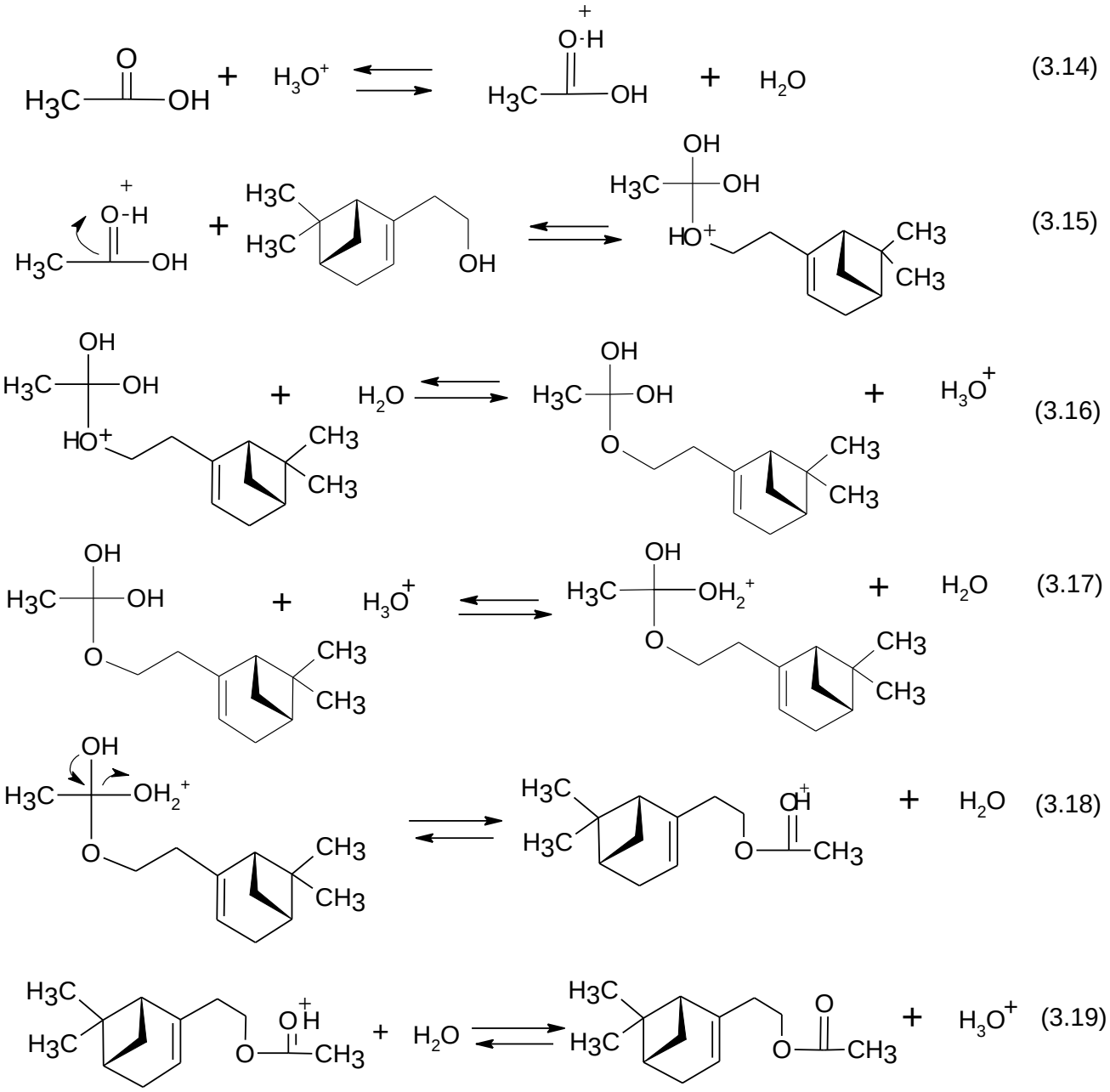

Figure 3.20 Mechanism of bimolecular reaction for the synthesis of nopyl acetate [96].

3.4 Chapter conclusions

The internal mass transfer resistance can be neglected over Amberlyst-15 and Sn-SBA-15 average particle sizes 58-76.5 μm for nopol esterification. The initial reaction rate is not significantly differed by varying the stirring speed. Stirring speeds of 750 rpm over Sn-SBA-15 and 1000 rpm over both Amberlyst-15 and Sn-MCM-41 are most convenient in

achieving the highest initial nopol disappearance and nopyl acetate formation reaction rates. Thus, nopol esterification reaction over Amberlyst-15 is not external diffusion controlled at stirring speeds between 500 and 1000 rpm.

Synthesis of nopyl acetate was satisfactory using the homogeneous catalyst *p*-TSA, achieving a selectivity of 45.6 % and a substrate conversion of 99.7 % compared to 9 and 57.6 % respectively over Amberlyst-15. It is evident that the esterification of nopol is more favored on sulfonic acids than with tin incorporated silicas, due to its high density of acid sites per gram (5.25 mmol/g for *p*-TSA and 4.7 mmol/g for Amberlyst-15). However *p*-TSA use exhibits disadvantages due to the difficulty of waste disposal and separation of the reaction medium.

Sn-SiO_2 exhibits best catalytic performance for nopyl acetate synthesis in presence of acetic anhydride, 98 % nopol conversion and 100 % ester selectivity. Sn-SBA-15 displays moderate substrate conversion (19 %) and high ester selectivity (78 %) with acetic acid. Acetic anhydride is a more effective esterifying agent than acetic acid. The economic feasibility of Sn-SiO_2 and structural properties of Sn-SBA-15 make them potential materials for replacing toxic and corrosive homogeneous catalysts. Table 3.23 summarizes most active catalytic conditions for nopol esterification.

Table 3.23 Best reaction conditions tested for nopyl acetate synthesis

Catalyst	Catalyst conc. (mg/mL)	Acid[1], anhydride[2]/ alcohol	Solvent	T (°C)	Time (min)	X_{nopol} (%)	$S_{nop.\ ac.}$ (%)
Amberlyst-15	6.1	1:1[1]	Toluene	80	480	81.6	8.7
Amberlyst-15	6.1	2:1[1]	Toluene	80	90	66.4	8.2
Amberlyst-15	3.7	2:1[1]	n-hexane	50	120	13.5	10.3
Sn-SBA-15	3.7	2:1[1]	n-hexane	50	1440	10.3	15.2
Sn–SiO_2	3.7	3:1[2]	Toluene	80	60	75.0	100

[1]Acid: acetic acid, [2]anhydride: acetic anhydride

CONCLUSIONS

4. GENERAL CONCLUSIONS

The characterization performed to synthesized materials verifies that MCM-41 and SBA-15 materials are ordered hexagonal mesostructures of high surface area (MCM-41: 596.2 m^2/g; Sn-MCM-41: 575.8 m^2/g, SBA-15: 530.6 m^2/g, Sn-SBA-15: 470.5 m^2/g, SiO_2: 433.8 m^2/g) and Sn-SiO_2: 363.6 m^2/g). All synthesized materials exhibit a type IV adsorption - desorption isotherm, typical of mesoporous materials. High surface area of Sn-SBA-15 (470.5 m^2 / g) and Sn-MCM-41 (575.8 m^2 / g) with Sn active species induce a better selectivity to the ester (8 - 17.8%) compared to Amberlyst- 15 (6%). Amberlyst-15 with the highest acid value (4.7 mmol NH^3 / g cat.) exhibits an extremely high nopol conversion (98.2%) compared to siliceous materials (3 - 6%). For Amberlyst-15 and Sn-SBA-15, an average particle size of 58-76.5 μm and stirring speeds between 500 and 1000 rpm guarantee the absence of diffusion effects. Sn-SBA-15 and Sn-SiO_2 materials display highest total acidity values, 0.34 and 0.4 mmol NH_3/g cat. H_2 -TPR analysis was performed on Sn-MCM-41 and Sn-SBA-15. These show a peak at 890 ° C corresponding to SnOx species and two other peaks at 215 and 525 ° C attributed to the presence of thin SnOx films. This analysis showed no signal in the case of Sn-SiO_2. This leads to think that the presence of Sn oxides is not essential to obtain high ester yields.

Best nopyl acetate selectivity in n-hexane is obtained over Sn-SBA-15 (15.2 %) and Sn-MCM-41 displayed best ester selectivity in toluene, 17.8 % at a 2:1 acid: alcohol molar ratio. Selectivity to nopyl acetate over Amberlyst-15 was greater with apolar aprotic solvents (ethyl acetate: 8.9 %, n-hexane: 10.5 %, toluene: 6.3 %) or the protic solvent ethanol (6.3 %) than with the dipolar aprotic solvent acetonitrile (0.6 %). High ester selectivity in n-hexane may be due not only to its aprotic apolar nature but also to the low solubility (0.014% at 20 °C) in this solvent of the water produced in the esterification reaction. Amberlyst-15 reaches 100 % nopol conversion in presence of toluene at acid: alcohol molar ratios of 1:2, 1:1 and 2:1. Synthesis of nopyl acetate was satisfactory using homogeneous catalyst *p*-TSA, achieving a selectivity of 45.6 % and a nopol conversion of 99.7 % compared to 9 and 57.6 % respectively with Amberlyst-15. Sulfonic acids (*p*-TSA, Amberlyst-15) displaying high density of acid sites per gram, 5.25 mmol/g and 4.7 mmol/g respectively, are more active for nopol esterification than tin-containing

mesoporous materials (0.15 mmol NH_3/g cat. for Sn-MCM-41, 0.34 mmol NH_3/g cat. for Sn-SBA-15 and 0.40 mmol NH_3/g cat. for Sn-SiO_2).

Sn-SiO_2, exhibiting highest total acidity (0.4 mmol NH_3/g cat) among tin-containing materials, with acetic anhydride as esterifying agent, achieves a 75 % nopol conversion and 100 % nopyl acetate selectivity at 60 min making it an active and selective material for nopyl acetate synthesis. In contrast, Sn-MCM-41 displays 48 % conversion and 100 % selectivity, whilst Sn-SBA-15 presents 45 % conversion and 100% selectivity. Acetic anhydride enhances the reaction by removing the by-product water.

The re-use of Amberlyst-15 reveals that the material loses catalytic activity during cycles performed. The study of Amberlyst-15 heterogeneity in the esterification of nopol with acetic acid confirms that leaching of the active species does not occur. The structural properties of Sn-SBA-15, the high catalytic performance and the economic viability of Sn-SiO_2 make these potential materials to replace homogeneous acid catalysts in the nopol esterification reaction.

Through this project, environmentally sustainable synthesis conditions for the nopyl acetate production were established, since it was worked at low pressures (atmospheric pressure) and temperatures (< 80 ° C), using reagents and materials that avoid difficult to dispose toxic and corrosive waste generation. The results of this project are intended to contribute not only to a future modeling and design of the reaction system but also to the value added chain of essential oils, because it presents a process through which it is possible to transform an alcohol obtained from one of the components of turpentine oil into an ester widely used in the pharmaceutical, perfume and general cleaning industry.

RECOMMENDATIONS

5. RECOMMENDATIONS

To further complement the work performed in this research, it would be desirable to perform additional characterizations to materials, such as XPS and nuclear magnetic resonance (NMR) solids. The above in order to establish with greater depth the state of the metal species in the tin supported catalysts (Sn-MCM-41, Sn-SBA-15 and Sn-SiO_2) and its relation on activity.

With the XPS analysis all the elements except hydrogen and helium that are present in the materials can be detected. It is also useful to determine the concentration of the materials in the outer surface layers (2 to 10 nm) and the evaluation of the degree of oxidation or electronic status of the aforementioned elements. This analysis would contribute to establish the state of oxidation of tin in the catalysts.

The nuclear magnetic resonance, NMR, of solids allows extending the analysis on the state of the metallic species in the catalyst. The ^{119}Sn NMR would be the analysis indicated in the evaluation of the state of Sn species in the materials. Additionally it is of interest to analyze ^{28}Si to establish Sn-Si bonds between different structures and relate them with structural properties.

APPENDIXES

6. APPENDIXES

6.1 Calibration curves of interest compounds

Five standard solutions were prepared with different concentrations of acetic acid, nopol and nopyl acetate. Starting from 100 μL of standard solution and 300 μL of a 0.0625 M dodecane-toluene solution, 5 samples were prepared, injected and analyzed by gas chromatography.

Table 6.1 Standard solution concentrations of acetic acid, nopol and nopyl acetate

Solution	Conversion (%)	$C_{acetic\ acid}$ (M)	C_{nopol} (M)	$C_{nopyl\ ac.}$ (M)
1	0	0.5000	0.5000	0.0000
2	25	0.3750	0.3750	0.1250
3	50	0.2500	0.2500	0.2500
4	75	0.1250	0.1250	0.3750
5	100	0.0000	0.0000	0.5000

The calibration curves, Figures 6.1 - 6.3, exhibit a linear relationship that can be expressed using the equation for a straight line, $y = mx + b$. In this equation, y is the instrument response, x is the concentration, m represents the slope of the line, and b is the y-intercept [97]. The correlation coefficient is used to make certain that a curve is linear. Best correlation coefficients were obtained for nopol and nopyl acetate calibration (Figures 6.2 – 6.3) curves, ~0.995, whereas in acetic acid calibration (Figure 6.1), this value was ~0.985.

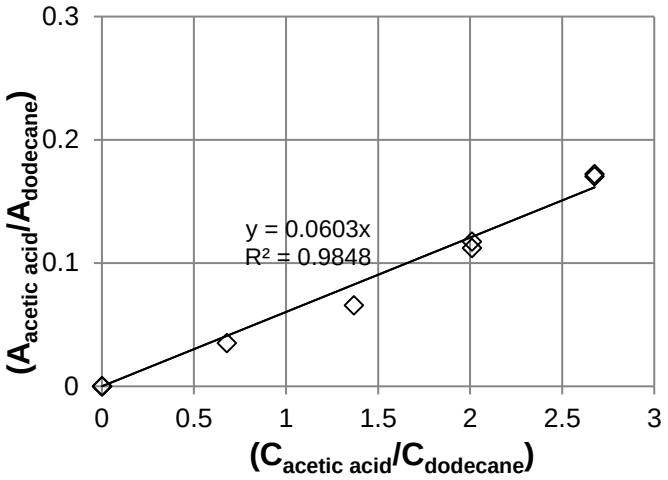

Figure 6.1 Calibration curve of acetic acid.

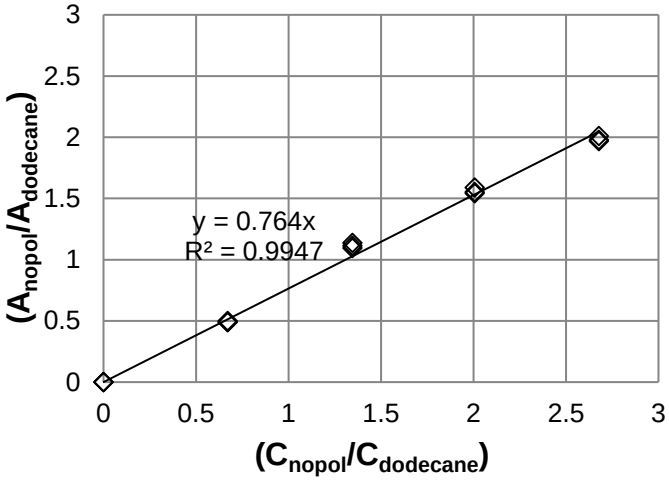

Figure 6.2 Calibration curve of nopol.

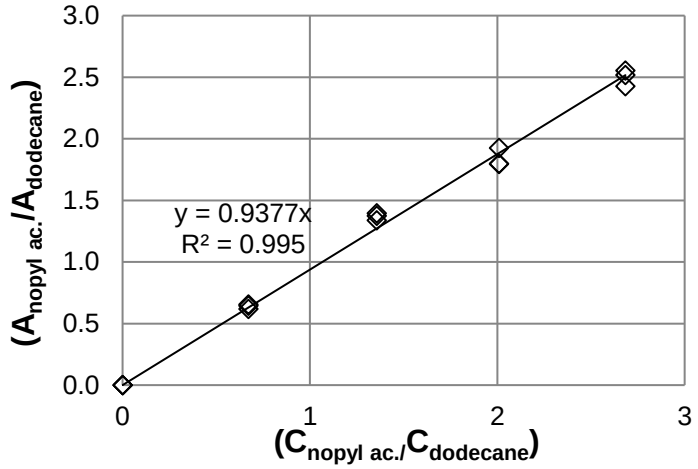

Figure 6.3 Calibration curve of nopyl acetate.

6.2 Chromatographic conditions for sample analysis

When a signal is integrated, the software ChemStation Integrator:

• Identifies a start and an end time for each peak and marks these points with vertical tick marks.

• Finds the apex of each peak; that is, the retention/migration time.

• Constructs a baseline.

• Calculates the area, height and peak width for each peak.

This process is controlled by parameters called integration events.

The following information describes the chromatographic conditions for sample analysis.

```
INSTRUMENT CONTROL PARAMETERS:    GC MSD
----------------------------------------
Control Information
------- -----------

Sample Inlet      :  GC
Injection Source  :  GC ALS
Mass Spectrometer :  Disabled


No Sample Prep method has been assigned to this method.

GC
Oven
Temperature
```

Setpoint	On
(Initial)	70 °C
Hold Time	3 min
Post Run	70 °C
Program	
#1 Rate	10 °C/min
#1 Value	180 °C
#1 Hold Time	1 min
Equilibration Time	1 min
Max Temperature	230 °C
Slow Fan	Disabled
Cryo	Off
ALS	
Front Injector	
Syringe Size	10 µL
Injection Volume	1 µL
Injection Repetitions	1
Injection Delay	0 sec
Solvent A Washes (PreInj)	3
Solvent A Washes (PostInj)	3
Solvent A Volume	8 µL
Solvent B Washes (PreInj)	0
Solvent B Washes (PostInj)	3
Solvent B Volume	8 µL
Sample Washes	0
Sample Wash Volume	8 µL
Sample Pumps	3
Dwell Time (PreInj)	0 min
Dwell Time (PostInj)	0 min
Solvent Wash Draw Speed	300 µL/min
Solvent Wash Dispense Speed	6000 µL/min
Sample Wash Draw Speed	300 µL/min
Sample Wash Dispense Speed	6000 µL/min
Injection Dispense Speed	6000 µL/min
Viscosity Delay	0 sec
Sample Depth	Disabled
Sample Overlap	
Mode	Sample overlap is not enabled
ALS Errors	Pause for user interaction

Front SS Inlet He		
Mode	Split	
Heater	On	250 °C
Pressure	On	15.987 psi
Total Flow	On	62.571 mL/min
Septum Purge Flow	On	3 mL/min
Gas Saver	Off	
Split Ratio	25 :1	
Split Flow	39.674 mL/min	
Back SS Inlet He		
Mode	Split	
Heater	On	150 °C
Pressure	On	5.8639 psi
Total Flow	On	9 mL/min
Septum Purge Flow	On	3 mL/min
Gas Saver	Off	
Split Ratio	5 :1	
Split Flow	5 mL/min	
Thermal Aux 2 (MSD Transfer Line)		
Temperature		
Setpoint	On	
(Initial)	280 °C	
Hold Time	2 min	
Post Run	0 °C	
Column		
Column #1		
Flow		
Setpoint	On	
(Initial)	1.5869 mL/min	
Hold Time	2 min	
Post Run	0.57353 mL/min	
Agilent 123-7033		
DB-WAX		
-60 °C—240 °C (240 °C): 30 m x 320 µm x 0.5 µm		
In	Front SS Inlet He	
Out	Aux EPC 1	
(Initial)	70 °C	
Pressure	13.567 psi	

Flow	1.5869 mL/min
Average Velocity	22.28 cm/sec
Holdup Time	2.2442 min
Column #2	
Flow	
Setpoint	Off
(Initial)	2.2912 mL/min
Hold Time	2 min
Post Run	0 mL/min
J&W 123-1032: 006	
DB-1	
-60 °C—325 °C (325 °C): 30 m x 320 µm x 0.25 µm	
In	Front SS Inlet He
Out	Aux EPC 1
(Initial)	70 °C
Pressure	15.987 psi
Flow	2.2912 mL/min
Average Velocity	30.462 cm/sec
Holdup Time	1.6414 min
Column #3	
Flow	
Setpoint	On
(Initial)	1 mL/min
Hold Time	2 min
Post Run	1.9054 mL/min
Agilent 123-7033	
DB-WAX	
-60 °C—240 °C (240 °C): 30 m x 320 µm x 0.5 µm	
In	Back SS Inlet He
Out	Other
(Initial)	70 °C
Pressure	5.8639 psi
Flow	1 mL/min
Average Velocity	19.826 cm/sec
Holdup Time	2.5219 min
Column #4	
Pressure	
Setpoint	On
(Initial)	7 psi
Hold Time	2 min

Post Run	0 psi
Agilent 160-2615: 0004	
Retention Gap	
-60 °C—350 °C (350 °C): 5 m x 180 µm x 0 µm	
In	Aux EPC 1 He
Out	Other
(Initial)	70 °C
Pressure	7 psi
Flow	0.74948 mL/min
Average Velocity	45.074 cm/sec
Holdup Time	0.18488 min
Column #5	
Pressure	
Setpoint	On
(Initial)	7 psi
Hold Time	2 min
Post Run	0 psi
Agilent 160-2615-2: 005	
Retention Gap	
-60 °C—350 °C (350 °C): 2 m x 180 µm x 0 µm	
In	Aux EPC 1 He
Out	Front Detector FID
(Initial)	70 °C
Pressure	7 psi
Flow	1.8737 mL/min
Average Velocity	112.68 cm/sec
Holdup Time	0.029581 min
Front Detector FID	
Heater	On 250 °C
H2 Flow	On 40 mL/min
Air Flow	On 450 mL/min
Makeup Flow	On 5 mL/min
Carrier Gas Flow Correction	Does not affect Makeup or Fuel Flow
Flame	On
Electrometer	On
Back Detector TCD	
Heater	On 200 °C

```
Reference Flow                                  On    10 mL/min

Makeup Flow                                     On    5 mL/min
Negative Polarity                               Off
Filament                                        Off

Valve 1
Type                                            Gas Sampling Valve

GSV Loop Volume                                 0.25 µL
Load Time                                       0.5 min
Inject Time                                     0.5 min

Valve 2
Switching Valve                                 On

Aux EPC 1 2    3
Aux EPC 1 He
***Excluded from Affecting GC's Readiness State***
Aux EPC 1 He                                    Supplies Column 4


Aux EPC 2 He
Pressure
Setpoint                                        On
(Initial)                                       7 psi
Hold Time                                       2.6 min
Post Run                                        0 psi

***Excluded from Affecting GC's Readiness State***

Aux EPC 3 He
Pressure
Setpoint                                        On
(Initial)                                       3 psi
Hold Time                                       0 min
Post Run                                        0 psi

***Excluded from Affecting GC's Readiness State***


Aux EPC 4 5    6
Aux EPC 4 He
Pressure
Setpoint                                        Off
(Initial)                                       16 psi
Hold Time                                       0 min
```

```
Post Run                                        0 psi

***Excluded from Affecting GC's Readiness State***

Aux EPC 5 He
Pressure
Setpoint                                        Off
(Initial)                                       0 psi
Hold Time                                       0 min
Post Run                                        0 psi

***Excluded from Affecting GC's Readiness State***

Aux EPC 6 He
Pressure
Setpoint                                        Off
(Initial)                                       0 psi
Hold Time                                       0 min
Post Run                                        0 psi

***Excluded from Affecting GC's Readiness State***


Valve Box
Heater                                          On    200 °C

Signals
Signal #1:  Front Signal
Description                                     Front Signal
Details                                         Front Signal (FID)

Save                                            On
Data Rate                                       20 Hz
Dual Injection Assignment                       Front Sample

Signal #2:  Test Plot
Description                                     Test Plot
Details
Save                                            Off
Data Rate                                       50 Hz
Dual Injection Assignment                       Back Sample

Signal #3:  Test Plot
Description                                     Test Plot
Details
Save                                            Off
Data Rate                                       50 Hz
```

```
Dual Injection Assignment                    Back Sample

Signal #4:  Test Plot
Description                                  Test Plot
Details
Save                                         Off
Data Rate                                    50 Hz
Dual Injection Assignment                    Back Sample



TUNE PARAMETERS for SN: US81819751
------------------------------

Trace Ion Detection is OFF.

EMISSION    :      34.610
ENERGY      :      69.922
REPELLER    :      24.427
IONFOCUS    :      90.157
ENTRANCE_LE :      28.500
EMVOLTS     :    1447.059
Actual EMV  :    1447.06
GAIN FACTOR :       0.18
AMUGAIN     :    2345.000
AMUOFFSET   :     122.938
FILAMENT    :       1.000
DCPOLARITY  :       0.000
ENTLENSOFFS :      17.569
MASSGAIN    :    -342.000
MASSOFFSET  :     -36.000

END OF TUNE PARAMETERS
----------------------------------



END OF INSTRUMENT CONTROL PARAMETERS
```

6.3 Chromatograms of interest compounds

The GC chromatograms of interest compounds, acetic acid, dodecane, nopol and nopyl acetate are shown in Figure 6.4, obtained by injecting a sample of a syringe drop of each component in toluene. Retention times are presented in Table 6.2.

Table 6.2 Retention times of interest compounds

Compound	Retention time, min
Acetic acid	2.034
Dodecane	9.430
Nopol	10.391
Nopyl acetate	12.359

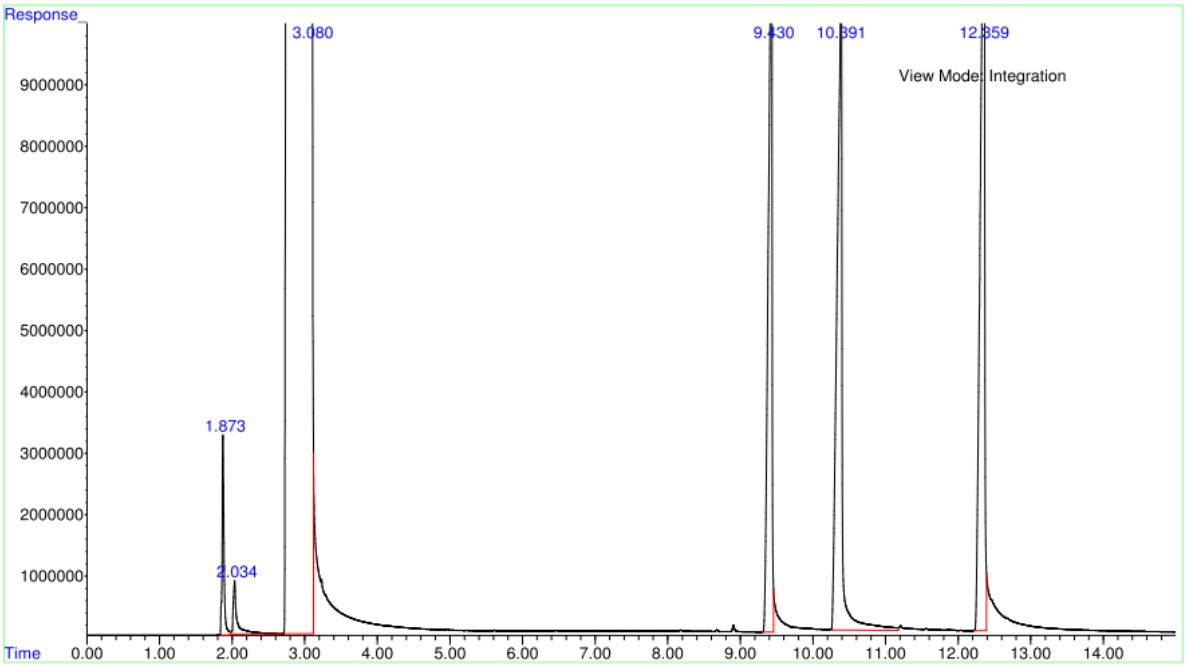

Figure 6.4 Chromatogram of interest compounds.

BIBLIOGRAPHY

7. BIBLIOGRAPHY

[1] E. E. Stashenko, *Aceites Esenciales*, Primera ed. Bucaramanga (Colombia): División de Publicaciones UIS, 2009.

[2] K.-H. Kubeczka, “History and Sources of Essential Oil Research,” in *Handbook of Essential Oils Science, Technology, and Applications*, Boca Raton (FL): CRC Press, 2016.

[3] W. S. Brud, *Industrial Uses of Essential Oils*. Boca Raton (FL): Taylor & Francis Group, 2016.

[4] H. F. Gscheidmeier M, “Turpentines,” in *Ullmann’s Enc. of Industrial Chemistry*, Weinheim (Germany): Wiley-VCH John Wiley & Sons, 2005, p. 17.

[5] R. E. Kirk and D. F. Othmer, “Kirk-Othmer Chemical Technology of Cosmetics,” New York: John Wiley & Sons, 2012, p. 832.

[6] L. G. Wade, *Organic Chemistry*, 7th ed. Upper Saddle River (NJ): Prentice Hall, 2009.

[7] G. D. Yadav and R. D. Bhagat, “Clean esterification of mandelic acid over Cs2.5 H0.5PW12O40 supported on acid treated clay,” *Clean Technol. Environ. Policy*, vol. 7, no. 4, pp. 245–251, 2005.

[8] D. P. Sawant, A. Vinu, J. Justus, P. Srinivasu, and S. B. Halligudi, “Catalytic performances of silicotungstic acid/zirconia supported SBA-15 in an esterification of benzyl alcohol with acetic acid,” *J. Mol. Catal. A Chem.*, vol. 276, no. 1–2, pp. 150–157, 2007.

[9] G. Corro, F. Bañuelos, E. Vidal, and S. Cebada, “Measurements of surface acidity of solid catalysts for free fatty acids esterification in Jatropha curcas crude oil for biodiesel production,” *Fuel*, vol. 115, pp. 625–628, 2014.

[10] J. J. N. Otera, *Esterification Methods, Reactions, and Applications*. Weinheim: Wiley VCH Verlag GmbH & Co. KGaA, 2010.

[11] S. Khire, P. V. Bhagwat, M. Fernandes, P. B. Gangundi, and H. Vadalia, “Esterification of lower aliphatic alcohols with acetic acid in presence of different acid catalysts,” *Indian J. Chem. Technol.*, vol. 19, no. September, pp. 342–350, 2012.

[12] Y. Liu, E. Lotero, and J. G. Goodwin, “A comparison of the esterification of acetic acid with methanol using heterogeneous versus homogeneous acid catalysis,” *J. Catal.*, vol. 242, no. 2, pp. 278–286, 2006.

[13] M. Alvaro, A. Corma, D. Das, V. Fornés, and H. García, “‘Nafion’-functionalized

mesoporous MCM-41 silica shows high activity and selectivity for carboxylic acid esterification and Friedel-Crafts acylation reactions," *J. Catal.*, vol. 231, no. 1, pp. 48–55, 2005.

[14] M. Sharma, R. K. Wanchoo, and A. P. Toor, "Amberlyst 15 Catalyzed Esterifi cation of Nonanoic Acid with 1 - Propanol : Kinetics, Modeling, and Comparison of Its Reaction Kinetics with Lower Alcohols," *Ind. Eng. Chem. Res.*, vol. 53, pp. 2167–2174, 2014.

[15] A. Corma, "From Microporous to Mesoporous Molecular Sieve Materials and Their Use in Catalysis," *Chem. Rev.*, vol. 97, pp. 2373–2419, 1997.

[16] H. E. Hoydonckx, D. E. De Vos, S. A. Chavan, and P. A. Jacobs, "Esterification and transesterification of renewable chemicals," *Top. Catal.*, vol. 27, no. 1–4, pp. 83–96, 2004.

[17] N. Linares, A. M. Silvestre-Albero, E. Serrano, J. Silvestre-Albero, and J. García-Martínez, "Mesoporous materials for clean energy technologies," *Chem. Soc. Rev.*, vol. 43, no. 22, pp. 7681–7717, 2014.

[18] L. Li, S. Yu, F. Liu, J. Yang, and S. Zhaug, "Reactions of turpentine using Zr-MCM-41 family mesoporous molecular sieves," *Catal. Letters*, vol. 100, no. 3–4, pp. 227–233, 2005.

[19] M. Selvaraj and Y. Choe, "Well ordered two-dimensional SnSBA-15 catalysts synthesized with high levels of tetrahedral tin for highly efficient and clean synthesis of nopol," *Appl. Catal. A Gen.*, vol. 373, no. 1–2, pp. 186–191, Jan. 2010.

[20] A. Corma, "Water-resistant Lewis-acid sites: carbonyl-ene reactions catalyzed by tin-containing, hydrophobic molecular sieves," *Arkivoc*, vol. 8, pp. 40–48, 2007.

[21] "Nopyl acetate Sigma Aldrich." [Online]. Available: nopyl+acetate.+http://www.sigmaaldrich.com/catalog/ProductDetail.do?lang=en&N4=W516309%7CALDRICH&N5=SEARCH_CONCAT_PNO%7CBRAND_KEY&F=SPEC. [Accessed: 15-Apr-2017].

[22] "Nopyl acetate," *Food Cosmet. Toxicol.*, pp. 943–944, 1974.

[23] G. M. Barton, "Can trees cure cancer?," *Can. Chem. News*, 1992.

[24] J. P. Bain, "Nopol . I . The Reaction of b-Pinene with Formaldehyde," *J. Am. Chem. Soc.*, vol. 68, no. 4, pp. 638–641, 1946.

[25] S. Watanabe, "Thermal condensation of formaldehyde with cycloolefins," *Bulletin of the Chemical Society of Japan*, vol. 38, no. 8. pp. 1231–1235, 1965.

[26] V. Heitmann, W., Marietta Ga., Maetzel, "Process for preparing of cis-dihydronopol," US5175347, 1992.

[27] Z. Wang, Z. Xiao, and J. Chen, “Synthesis and identification of nopol and its derivatives,” *Chem. World*, vol. 45, no. 2, pp. 89–92, 2004.

[28] Z. Wang and Z. Xiao, “Synthesis and 13C NMR chemical shift analysis of nopol derivatives.,” *Chem. Ind. For. Prod.*, vol. 19, no. 05, pp. 497–498, 2002.

[29] Z.-D. Wang, Z.-Q. Xiao, and J.-Z. Chen, “Studies of synthesis and oxidation of nopyl acetate.,” *Chem. Ind. For. Prod.*, vol. 24, no. 01, 2004.

[30] J.-Z. Chen, Z.-Q. Xiao, Z.-J. Li, and S.-U. Wu, “The synthesis of nopyl esters by azeotropic deacidification.,” *J. Chem. Ind. For. Prod.*, vol. 06, 2002.

[31] A. J. Baggio RF, Sparks AL, Juo R, “Constrained cis-diol-borate bioconjugation system,” US 7,399,645 B2, 2008.

[32] X. J. Khaja SD, “Ceric Ammonium Nitrate: Novel and Robust Acetylating Catalyst.,” *Lett. Org. Chem.*, vol. 3, no. 7, 2006.

[33] V. V Costa, K. A. da Silva Rocha, L. C. A. Oliveira, E. F. Kozhevnikova, I. V Kozhevnikov, and E. V Gusevskaya, “Heteropoly acid catalysts for the synthesis of fragrance compounds from bio-renewables: acetylation of nopol and terpenic alcohols,” *RSC Adv.*, vol. 6, no. 49, pp. 43217–43222, 2016.

[34] L. C. Luo Jin-yue, “Synthesis of Nopyl Acetate Catalyzed by SO4(2-)/ZrO2-TiO2,” *Chem. Ind. For. Prod.*, vol. 28, no. 6, 2008.

[35] J. Z. Chen, Z. Xiao, Z. Li, and S. Wu, “The Synthesis of Nopyl Esters by Azeotropic Deacidification,” *Chem. For. Prod.*, vol. 36, no. 6, 2002.

[36] “http://www.thegoodscentscompany.com/data/rw1344431.html,” *The Good Scents Company Information System*, 2016. [Online]. Available: http://www.thegoodscentscompany.com/data/rw1344431.html. [Accessed: 10-May-2017].

[37] R. E. Kirk and D. F. Othmer, “Terpenoids,” in *Kirk-Othmer Encyclopedia of Chemical Technology*, 4th ed., New York: John Wiley & Sons, Inc, 2000.

[38] L. F. Correa Montes, “Síntesis de nopol empleado los catalizadores Sn-SBA-15 y Sn-MCM-41,” Trabajo de Maestría en Ciencias Químicas, Universidad de Antioquia, 2012.

[39] “(1R)-(−)-Nopol.” [Online]. Available: http://www.sigmaaldrich.com/catalog/product/aldrich/340367?lang=en&region=CO. [Accessed: 28-May-2017].

[40] “Scavage Colombia.” [Online]. Available: http://www.scavage.com/trade?menu=co.import&query=product:alcoholes. [Accessed: 09-Apr-2017].

[41] U. Comtrade, “United Nations Commodity Trade Statistics Database,” 2015.

[Online]. Available: https://comtrade.un.org/db/mr/rfCommoditiesList.aspx?px=H1&cc=3301. [Accessed: 06-Feb-2017].

[42] H. S. Fogler, *Elements of Chemical Reaction Engineering*, 3rd ed. Upper Saddle River (NJ): Prentice Hall, 1999.

[43] S. H. Ali, A. Tarakmah, S. Q. Merchant, and T. Al-Sahhaf, “Synthesis of esters: Development of the rate expression for the Dowex 50 Wx8-400 catalyzed esterification of propionic acid with 1-propanol,” *Chem. Eng. Sci.*, vol. 62, no. 12, pp. 3197–3217, 2007.

[44] Y. Liu, E. Lotero, and J. G. Goodwin, “Effect of water on sulfuric acid catalyzed esterification,” *J. Mol. Catal. A Chem.*, vol. 245, no. 1–2, pp. 132–140, 2006.

[45] R. Schwarzer, “Esterification of acetic acid with methanol : A Kinetic Study on Amberlyst 15,” Masters of Engineering (Chemical Engineering), University of Pretoria, 2006.

[46] H. L. H. A. Iszi, “Kinetics of Synthesis of Isobutyl Propionate over Amberlyst-15,” *Turk J Chem*, vol. 31, pp. 493–499, 2007.

[47] E. O. Akbay and M. R. Altiokka, “Kinetics of esterification of acetic acid with n-amyl alcohol in the presence of Amberlyst-36,” *Appl. Catal. A Gen.*, vol. 396, no. 1–2, pp. 14–19, 2011.

[48] E. Sert, A. D. Buluklu, S. Karakuş, and F. S. Atalay, “Kinetic study of catalytic esterification of acrylic acid with butanol catalyzed by different ion exchange resins,” *Chem. Eng. Process. Process Intensif.*, vol. 73, pp. 23–28, 2013.

[49] R. Pal, T. Sarkar, and S. Khasnobis, “Amberlyst-15 in organic synthesis,” *Arkivoc*, vol. 2012, no. 1, pp. 570–609, 2012.

[50] B. Das, P. Thirupathi, I. Mahender, V. S. Reddy, and Y. K. Rao, “Amberlyst-15: An efficient reusable heterogeneous catalyst for the synthesis of 1,8-dioxo-octahydroxanthenes and 1,8-dioxo-decahydroacridines,” *J. Mol. Catal. A Chem.*, vol. 247, no. 1–2, pp. 233–239, 2006.

[51] Y. Zhang, D. Wu, Y. H. Sun, S. Y. Peng, D. Y. Zhao, Q. Luo, and F. Deng, “Synthesis and properties of aluminosilicate mesoporous material with adjustable pore structure,” *Stud. Surf. Sci. Catal.*, vol. 146, pp. 161–164, 2003.

[52] J. Zheng, C. Song, X. Xu, U. T. Turaga, and X. S. Zhao, “Acidity measurement of nanoporous aluminosilicates-zeolites and MCM-41,” in *Nanoporous Materials*, London: Imperial College Press, 2004, p. 465.

[53] F. Kleitz, “Ordered Mesoporous Materials,” in *Handbook of Heterogeneous Catalysis*, 2nd ed., no. March, Weinheim (Germany), 2008, pp. 177–214.

[54] A. Vinu, T. Mori, and K. Ariga, “New families of mesoporous materials,” *Sci.*

Technol. Adv. Mater., vol. 7, no. 8, pp. 753–771, 2006.

[55] E. You, “Synthesis and adsorption studies of the micro-mesoporous material SBA-15,” Master of Science in Chemical Engineering, University of Massachusetts Amherst, 2007.

[56] O. W. Flörke, H. A. Graetsch, F. Brunk, D. C. O. Feuerfest, L. Benda, Paschen, H. E. Bergna, W. O. Roberts, W. A. Welsh, and D. M. Chapman, “Silica,” in *Ullmann´s Enc. of Industrial Chemistry*, 2005, pp. 1–58.

[57] E. G. Vieira, I. V. Soares, N. L. Dias Filho, N. C. da Silva, E. F. Garcia, A. C. Bastos, S. D. Perujo, T. T. Ferreira, A. H. Rosa, and L. F. Fraceto, “Preconcentration and determination of metal ions from fuel ethanol with a new 2,2’-dipyridylamine bonded silica,” *J. Colloid Interface Sci.*, vol. 391, no. 1, pp. 116–124, 2013.

[58] S. E. Dann, “Solid State Chemistry,” in *Reactions and Characterization of Solids*, 1st ed., Cambridge (UK): The Royal Society of Chemistry, 2000, pp. 48–80.

[59] S. Brunauer, P. H. Emmett, and E. Teller, “Adsorption of Gases in Multimolecular Layers,” *J. Am. Chem. Soc.*, vol. 60, no. 1, pp. 309–319, 1938.

[60] K. S. W. Sing, D. H. Everett, R. a. W. Haul, L. Moscou, R. a. Pierotti, J. Rouquérol, and T. Siemieniewska, “Reporting Physisorption Data for Gas / Solid Systems with Special Reference to the Determination of Surface Area and Porosity,” *Pure Appl. Chem.*, vol. 54, no. 11, pp. 2201–2218, 1982.

[61] B. Welz and M. Vale, “Atomic Absorption Spectrometry and Related Techniques,” *Ewing’s Anal. Instrum. Handbook, 3rd Ed.*, p. 1037, 2005.

[62] D. Jariel, “Scanning electron microscopy,” *Encyclopedia of Science*. Salem Press, Amenia (NY), 2016.

[63] P. R. Boehlke, “Scanning Electron Microscopy,” *Encyclopedia of Science*. Salem Press, Amenia (NY), 2016.

[64] S. Wang, X. Ma, J. Gong, X. Yang, H. Guo, and G. Xu, “Transesterification of Dimethyl Oxalate with Phenol under SnO2/SiO2 Catalysts,” *Ind. Eng. Chem. Res.*, vol. 43, pp. 4027–4030, 2004.

[65] A. Parmaliana, F. Frusteri, F. Arena, N. Mondello, and N. Giordano, “Activity and Characterization of Alkali Doped Ni/MgO Catalysts,” *Stud. Surf. Sci. Catal.*, vol. 48, no. C, pp. 739–748, 1989.

[66] M. Hunger and J. Weitkamp, “In situ IR, NMR, EPR, and UV_Vis Spectroscopy_ Tools for New Insight into the Mechanisms of Heterogeneous Catalysis - Hunger - 2001 - Angewandte Chemie International Edition - Wiley Online Library.pdf,” *Angew. Chemie - Wiley -VCH*, vol. 40, pp. 2954–2971, 2001.

[67] Princeton Instruments, “Raman Spectroscopy Basics - Application Note,” 2012.

[Online]. Available: http://content.piacton.com/Uploads/Princeton/Documents/Library/UpdatedLibrary/Raman_Spectroscopy_Basics.pdf. [Accessed: 20-Apr-2018].

[68] T. R. Crompton, *Thermal Methods of Polymer Analysis*. Shawbury, Shrewsbury, Shropshire (UK): Smithers Rappa, 2013.

[69] M. Grün, K. K. Unger, A. Matsumoto, and K. Tsutsumi, “Novel pathways for the preparation of mesoporous MCM-41 materials: control of porosity and morphology,” *Microporous Mesoporous Mater.*, vol. 27, pp. 207–216, 1999.

[70] P. Shah, A. V. Ramaswamy, K. Lazar, and V. Ramaswamy, “Synthesis and characterization of tin oxide-modified mesoporous SBA-15 molecular sieves and catalytic activity in trans-esterification reaction,” *Appl. Catal. A Gen.*, vol. 273, no. 1–2, pp. 239–248, 2004.

[71] R. D. Gonzalez, T. Lopez, and R. Gomez, “Sol-gel preparation of supported metal catalysts,” *Catal. Today*, vol. 35, no. 3, pp. 293–317, 1997.

[72] P. W. Park, H. H. Kung, D. W. Kim, C. H. F. Peden, Staff, A. Yezeretz, W. Epling, N. Currier, H. Chen, H. Hess, O. Kresnawahjuesa, and D. Lafyatis, “Characterization of SnO2/Al2O3 Lean NO Catalysts,” *J. Catal.*, vol. 184, pp. 440–454, 1999.

[73] E. Alarcón, A. L. Villa, and C. Montes, “Síntesis de nopol a partir de β-pineno y aceite de trementina con el catalizador Sn-MCM-41,” *Rev. Fac. Ing. Univ. Antioquia*, vol. 46, pp. 45–55, 2006.

[74] V. Ramaswamy, P. Shah, K. Lazar, and a. V. Ramaswamy, “Synthesis, Characterization and Catalytic Activity of Sn-SBA-15 Mesoporous Molecular Sieves,” *Catal. Surv. from Asia*, vol. 12, no. 4, pp. 283–309, Nov. 2008.

[75] X. Liu, H. Sun, and Y. Yang, “Rapid synthesis of highly ordered Si-MCM-41,” *J. Colloid Interface Sci.*, vol. 319, pp. 377–380, 2008.

[76] Y. Liu, Y. Cao, N. Yi, W. Feng, W. Dai, S. Yan, H. He, and K. Fan, “Vanadium oxide supported on mesoporous SBA-15 as highly selective catalysts in the oxidative dehydrogenation of propane,” *J. Catal.*, vol. 224, pp. 417–428, 2004.

[77] V. Ramaswamy, P. Shah, K. Lazar, and a. V. Ramaswamy, “Synthesis, characterization and catalytic activity of Sn-SBA-15 mesoporous molecular sieves,” *Catal. Surv. from Asia*, vol. 12, pp. 283–309, 2008.

[78] G. Mitran, É. Makó, Á. Rédey, and I.-C. Marcu, “Esterification of Acetic Acid with n-Butanol Using Molybdenum Oxides Supported on γ-Alumina,” *Comptes Rendus Chim.*, vol. 15, pp. 793–798, May 2012.

[79] C. Toro, P. Hidalgo, and R. Navia, “Development of polyesters from glycerol for Na removal in biodiesel refining,” *J. Biobased Mater. Bioenergy*, vol. 5, no. 1, pp.

55–62, 2011.

[80] Z. He, Z. Hou, Y. Luo, Y. Dilixiati, and W. Eli, “Hydroesterification of styrene derivatives catalyzed by an acidic resin supporting palladium complexes,” *Catal. Sci. Technol.*, vol. 4, no. 4, pp. 1092–1103, 2014.

[81] E. A. Durango, A. L. V. De P, and C. M. De, “Síntesis de nopol a partir de β-pineno y aceite de trementina con el catalizador Sn-MCM-41,” *Rev. Fac. Ing. Univ. Antioquia*, vol. 46, pp. 45–55, 2006.

[82] P. Fejes, J. B. Nagy, K. Kovacs, and G. Vanko, “Synthesis of tin(IV) silicalites (MFI) and their characterization A Mössbauer and MAS NMR spectroscopy study,” *Appl. Catal. A Gen.*, vol. 145, pp. 155–184, 1996.

[83] E. Caponetti, A. Minoja, M. L. Saladino, and A. Spinella, “Characterization of Nd-MCM-41 obtained by impregnation,” *Microporous Mesoporous Mater.*, vol. 113, no. 1–3, pp. 490–498, 2008.

[84] C. J. Brinker, R. J. Kirkpatrick, D. R. Tallanta, B. C. Bunker, and B. Montez, “NMR confirmation of strained ‘defects’ in amorphous silica,” *J. Non. Cryst. Solids*, vol. 99, pp. 418–428, 1988.

[85] C. Cong-Yan, L. Hong-Xin, and M. E. Davis, “Studies on mesoporous materials I. Synthesis and characterization of MCM 41,” *Microporous Mater.*, vol. 2, no. 2, pp. 17–26, 1993.

[86] S. Huang, Y. Chen, H. Xiao, and F. Lu, “Characterization of Sn and Si nanocrystals embedded in SiO2 matrix fabricated by magnetron co-sputtering,” *Surf. Coatings Technol.*, vol. 205, no. 7, pp. 2247–2250, 2010.

[87] J. P. Thielemann, T. Ressler, A. Walter, G. Tzolova-Müller, and C. Hess, “Structure of molybdenum oxide supported on silica SBA-15 studied by Raman, UV-Vis and X-ray absorption spectroscopy,” *Appl. Catal. A Gen.*, vol. 399, no. 1–2, pp. 28–34, 2011.

[88] P. Shah, A. V Ramaswamy, K. Lazar, and V. Ramaswamy, “Direct hydrothermal synthesis of mesoporous Sn-SBA-15 materials under weak acidic conditions,” *Microporous Mesoporous Mater.*, vol. 100, pp. 210–226, 2007.

[89] I. M. Smallwood, *Handbook of organic solvent properties*. New York: Halsted Press, 1996.

[90] G. Mitran, É. Makó, Á. Rédey, and I. C. Marcu, “Esterification of acetic acid with n-Butanol using vanadium oxides supported on γ-alumina,” *Comptes Rendus Chim.*, vol. 140, pp. 32–37, 2010.

[91] J. Yang, S. Cho, H. Kim, H. Joo, H. Jung, and K. Lee, “Production of 4-Hydroxybutyl Acrylate and Its Reaction Kinetics over Amberlyst 15 Catalyst,” *Can. J. Chem. Eng.*, vol. 85, no. February, pp. 83–91, 2007.

[92] S. H. Ali and S. Q. Merchant, “Kinetics of the esterification of acetic acid with 2-propanol: Impact of different acidic cation exchange resins on reaction mechanism,” *Int. J. Chem. Kinet.*, vol. 38, no. 10, pp. 593–612, 2006.

[93] N. Villandier and A. Corma, “One pot catalytic conversion of cellulose into biodegradable surfactants,” *Chemical Communications*, vol. 46, no. 24. p. 4408, 2010.

[94] M. L. Testa, V. La Parola, L. F. Liotta, and A. M. Venezia, “Screening of different solid acid catalysts for glycerol acetylation,” *J. Mol. Catal. A Chem.*, vol. 367, pp. 69–76, 2013.

[95] D. H. Pybus and C. S. Sell, *The Chemistry of Fragrances*. Ashford, Kent, UK: Royal Society of Chemistry, 1999.

[96] Z. Zeng, L. Cui, W. Xue, J. Chen, and Y. Che, “Recent Developments on the Mechanism and Kinetics of Esterification Reaction Promoted by Various Catalysts,” *Chemical Kinetics*, no. 2. pp. 256–282, 2011.

[97] Audra Clark, “Back to the Basics The Importance of a Good Calibration.” [Online]. Available: http://www.apgqa.com/era_and_apg.asp. [Accessed: 25-May-2018].